

Title	SUPERCONDUCTING AND MAGNETIC PROPERTIES OF PB <sub>1-2-x</sub> EU <sub>x</sub> MO <sub>6</sub> S <sub>8</sub> AND CE <sub>x</sub> LA <sub>1-x</sub> MO <sub>6</sub> S <sub>8</sub>
Author(s)	野口, 悟
Citation	大阪大学, 1986, 博士論文
Version Type	VoR
URL	<a href="https://hdl.handle.net/11094/1333">https://hdl.handle.net/11094/1333</a>
rights	
Note	

*Osaka University Knowledge Archive : OUKA*

<https://ir.library.osaka-u.ac.jp/>

Osaka University

SUPERCONDUCTING AND MAGNETIC PROPERTIES OF

$\text{Pb}_{1.2-x}\text{Eu}_x\text{Mo}_6\text{S}_8$  AND  $\text{Ce}_x\text{La}_{1-x}\text{Mo}_6\text{S}_8$

BY

SATORU NOGUCHI

DISSERTATION IN PHYSICS



**THE OSAKA UNIVERSITY**  
**GRADUATE SCHOOL OF SCIENCE**  
**TOYONAKA, OSAKA**

SUPERCONDUCTING AND MAGNETIC PROPERTIES OF

$\text{Pb}_{1.2-x}\text{Eu}_x\text{Mo}_6\text{S}_8$  AND  $\text{Ce}_x\text{La}_{1-x}\text{Mo}_6\text{S}_8$

by

Satoru NOGUCHI

DISSERTATION IN PHYSICS

THE OSAKA UNIVERSITY  
GRADUATE SCHOOL OF SCIENCE

TOYONAKA, OSAKA

September, 1986

## CONTENTS

PART I. SUPERCONDUCTING AND MAGNETIC PROPERTIES	
OF $\text{Pb}_{1.2-x}\text{Eu}_x\text{Mo}_6\text{S}_8$	
ABSTRACT	1
§ 1. INTRODUCTION	2
§ 2. CRYSTAL STRUCTURE AND ELECTRONIC PROPERTIES	9
§ 3. EXPERIMENTAL PROCEDURES	12
3.1. Sample Preparation	12
3.2. Resistance and Susceptibility Measurements under a Static Field	15
3.3. High Field Magnetoresistance and Magnetization Measurements	21
§ 4. RESULTS AND DISCUSSIONS	38
4.1. Superconducting and Structural Phase Transitions	38
4.2. Upper Critical Field $H_{c2}$	48
4.3. Magnetic Properties of $\text{Eu}_{1.2}\text{Mo}_6\text{S}_8$	66
§ 5. CONCLUDING REMARKS	73
APPENDIX	74
REFERENCES	77
PART II. VALENCE OF Ce AND KONDO EFFECT IN $\text{Ce}_x\text{La}_{1-x}\text{Mo}_6\text{S}_8$	
ABSTRACT	81
§ 1. INTRODUCTION	82
§ 2. EXPERIMENTAL	87
§ 3. VALENCE OF Ce IN $\text{CeMo}_6\text{S}_8$	91
§ 4. SUPERCONDUCTING PROPERTIES	97

§ 5.	MAGNETIC PROPERTIES	105
§ 6.	CONCLUDING REMARKS	125
	APPENDIX I	127
	APPENDIX II	129
	REFERENCES	131
	ACKNOWLEDGEMENTS	133

## PART I

### SUPERCONDUCTING AND MAGNETIC PROPERTIES OF $\text{Pb}_{1.2-x}\text{Eu}_x\text{Mo}_6\text{S}_8$

#### ABSTRACT

Effect of magnetic ions on the superconductivity is investigated in the pseudo-ternary Chevrel compounds  $\text{Pb}_{1.2-x}\text{Eu}_x\text{Mo}_6\text{S}_8$  by measuring the electrical resistance and magnetization in the range of temperature down to 0.1 K and magnetic field up to 650 kOe.

Superconducting and structural transformation temperatures,  $T_c$  and  $T_s$ , are obtained as a function of Eu concentration. A clear enhancement of  $H_{c2}$  is found around the composition  $\text{Pb}_{0.7}\text{Eu}_{0.5}\text{Mo}_6\text{S}_8$  and the  $H_{c2}(0)$  is estimated to be 630 kOe. The dependences of  $T_c$  and  $H_{c2}$  on the temperature and Eu concentration are successfully explained by the theory of Maekawa and Tachiki with the antiferromagnetic coupling of  $-3.2 \pm 0.6$  meV between the conduction electrons and Eu spins. Valence mixing of  $\text{Eu}^{2+}$  and  $\text{Eu}^{3+}$  is suggested in  $\text{Eu}_{1.2}\text{Mo}_6\text{S}_8$  from the high field magnetization data. A large negative magnetoresistance is found in  $\text{Eu}_{1.2}\text{Mo}_6\text{S}_8$  near the magnetic ordering temperature  $T_m$ , which indicates that the spin fluctuation effect is large in the compound.

## § 1. INTRODUCTION

Recently, the utility of high magnetic field is highlighted with respect to not only a basic interest in physical subjects but its applications to nuclear fusion or high resolution NMR etc. By the present time, however, the generation of static field above 30 Tesla is difficult because the energy loss due to Joule heating is too much. In order to obtain high magnetic field without energy loss, superconducting materials with a high critical field are needed. So, high field superconductors have been extensively developed by many researchers as well as high  $T_c$  superconductors.

Fig.1 shows the  $H_{c2}(T)$  curves in some of the high field superconductors. NbTi alloy is commercially used as a standard superconducting wire for practical application.  $Nb_3Sn$  and  $Nb_3Ge$  are A-15 type superconductors<sup>1)</sup> which have been extensively investigated with great interest in basic and applied research.  $Nb_3Ge$  has the highest superconducting transition temperature with 23 K.  $Nb_3Sn$  is commercially used for high field superconducting magnet up to 15 Tesla.  $PbMo_6S_8$  and  $SnMo_6S_8$  are Chevrel phase compounds<sup>2)</sup>, having a very high critical field and a large initial slope  $-(dH_{c2}/dT)_{T_c}$ . In particular,  $Pb_xMo_6S_8$  with  $x \approx 1$  has an extremely high critical field. The upper critical field  $H_{c2}$  of this system has been investigated by three groups; Foner<sup>3)</sup>, Fischer<sup>4)</sup> and our group<sup>5)</sup>. They found the highest  $H_{c2}(0)$  of  $Pb_xMo_6S_8$  to be 600 kOe as is seen in Fig.1. At 4.2 K,  $H_{c2}$  of this compound is about 4 times higher than that of NbTi. If the compound is developed as practical superconducting wire, it may be

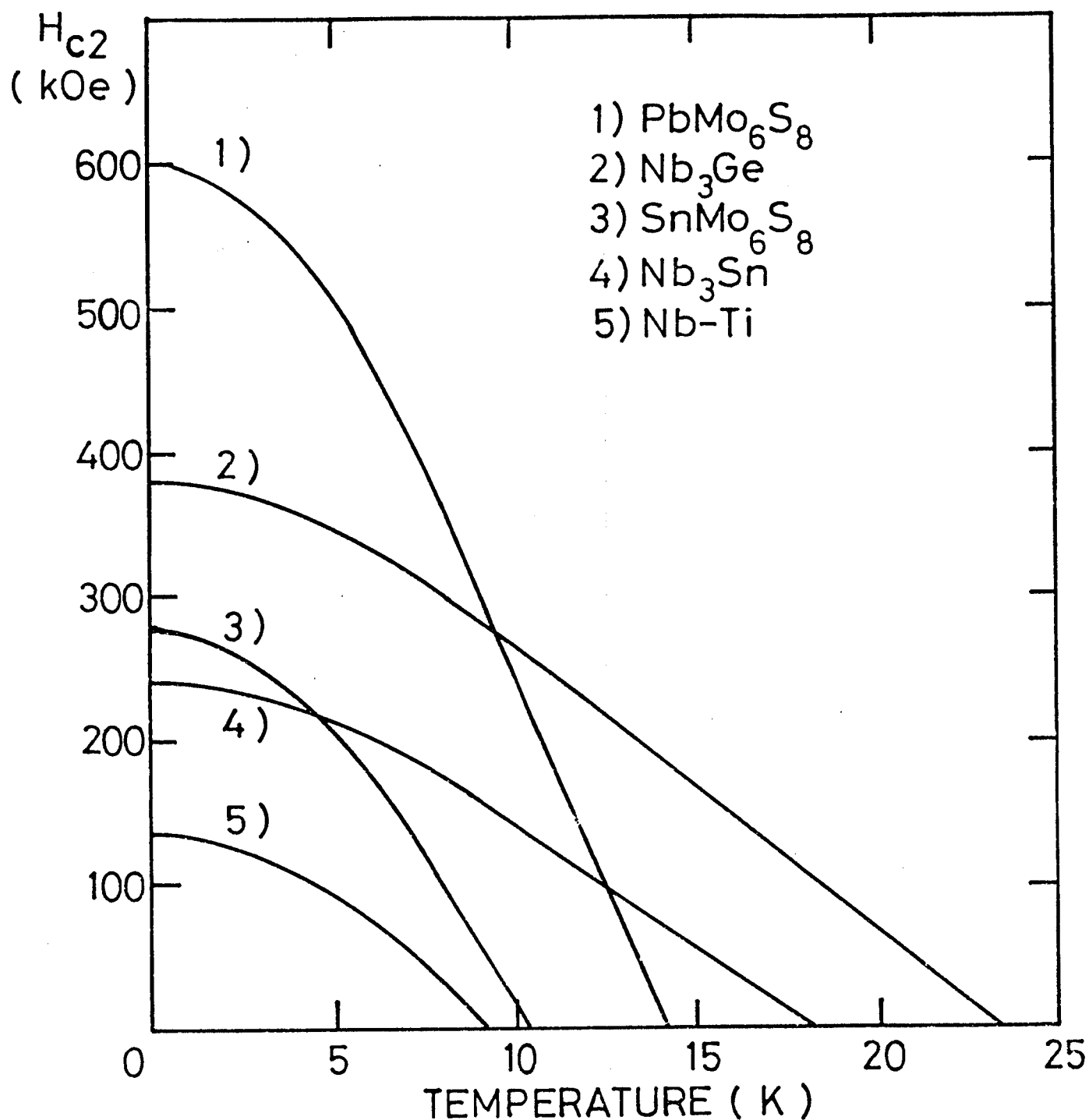


FIG.1 Upper critical field as a function of temperature for high field and high temperature superconductors.



possible to generate the static field up to 50 Tesla. The development is extensively done by many groups including ourselves.<sup>6)- 9)</sup>

Generally, external magnetic field destroys the superconductivity by interacting with orbits and spins of the conduction electrons. In a Type II superconductor, orbital critical field  $H_{c2}^*$  is given by

$$H_{c2}^* = \frac{\phi_0}{2\pi\xi^2}, \quad (1-1)$$

where  $\xi$  is the Ginzburg-Landau coherence length and  $\phi_0$  the flux quantum.<sup>10)</sup> In a dirty limit ( $\ell < \xi$ ), we have

$$\xi^2 \sim \ell \cdot v_F / T_C, \quad (1-2)$$

where  $\ell$  is the mean free path of the electrons in the normal state and  $v_F$  being Fermi velocity. Therefore, a high critical field is obtained in compounds with a high  $T_C$ , a short mean free path and a low Fermi velocity, i.e. narrow band structure.

Interaction of the field with the conduction-electron spins leads to the paramagnetic limiting field,  $H_{p0}$ , given by

$$H_{p0} = 18.4 T_C \quad [\text{kOe}].^{11)} \quad (1-3)$$

In the high field superconductors, however, observed critical fields are much higher than this limit. One of the reason for this is probably to be found in a strong spin-orbit coupling of the two states forming a Cooper pair.<sup>12)</sup> In this case, the para-

magnetic limit  $H_p$  is given with the spin-orbit coupling parameter  $\lambda_{so}$ , as follows,

$$H_p = 1.33 \sqrt{\lambda_{so}} \cdot H_{p0}. \quad (1-4)$$

For  $\lambda_{so} \rightarrow \infty$  we have  $H_p \rightarrow \infty$  and no paramagnetic limitation will occur in this extreme case. On the other hand, it is pointed out by Orland et al. that  $H_p$  is substantially enhanced by the strong coupling contributions.<sup>13)</sup> Anyway, the basic properties of high field superconductors are still not completely understood.

Chevrel compounds are written with the general formula  $M_x Mo_6 - X_8$ ,<sup>14)</sup> where M stands for a large number of metals as is shown in Fig.2 and x may take a value between 1 and 4 depending on the element M. X is a substitute for Chalcogens ( S, Se or Te ). Since Matthias et al. reported in 1972 that many of these new phases were superconducting with reasonably high critical temperatures,<sup>15)</sup> they have attracted much attention because of their peculiar superconducting and magnetic properties. One of the attractive characters of the compounds appears in the rare-earth molybdenum sulfides  $REMo_6S_8$ .<sup>16)</sup> Various phases of  $REMo_6S_8$  are shown in Fig.3. With exception of Ce and Eu compounds, they are all superconducting in spite of the fact that they contain nearly 7 at.% magnetic rare earth ion. For RE = Gd, Tb, Dy and Er, they show coexistence of antiferromagnetic order and superconductivity at low temperatures. Only  $HoMo_6S_8$  becomes ferromagnetic at low temperatures where superconductivity is destroyed. These fascinate physical properties are also found in  $RERh_4B_4$  compounds.<sup>17)</sup> At

Li r	Be											B	C	N	O	F	Ne
Na r	Mg r											Al r	Si	P	S	Cl	Ar
K	Ca r	Sc t	Ti	V	Cr t	Mn t,r	Fe t,r	Co r	Ni r	Cu r	Zn r	Ga	Ge	As	Se	Br	Kr
Rb	Sr r	Y r	Zr	Nb	Mo	Tc	Ru	Rh	Pd r	Ag r	Cd r	In r	Sn r	Sb	Te	I	Xe
Cs	Ba r	La r	Hf	Ta	W	Re	Os	Ir	Pt	Au	Hg	Tl	Pb	Bi	Po	At	Rn
Fr	Ra	Ac															
			Ce r	Pf t	Nd t	Pm	Sm r	Eu r	Gd	Tb	Dy	Ho	Er	Tm	Yb	Lu	
			Th r	Po	U r	Np	Pu	Am	Cm	Bk	Cf	Es	Fm	Md	No	Lw	

FIG.2 Periodic table indicating the element M for which the compounds  $M_xMo_6S_8$  form. r and t indicate that the room temperature phase is rhombohedral or triclinic, respectively. Shaded members have superconducting transitions above 1.2 K.

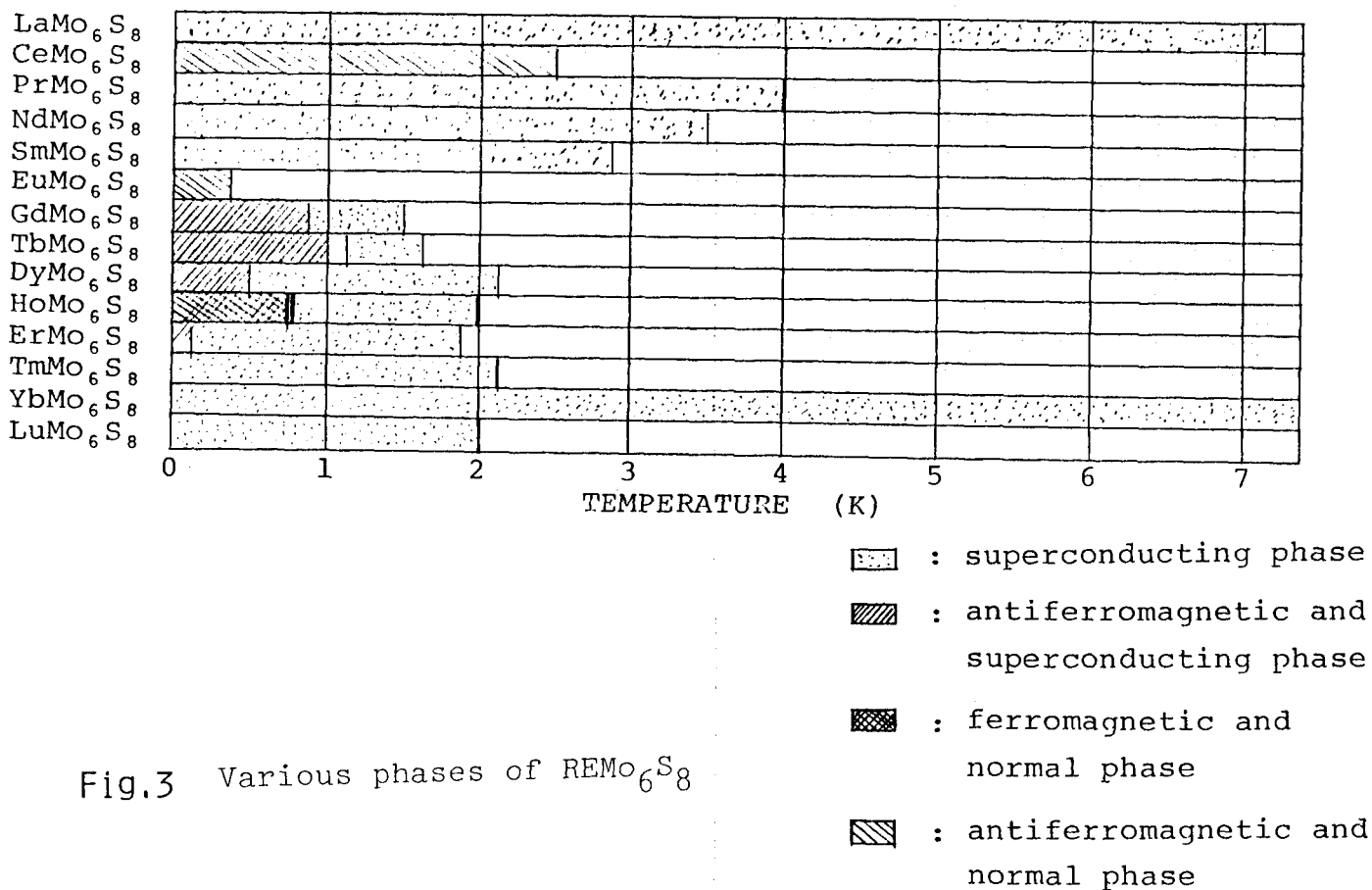


Fig.3 Various phases of  $REMo_6S_8$

present, these materials are called as "magnetic superconductors" and have been investigated extensively in connection with the interplay between superconductivity and long range magnetic ordering of the RE magnetic moments.<sup>18)</sup>

In a high field superconductor with localized magnetic impurities, the external field may be of the same order of magnitude as the exchange field coming from the localized spins. So, the  $H_{c2}$  behavior depends on the sign of the exchange field. If the exchange is negative, it is possible to observe an enhancement of  $H_{c2}$  with respect to the equivalent non-magnetic compound as a result of a compensation of the external field by the exchange field acting on the conduction-electron spins. This idea was first proposed by Jaccarino and Peter.<sup>19)</sup> Nuclear magnetic resonance and Mössbauer effect studies by Fradin et al. on  $\text{Sn}_{0.5}\text{Eu}_{0.5}\text{Mo}_6\text{S}_8$  showed a negative s-band polarization at the Mo sites.<sup>20)</sup> These results indicate that the exchange interaction between the conduction electron spins and the Eu magnetic moments is antiferromagnetic in the Chevrel compounds. In this case it is expected that the  $H_{c2}$  is effectively enhanced.

The energy band calculations done by Jarlborg and Freeman show the high Mo d-band density of states ( DOS ) at the Fermi energy  $E_F$  and low conduction electron DOS at the RE site.<sup>21)</sup> The former Mo d-electrons with high DOS contribute to the superconductivity of the compounds and the latter low conduction electron DOS yields the weak coupling with 4f electrons. On the basis of this model, Maekawa and Tachiki calculated the effect of magnetic spins on the superconductivity by taking account of the inelastic scat-

tering of conduction electrons with the magnetic spins which correlate each other through exchange interaction.<sup>22)</sup> They give a general formula for the temperature dependence of upper critical field  $H_{c2}(T)$  and show a quantitative explanation to the Jaccarino-Peter effect.

These theoretical and experimental results stimulate us to investigate the effect of magnetic impurities on the upper critical field in the high field superconductors  $Pb_xMo_6S_8$ , for the possibility of getting even higher critical field than 600 kOe.<sup>23)</sup> Fischer et al. tried to observe the critical field in  $Pb_{0.7}Eu_{0.3}Mo_6S_8$ .<sup>24)</sup> However, their magnetic field was not enough to see whole aspect of the phenomena because the magnetic field higher than 600 kOe are needed to observe a complete transition at low temperatures. These requirements are satisfied with the facilities in our High Magnetic Field Laboratory of Osaka University.<sup>25,26)</sup>

In the present work, a systematic study of electrical resistance, magnetoresistance and magnetization is done in the pseudoternary compounds  $Pb_{1.2-x}Eu_xMo_6S_8$ .<sup>27,28)</sup> In Section 2, a brief overview of the crystal structure and electronic properties is given. The experimental procedures used in these investigations are outlined in Section 3. Results and discussions are given in Section 4 and concluding remarks drawn from the study are summarized in Section 5.

## § 2. CRYSTAL STRUCTURE AND ELECTRONIC PROPERTIES

Ternary molybdenum sulfides  $M_x Mo_6 S_8$  crystallize in a hexagonal-rhombohedral structure with the rhombohedral angle  $\alpha$  close to  $90^\circ$ . As is shown in Fig.4 these compounds contain building blocks with the formula  $Mo_6 S_8$ . The block is slightly deformed cube where the S atoms sit at the corner of the cube and the Mo atoms are located at the cube faces. The Mo atoms in one unit form a slightly deformed octahedron cluster. The shortest Mo-Mo intercluster distance becomes very large compared with the intracluster distances. The element M is situated in two different sites to satisfy the hexagonal rhombohedral symmetry. One is centered about the origin of the rhombohedral unit cell (000) surrounded by 8 units  $Mo_6 S_8$  and the other is centered at  $(\frac{1}{2}00)$  surrounded by 4 units  $Mo_6 S_8$ . So, x in  $M_x Mo_6 S_8$  may take a value between 1 and 4.

There are two types of non stoichiometry. In the materials of the first kind the element M is a small cation and the concentration x may vary continuously between two limits ( for example: Cu  $1.8 \leq x \leq 4$ ; Co  $1.32 \leq x \leq 2$  ). In the materials of the second kind, on the other hand, M is a large cation and x has a well defined value or the homogeneity domain where x may vary is very narrow.

$M_x Mo_6 S_8$  with M = Pb or rare-earth elements is the second type and it is found that most of the M-atoms occupy the first site (000). As a whole,  $M_x Mo_6 S_8$  can be seen CsCl type structure composed of the M-atom and the  $Mo_6 S_8$  cluster. The shortest distances of M-Mo and M-M are 4.2 and  $6.5 \overset{\circ}{\text{Å}}$ , respectively. These large distances

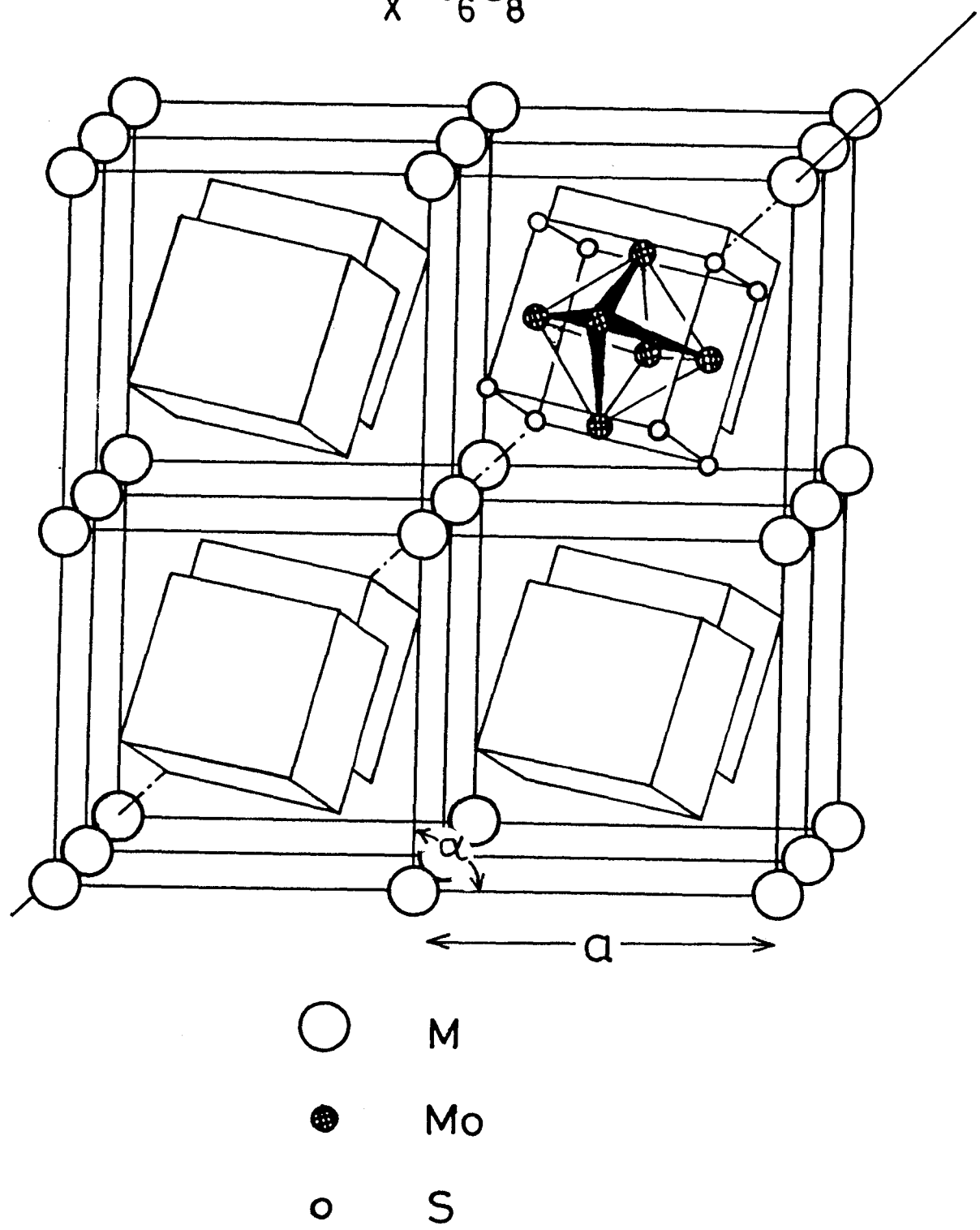
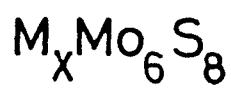


Fig.4 Crystal structure of  $M_x Mo_6 S_8$

imply that the magnetic interaction may be weak enough for the superconductivity to coexist with the magnetic long range order.

The large Mo-Mo intercluster distance and the large charge transfer from Mo to chalcogens result in the narrow Mo 4d-band and its high density of state ( DOS ) at the Fermi energy, which attributes to the superconductivity of the Chevrel compounds. Magnetic property is due to the localized 4f-electrons of rare-earth ions which are regularly located at the lattice points.

Recently, particular band calculations in these compounds were reported by Jarlborg and Freeman<sup>21)</sup>. They showed that the conduction electron DOS at the M site is reduced by an order of magnitude from its metallic state value. This low conduction electron DOS yields very weak coupling of the 4f-electrons to the conduction electrons and only a very weak Ruderman-Kittel-Kasuya-Yosida magnetic interaction, showing why all the rare-earth Chevrel compounds except Ce and Eu are superconducting despite their large local magnetic moments.



### § 3. EXPERIMENTAL PROCEDURES

#### 3.1. Sample preparation

Sintered samples of the pseudoternary compounds  $\text{Pb}_{1.2-x}\text{Eu}_x\text{Mo}_6\text{S}_8$  were prepared by the powder metallurgy technique. The procedure is summarized in Fig.5.

At the first step, europium sulfide, EuS, was obtained by the chemical reactions of  $\text{EuCl}_3$  and  $\text{H}_2\text{S}$  at 1000 °C for 1.5 hours after the desiccation of  $\text{EuCl}_3$  with pumping out at 150 °C for 2 hours. The product was checked to be a single phase of the europium sulfide by the X-ray powder diffraction.

Next, appropriate amount of starting materials  $\text{PbS}$ ,  $\text{MoS}_2$ , Mo and EuS were well ground together for 1 hour, pressed into tablets of 10 mmD x 1 mmT, sealed in a quartz tube evacuated down to  $10^{-5}$  Torr and then heated at 1100 °C for 40 hours after preheating at 400 °C for 24 hours. The preheating is necessary to suppress the vapour pressure of sulfur through the reaction. Subsequently, they were crushed, reground, pressed again into tablets and annealed in evacuated quartz tube at 1100 °C for 40 hours.

In these heat treatments total amounts of the powders in the tube were less than 4 grams to avoid bursting up the tube due to the excessive vapour pressure of sulfur. Compounds with nominal concentrations  $x = 0.0, 0.2, 0.4, 0.5, 0.6, 0.8, 1.0$  and 1.2 for  $\text{Pb}_{1.2-x}\text{Eu}_x\text{Mo}_6\text{S}_8$  were prepared in this manner.

At each step the crystal structure was checked by the X-ray powder diffraction. The diffraction pattern displayed the Chevrel

FIG.5. Sample Preparation Procedure of  $\text{Pb}_{1.2-x}\text{Eu}_x\text{Mo}_6\text{S}_8$

- 1)  $\text{EuCl}_3 \cdot n\text{H}_2\text{O} \longrightarrow \text{EuCl}_3 + n\text{H}_2\text{O}$  at 150 °C for 2 hours
- 2)  $2\text{EuCl}_3 + 3\text{H}_2\text{S} \longrightarrow 2\text{EuS} + 6\text{HCl}^\uparrow + \text{S}^\uparrow$  at 1000 °C for 1.5 hours
- 3) EuS : X-ray analysis
- 4)  $(1.2-x)\text{PbS} + x\text{EuS} + 3.4\text{MoS}_2 + 2.6\text{Mo}$   
mixed powder is pressed into tablet at 10 t/cm<sup>2</sup>  
 $\longrightarrow \text{Pb}_{1.2-x}\text{Eu}_x\text{Mo}_6\text{S}_8$   
sintered at 400 °C for 24 hours and at 1100 °C for 40 hour
- 5)  $\text{Pb}_{1.2-x}\text{Eu}_x\text{Mo}_6\text{S}_8$  : X-ray analysis
- 6) Annealed at 1100 °C for 40 hours
- 7)  $\text{Pb}_{1.2-x}\text{Eu}_x\text{Mo}_6\text{S}_8$  : X-ray analysis
- 8) Spark-cut into 0.5 mm x 1.0 mm x 7 mm for resistance measurement

phase with a small trace (  $\leq 5\%$  ) of binary phases  $\text{MoS}_2$  and  $\text{Mo}_2\text{S}_3$ . The lattice parameters of these samples well agree with the data in the Fischer's review<sup>2)</sup>. The obtained samples were spark-cut into small pieces of 0.1 mm x 1.0 mm x 7 mm for electrical resistance measurements.

### 3.2. Resistance and Susceptibility Measurements under a Static Field

The measurements of dc electrical resistance of  $\text{Pb}_{1.2-x}\text{Eu}_x\text{Mo}_6\text{S}_8$  were done by conventional four-probe methods. The measurement system in a temperature region from 4.2 K to 300 K is shown in Fig.6. Four copper wires of 0.05 mmD are spot-welded on to the specimen which is mounted on the copper stage with Apiezon N grease. The stage is insulated from the specimen with GE-7031 varnish coating and covered with a copper case to get a homogeneous temperature. The current below 10 mA is supplied by the dc current source ( Keithley model 225 ) to minimize the Joule heating. Temperature is measured by Au-0.07%Fe versus silver junction or germanium thermometer ( GR-200A-1000 ) calibrated by Lake Shore Cryotronics in the temperature region from 1.5 K to 100 K.

Temperature regulation is done by the automatic temperature control system developed in our laboratory.<sup>29)</sup> Heater A is used for heating the specimen, while B is immersed in liquid helium and used for cooling the specimen by evaporating cold helium gas. The difference between the voltage of the thermocouple and the reference is amplified by a microvolt meter ( Okura Electric AM-1001 ) and negatively fed back to the heaters through a heater current controller. According to the magnitude and the sign of the difference voltage, the heater current is controlled up to 500 mA. The temperature can be regulated within  $\pm 0.1$  K at the temperature region from 4.2 K to 200 K. Liquid helium lasts for about 6 ~ 8 hours at one run.

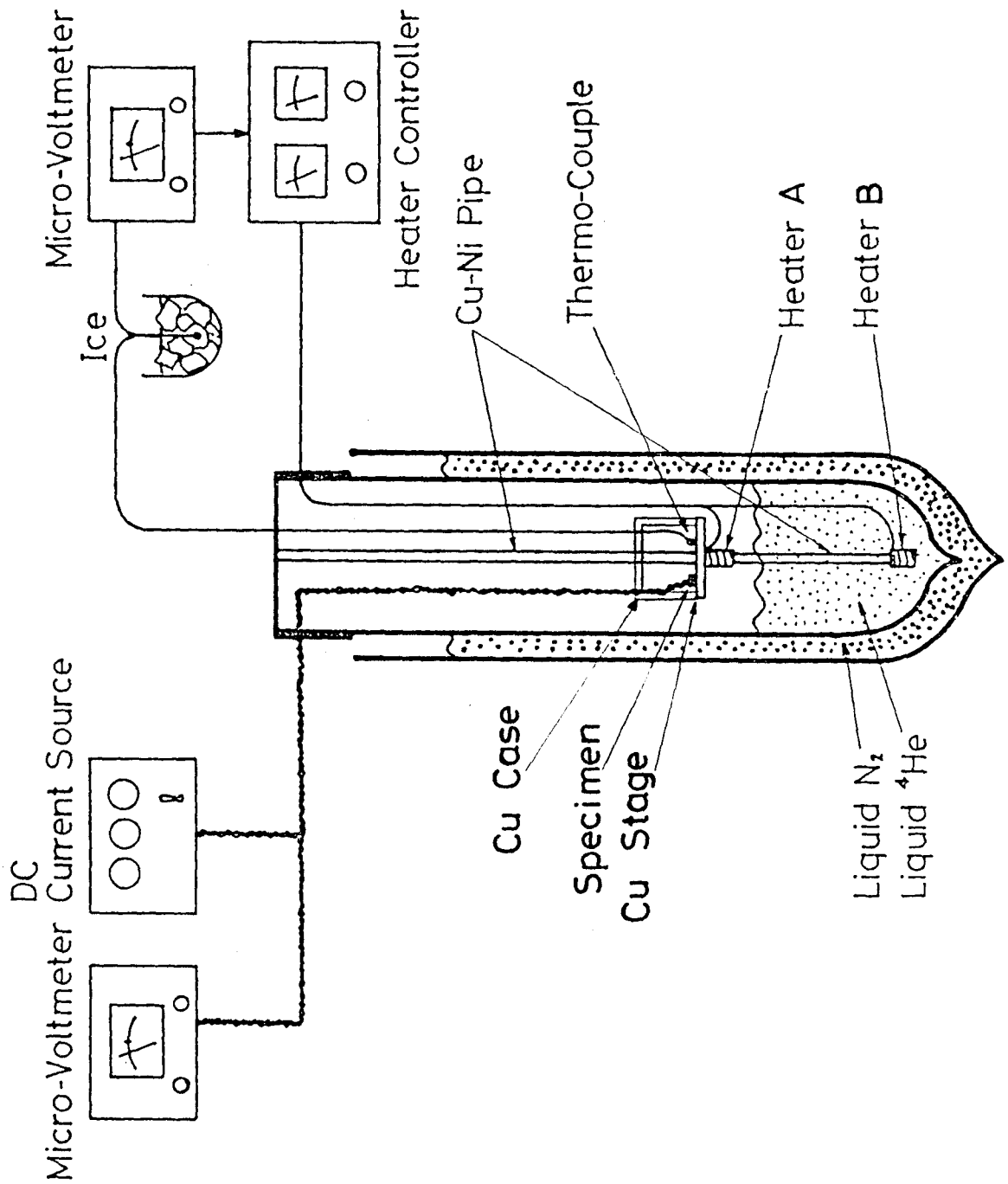


Fig.6 Illustration of resistance measurement system in the temperature range above 4.2 K.

In the measurements of magnetoresistance below 4.2 K a combined  $^3\text{He}$  and adiabatic demagnetization refrigerator was used. Illustration of the measurement system is shown in Fig.7. With slowly pumping of liquid  $^4\text{He}$  by Kenney type rotary pump of 3000 liters/min., the temperature is controlled from 4.2 K to 1.2 K through an exchange gas of about 1 Torr in adiabatic capsule. Around 1.2 K,  $^3\text{He}$  gas is liquified in a  $^3\text{He}$  pot and superconducting magnet A is operated up to about 25 kOe with the persistent current mode. After the exchange gas is evacuated to about  $10^{-6}$  Torr by a diffusion pump, the temperature down to 0.4 K is obtained with pumping of liquid  $^3\text{He}$  by a hermetically sealed rotary pump. Subsequently, the temperature is decreased down to 50 mK by slowly decreasing the magnetic field in the salt pile with decreasing rate of about 1 kOe/min.. The salt pile is made of a bakelite pipe in which about 40 grams of ferric ammonium alum,  $\text{FeNH}_4(\text{SO}_4)_2 \cdot 12\text{H}_2\text{O}$ , and about 2000 urethane coated 0.05 mmD copper wires are stuffed with thermal contact agent Apiezon J oil. Specimen is mounted on the thermal link which is made of about 200 urethane coated 0.05 mmD copper wire bundle to avoid the eddy current heating due to field sweep. Temperature is increased by using the manganin heater of 100  $\Omega$  which is immersed in the pile. Magnetic field up to 30 kOe is applied to the specimen by using superconducting magnet B and the magnetoresistance curve is recorded in X-Y recorder. Applied current to the specimen is suppressed below 1 mA. Automatic resistance bridge (Instruments for Technology Ltd.) and a carbon resistance thermometer which was previously calibrated by measuring CMN (  $\text{Ce}_2\text{Mg}_3(\text{NO}_3)_{12} \cdot 24\text{H}_2\text{O}$  ) susceptibility

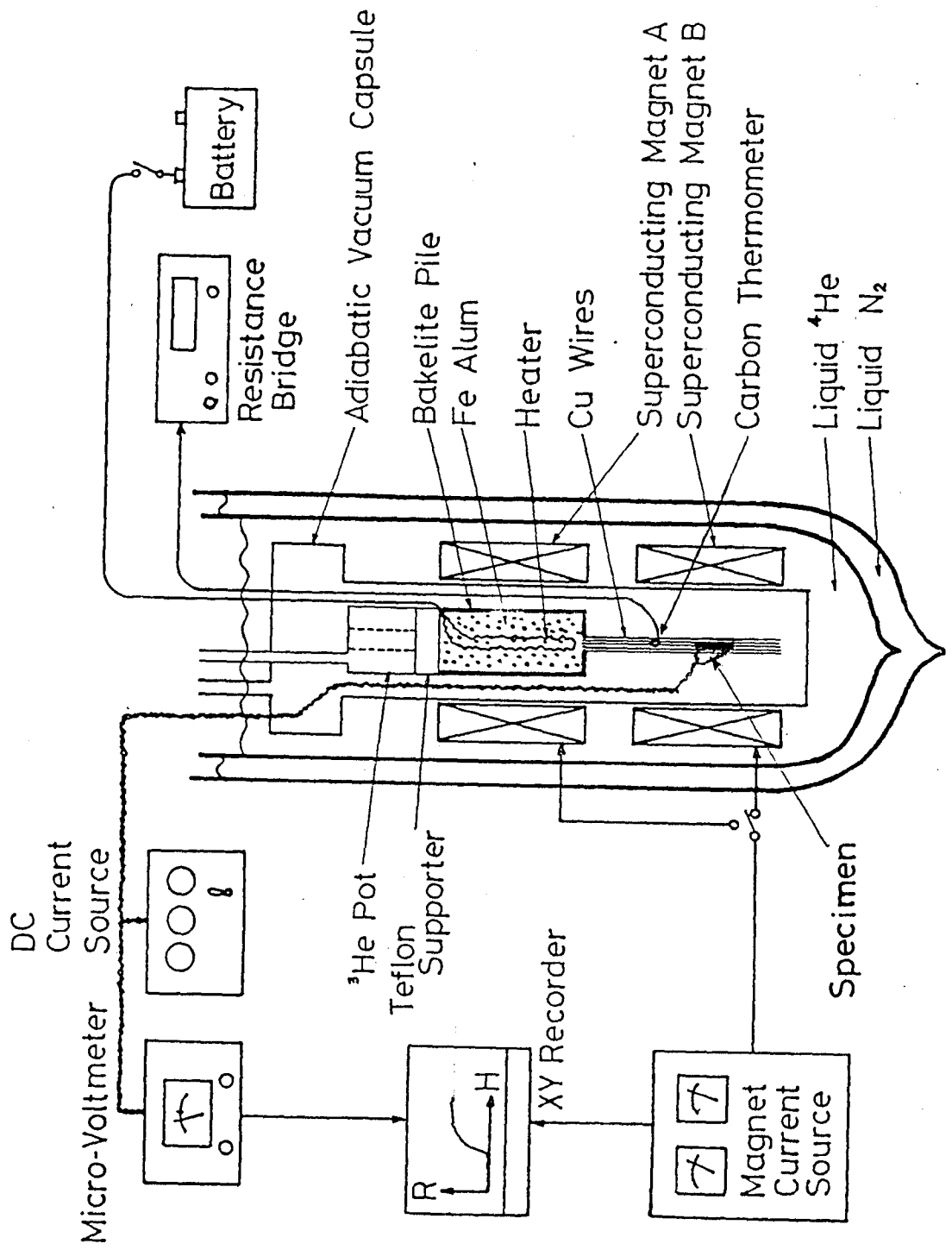


Fig.7 Illustration of magnetoresistance measurement system in the temperature range below 4.2 K.  $^4\text{He}$  and  $^3\text{He}$  gas pumping systems is not shown.

is used for the temperature measurement from 50 mK to 4.2 K.

The temperature dependence of magnetic susceptibility for Eu doped samples was measured in the temperature region from 1.5 K to 300 K by using the Farady type magnetometers ( CAHN 2000 ELECTRO-BALANCE ). Fig.8 shows illustration of the susceptibility measurement system. The balance system is set in a vacuum capsule with He exchange gas about 1 Torr. Sample in quartz basket is set at the position of maximum field gradient which was previously researched by the Hall magnetic sensor. With applying magnetic field, the sample is magnetized and the magnitude is measured by the electro-balance as the change of the magnetic force. After the correction for the blank data without the sample, the susceptibility of the sample is determined in comparison with the value of Mohr salt (  $\text{FeSO}_4(\text{NH}_4)_2\text{SO}_4 \cdot 6\text{H}_2\text{O}$ ;  $\chi_g = (31.22 \pm 0.32) \times 10^{-6}$  emu/g at 300 K ) as a standard sample. Temperature measurement and control system is the same as mentioned before.



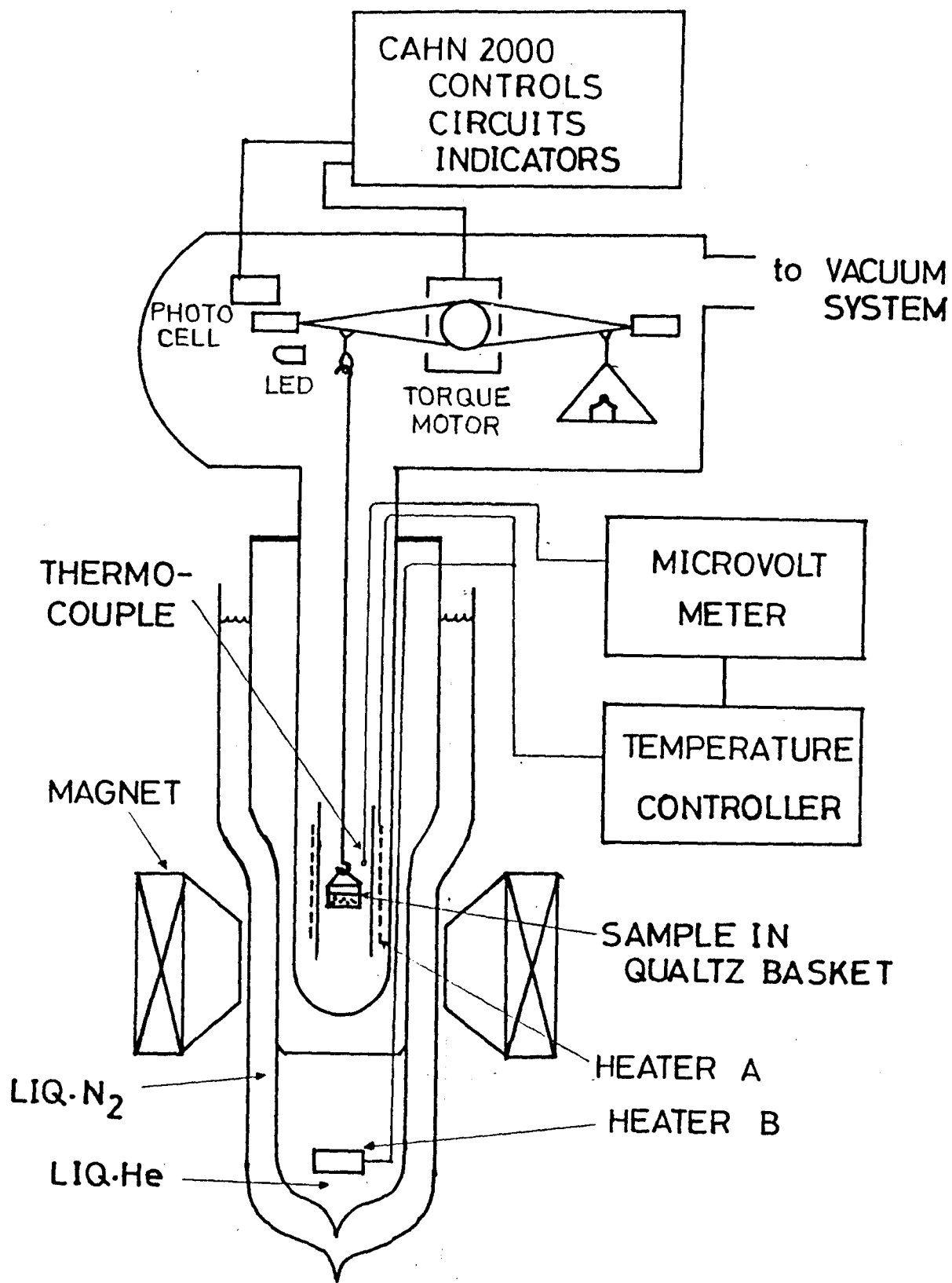


FIG.8 Illustration of magnetic susceptibility measurement system

### 3.3. High Field Magnetoresistance and Magnetization Measurements

High field magnetoresistance and magnetization measurements were done in High Field Laboratory of Osaka University.<sup>26)</sup> The laboratory has three capacitor bank systems; D-1 with 250 kJ, D-2 with 1250 kJ and D-3 with 50 kJ energy source and three types of the magnet are available for practical use; two-layer magnet 150(2L)20 for 700 kOe in 20 mm bore with pulse duration 0.4 ms, single-layer magnet with large bore 150(1L)60 for 500 kOe in 60 mm bore with pulse duration 0.35 ms and single-layer magnet 100(1L)34 for 500 kOe in 34 mm bore with pulse duration 0.3 ms. Our measurements were mainly done by two-layer magnet and large-bore magnet which are driven by the D-2 bank.

The electrical circuit of the D-2 bank system is shown in Fig.9. Discharge of the capacitor bank is attained by closing a pressurized spark-gap switch  $G_1$ . The same type switch  $G_2$  is used as a crowbar or diversion switch. Triggering pulse with small amplitude from pulse generators are amplified to trigger the main spark-gap switches  $G_1$  and  $G_2$  with small jitter time by passing through the two or three stages of spark-gap switch systems. In parallel with  $G_1$ , a mechanical switch MS is connected which should be operated with the charging voltage of the bank below 4 kV where the spark-gap switch does not operate effectively.

The cross-sectional view of the two-layer magnet 150(2L)20 is shown in Fig.10. The inner-layer coil a and outer-layer coil b are made of the maraging steel which is well known as one of the strongest steel ( hardness  $H_v \sim 700$ , yield strength  $> 200 \text{ kg/mm}^2$  ).

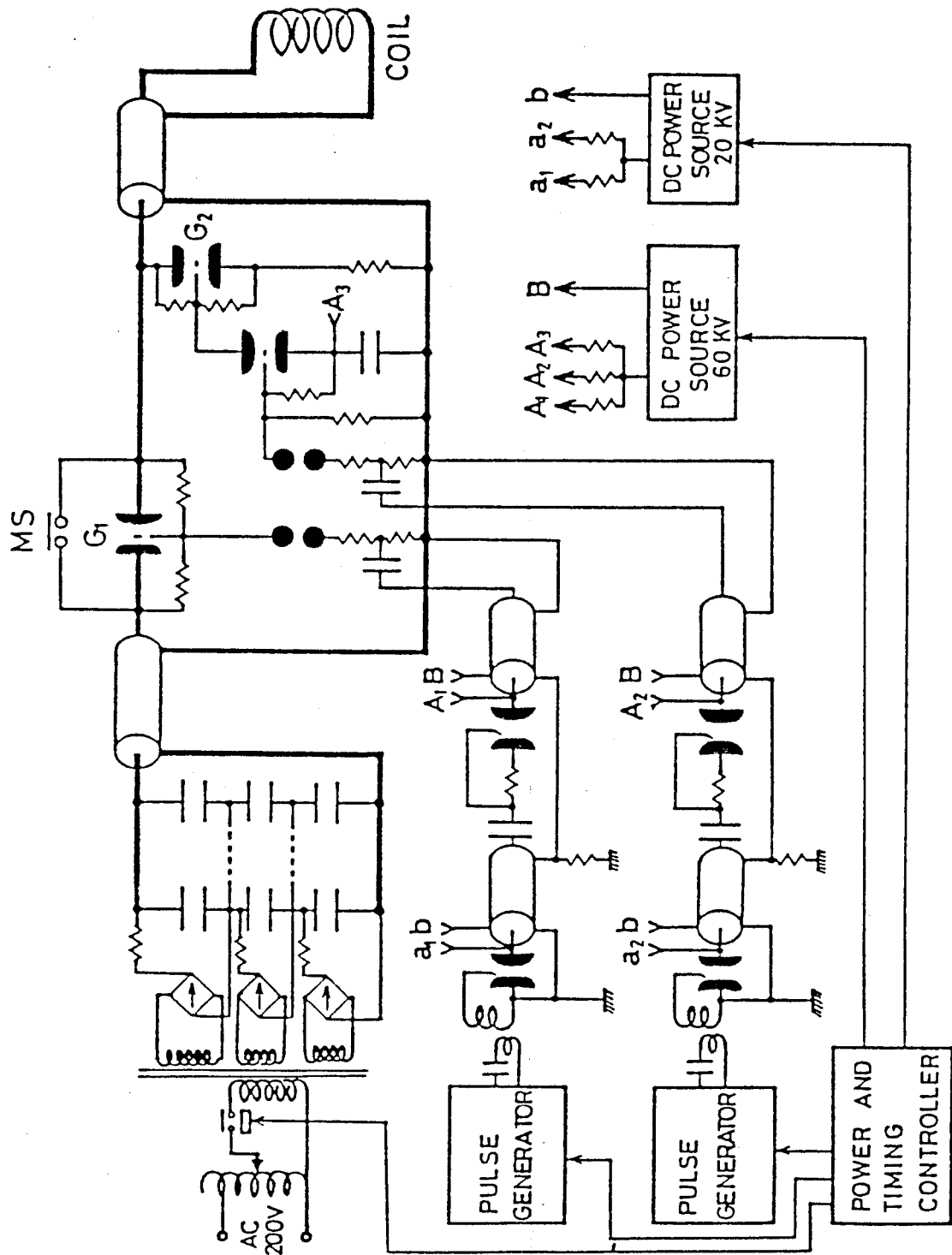


FIG.9 Electric circuit for the D-2 capacitor bank system.  $G_1$  and  $G_2$  are the pressurized air-gap switches and MS is the mechanical switch which is used in the range of low charging voltage ( $<4$  kV). The spark-gap switch  $G_1$  and  $G_2$  work effectively in the voltage range higher than 6 kV.

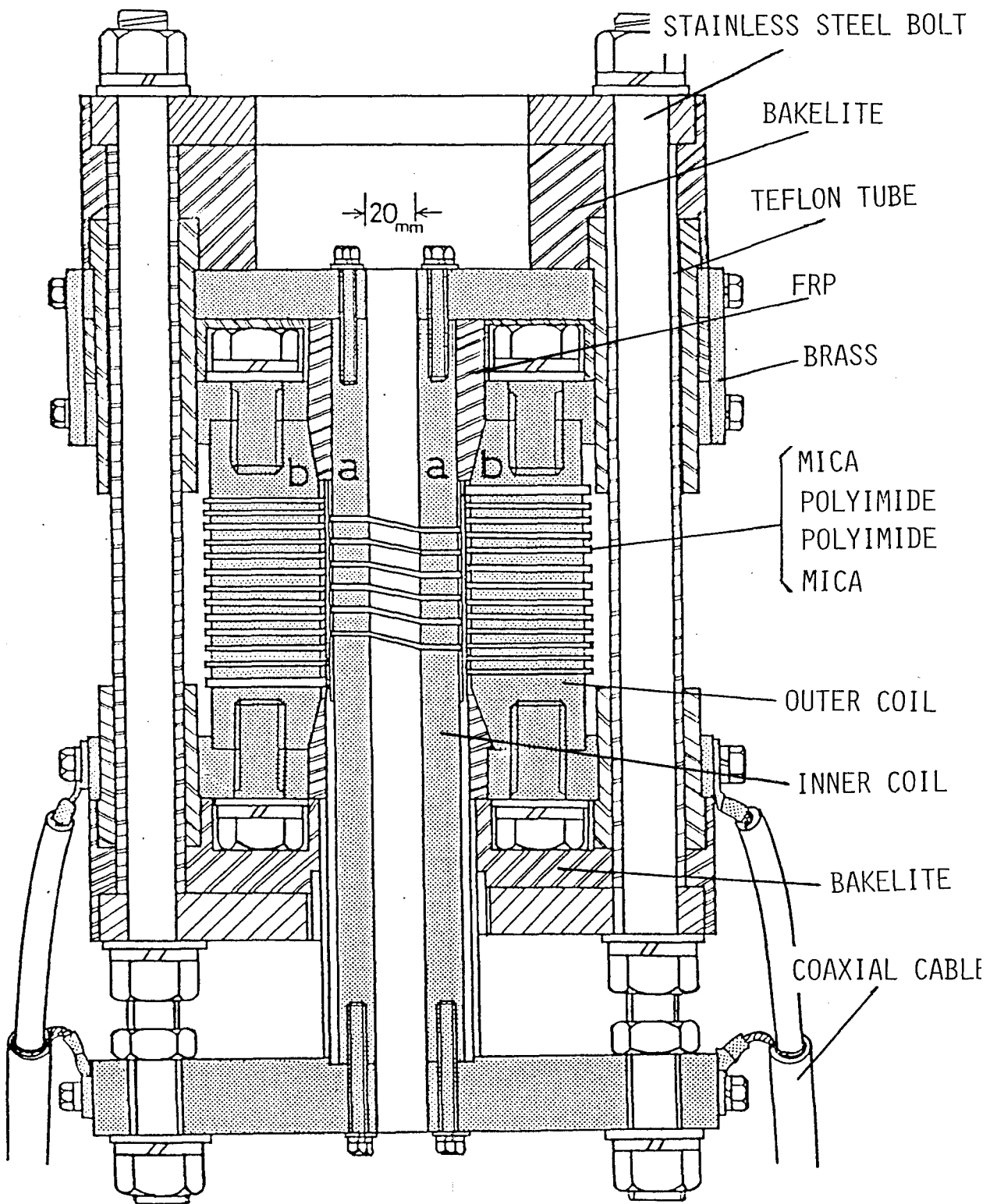


Fig.10 Cross-sectional view of the two-layer magnet.

They are connected electrically in series and pulsed current flows through the shadowed area of the magnet. Combinations of mica sheets and polyimide laminates are used for the insulation between the windings of the coil. They are strong enough against heat, compressive force and high voltage. Other insulators used to construct a magnet is shown in the figure. During experiments the magnet is covered with a thick iron hood to avoid unexpected accidents. A dewar with a sample is inserted into the magnet through a hole at the top of the hood.

The method of magnetoresistance measurement is basically the same as the dc four probe method. A block diagram for the  $Hc_2$  measurements is shown in Fig.11. In order to avoid excess Joule heating, a square-pulsed current  $I \leq 100$  mA which has a pulse width adjusted so as to cover that of magnetic field is used. The square-pulsed current and the magnetic field are applied to the specimen by operating a pulse generator. The output signal voltage and a trace of field are recorded in a digital recorder ( IWATSU, DM-901 ) through a dc amplifier and integrator, respectively. The recorder consists of 8-bit AD converter and 1024 x 2 words digital memory and it can record transient events with a minimum time resolution of 10 ns. The magnetoresistance curve, R versus H, is displayed on a X-Y recorder or an oscilloscope through a microcomputer ( IWATSU Data Processor SM-1330 ). A field trace is obtained by a field pick-up coil and the magnitude was previously calibrated at 283 kOe by submillimeter ESR of paramagnetic  $CuCl_2 \cdot 2H_2O$ <sup>30)</sup>. A stray signal induced by the flux change in the four probe circuit under the transient field is cancelled by using a compensation coil and



a bridge balance. The specimen is mounted on a tip of a bakelite rod for the measurement below 4.2 K and a sapphire holder for the measurement under temperature control above 4.2 K, respectively. An ohmic contact between the leading wires and the specimen is done effectively by the conductive adhesive ( DUPONT SILVER #4817 ). Copper wires of 0.05 mmD used for the current and signal leads of the specimen should be twisted well so as not to pick up the flux of the transient field.

Usually, the measurements are done by applying two shot of pulse field. The second shot is for the measurement with the opposite current direction to the first one. A final reduction of the background noise is done by making a subtraction between two data with the Data Processor. An example of data processing is shown in Fig.12. The specimen is  $\text{Pb}_{0.8}\text{Eu}_{0.4}\text{Mo}_6\text{S}_8$  and the measurement was done at 4.2 K by using two-layer magnet. (a) is a field trace obtained by integrating a pick-up voltage and the maximum field is 498.6 kOe. Two signals (b) and (c) are obtained by applying two shots of pulse field with the opposite current direction to a specimen, each other. The magnetoresistance signal (d) which is corrected for the background noise by calculating  $[(b)-(c)]/2$  with the Data Processor showed a complete transition between superconducting and normal state.

The method of temperature regulation is shown in Fig.13. Principle of the automatic temperature control system is the same as mentioned before. In order to contain the whole assembly for heating or cooling, a large bore magnet is needed. The magnet 150(1L)60 permits insertion of a 26 mmID glass dewar which is

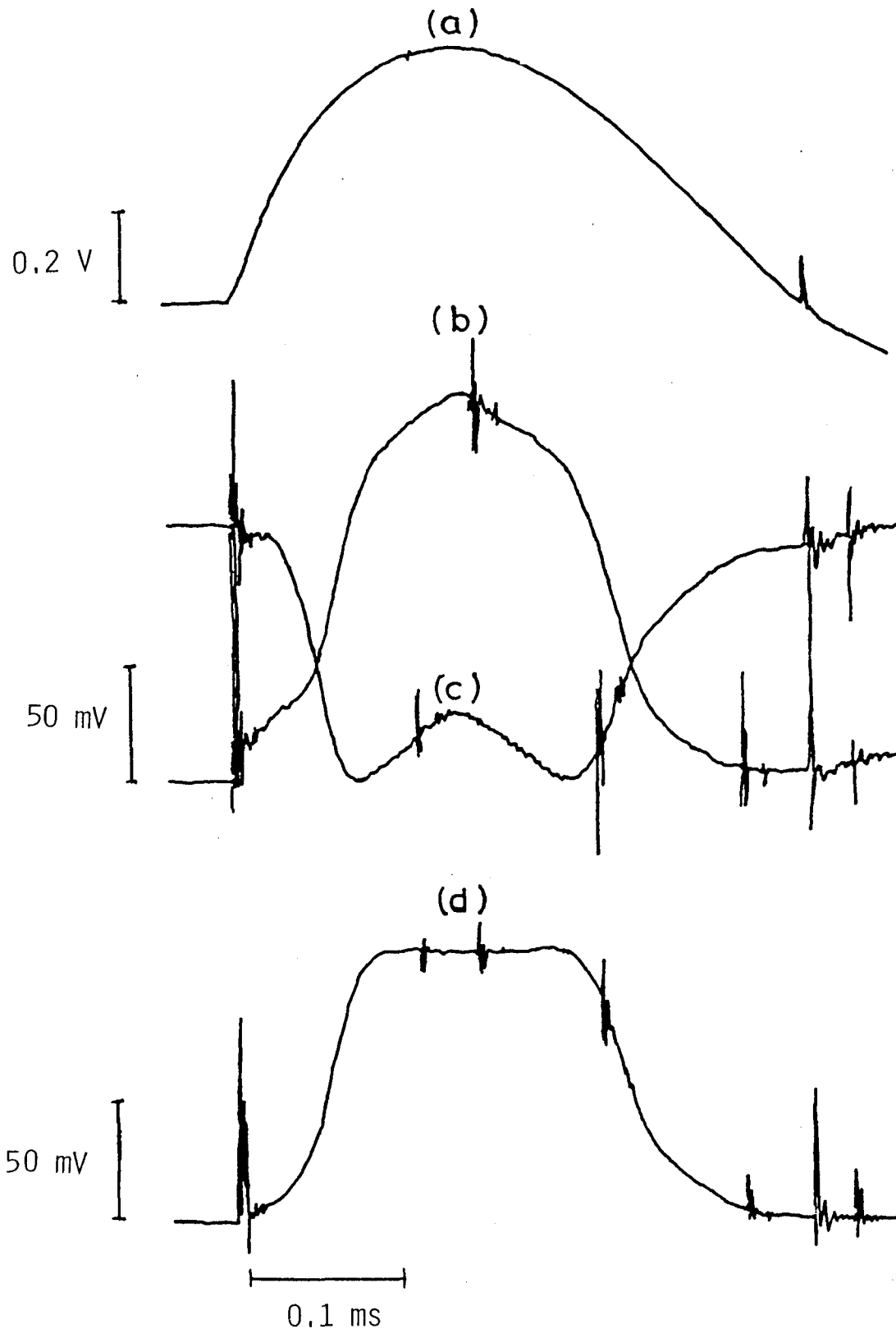


FIG.12 Example of data processing on  $\text{Pb}_{0.8}\text{Eu}_{0.4}\text{Mo}_6\text{S}_8$ . (a) is a trace of magnetic field. Two signals (b) and (c) are obtained by applying two shots of pulsed field with opposite current direction to a specimen. Background reduced signal (d) is obtained by calculating  $[(b)-(c)]/2$  at the Data Processor.



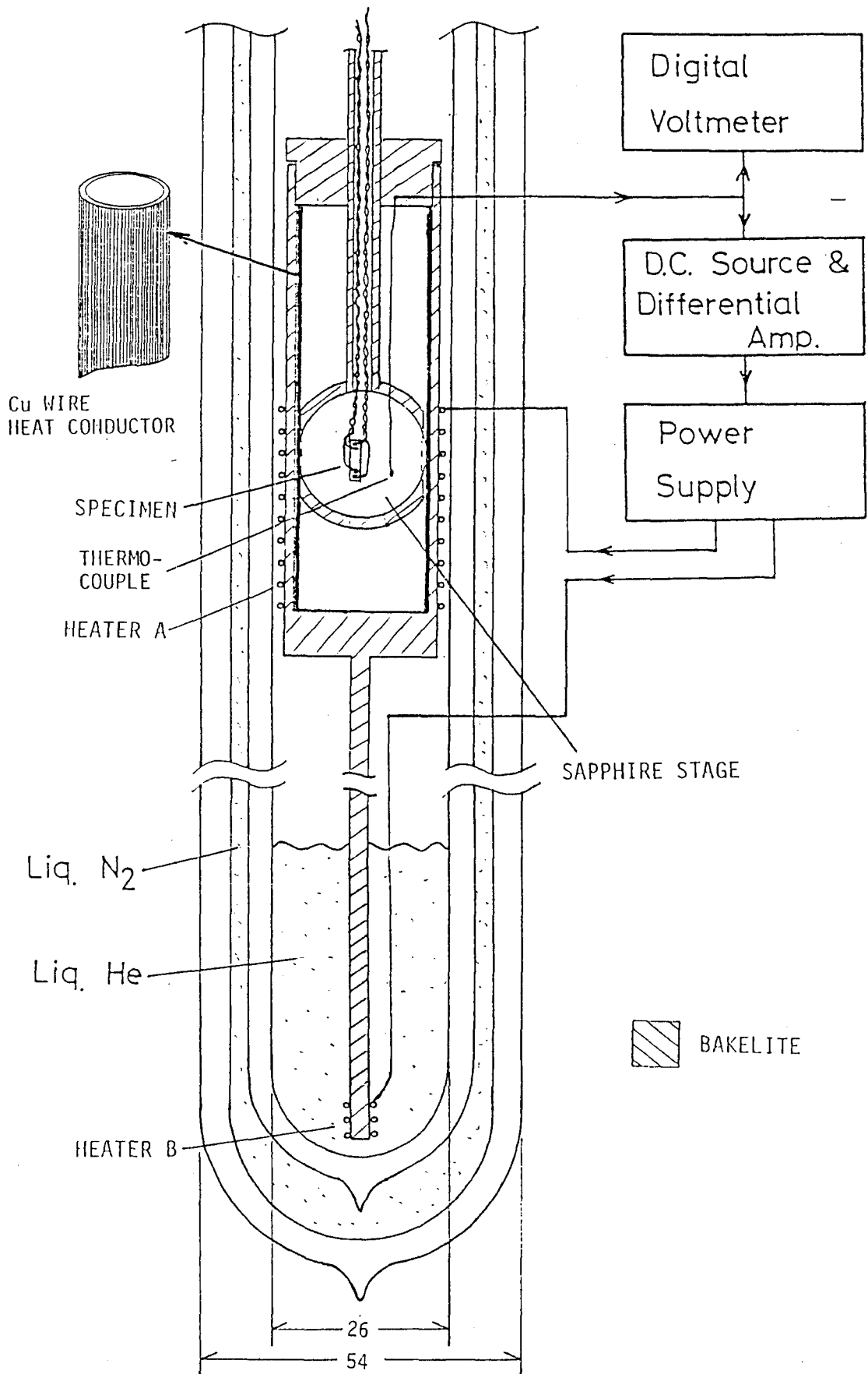


Fig.13 Illustration of the temperature control system for magnetoresistance measurements under pulsed field.

specially designed to contain liquid helium of about 120 cc below a specimen for cooling it and to have a large space for the temperature control assembly. Usual silver coating is done with slits of 10 mm on the dewar sides and it is found to have no problem on the field penetration or flux compensation of the pick-up coil. In the measurements under pulsed field, there exists one technical difficulty that bulk metallic materials cannot be used in the cryostat because of skin effect or Joule heating. As is shown in Fig.13, a specimen and a sapphire stage are contained in a thermal insulation cell. The specimen is mounted on the stage with Apiezon N grease and the thermocouple is attached close to it with GE-7031 varnish. The stage is made of a single crystal sapphire disc of 3 mm thick and 20 mm in diameter. The sapphire has good thermal conductivity which is comparable with that of metallic copper below 100 K, so that it is very useful insulating material for the present purpose. The cell is made of bakelite with 1.5 mm thick. An inside of the cell is covered with about 1200 urethane-coated 0.05 mmD copper wires, which is effective to get a homogeneous temperature under the transient field. By this arrangement uniformity of temperature around the specimen and thermometer can be obtained satisfactorily.

There are several cares in  $H_{c2}$  measurements under a transient magnetic field as follows; skin effect, eddy current, flux-flow and magnetocaloric effect. The sample thickness used in the measurements is 0.1 ~ 0.02 mm which is thin enough compared with the skin depth,  $\delta \approx 10$  mm, for the present compounds. The heating due to eddy current sometimes induces a hysteresis loop on the magnetoresistance curve. This effect is erased by thinning the sample down to about

0.1 mm.<sup>31)</sup> In order to minimize the flux-flow resistance the magnetic field is applied along the current direction. The surface effects such as  $H_{c3}$ , which is important in the measurements for a single crystal with clean surfaces, are negligible for the present sintered samples with many imperfections and voids<sup>32)</sup>. Special care must be taken for the magnetocaloric effect, on the other hand, because it is thermodynamically intrinsic. The effect which is the heating or cooling due to the adiabatic magnetization or demagnetization of Eu spins under transient magnetic field is not negligible in above material size when the Eu concentration  $x$  is higher than  $0.5 \sim 0.6$ . Fig.14 shows the magnetoresistance measurements for  $Pb_{0.6}Gd_{0.6}Mo_6S_8$  with various sample thickness and applied current to estimate the temperature change due to magnetocaloric effect. The sample is appropriate for the measurement because of its low  $H_{c2}$  ( $\sim 70$  kOe) and high Gd concentration. In the case of (a) where applied current and the sample thickness are 157 mA and 0.5 mm, respectively, the magnetoresistance curve shows the hysteresis due to Joule heating at the normal state under the magnetic field. In order to avoid Joule heating and skin effect the current is controlled below 50 mA and the sample is thinned below 0.1 mm. In the case of (b) the magnetoresistance curve on decreasing field is shifted to higher than that on increasing field. This is due to magnetocaloric effect. In order to reduce the effect a much thinner specimen is required to keep a much better heat contact with  $^4He$  heat bath. The magnetoresistance curve obtained in this way is shown in (c). Magnetocaloric effect is still remained but rather reduced and the temperature change is estimated about 0.2 K. In

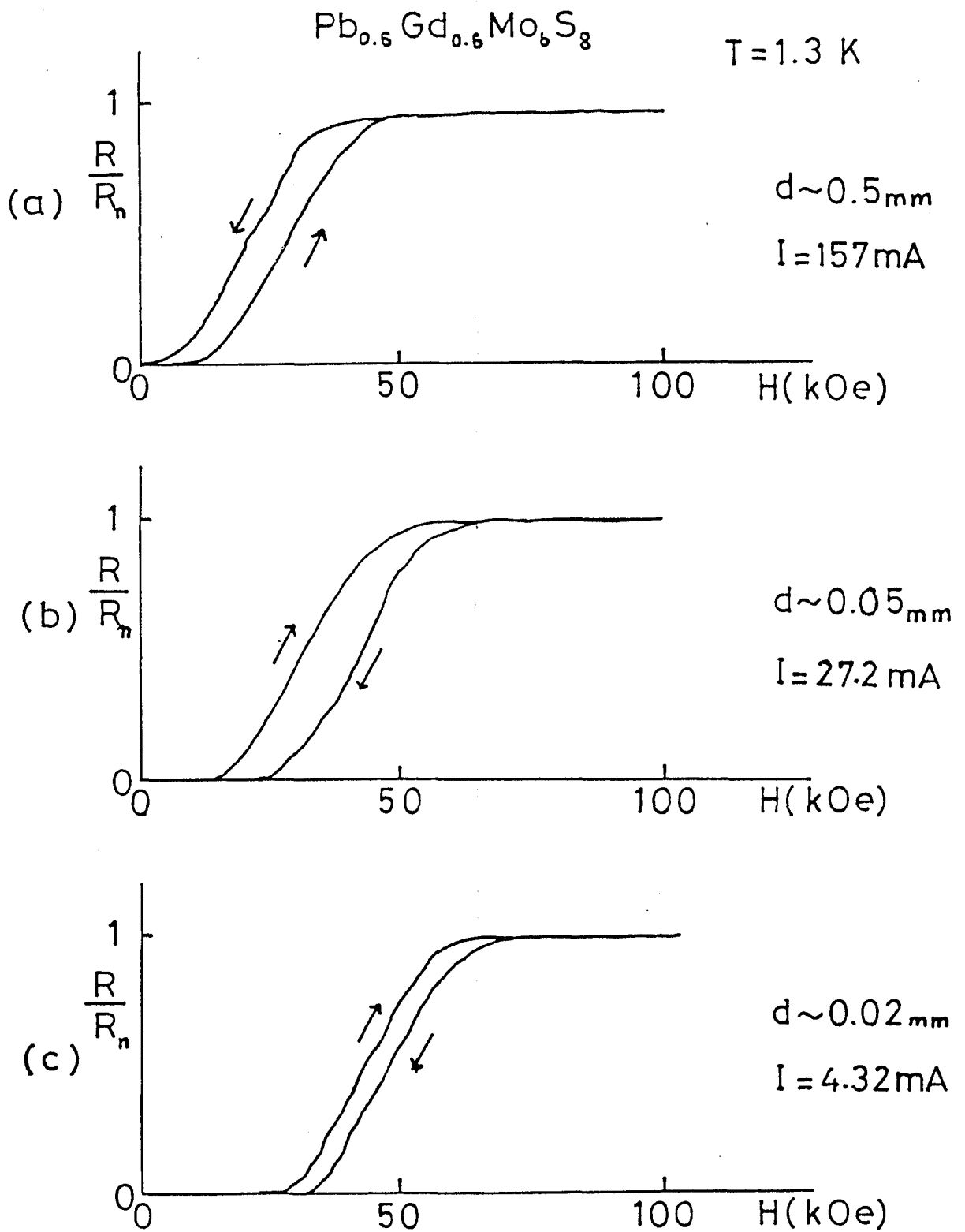


FIG.14 Magnetoresistance curves of  $\text{Pb}_{0.6}\text{Gd}_{0.6}\text{Mo}_6\text{S}_8$  with various sample thickness and applied current.  $R_n$  is the normal resistance well above  $H_{c2}$ .

the  $H_{c2}$  measurements of  $Pb_{1.2-x}Eu_xMo_6S_8$  for  $x \geq 0.5$ , the sample with 0.02 mm thick is used and the temperature change is suppressed down to 0.2 K.

The magnetization measurement is done by using a balanced pick-up coil.<sup>33)</sup> The technically important point is how to compensate background flux change due to a transient field, which is usually  $10^4 \sim 10^6$  times larger than the flux change due to the magnetization of the specimen. This is usually done by setting three coils as are shown schematically in Fig.15(a). Coil A picks up the magnetic flux change of the specimen while coil B is wound in the opposite direction to A in order to compensate the background flux change. Fine adjustment is done by one loop coil C taking a bridge balance as is shown in the figure.

Fig.15(b) is the cut view of the standard pick-up coil which has been used in our laboratory. Considering the field duration and frequency response, coil a is wound with 100 turns. The coil B is coaxially wound on a with 50 turns oppositely. The cross section of coil B is twice as large as that of A so as to make the net flux in A equal to that in B. Fine adjustment coil C is wound on B. The coil wire material is urethane-coated 2 % tin-doped copper of 0.1 mmD. The wire has large residual resistivity (  $2.5 \mu\Omega\text{cm}$  ) and is effective to improve the flux compensation especially at liquid helium temperature. The standard pick-up coil attains a flux compensation of  $10^{-4} \sim 10^{-5}$  at the signal output of the bridge balance circuit.

Fig.16 is a block diagram of the system where a cut view of a cryostat is also shown schematically. Three signal outputs of

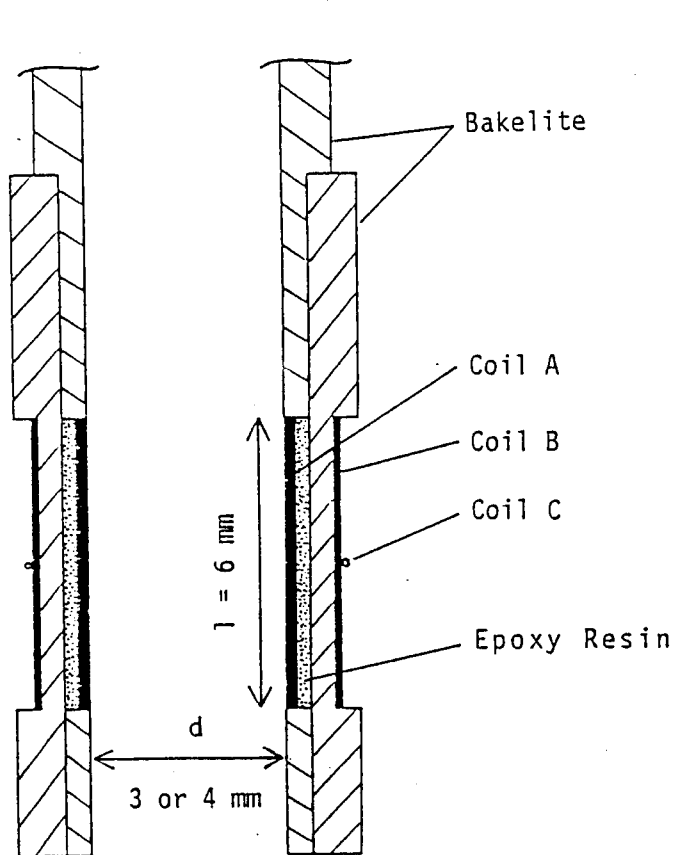
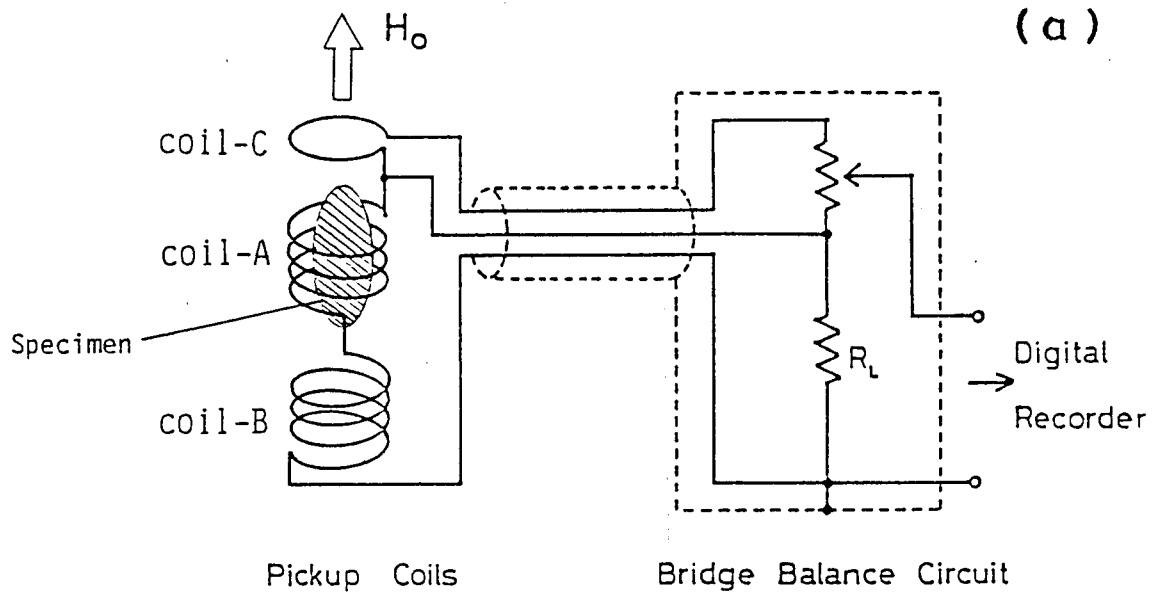
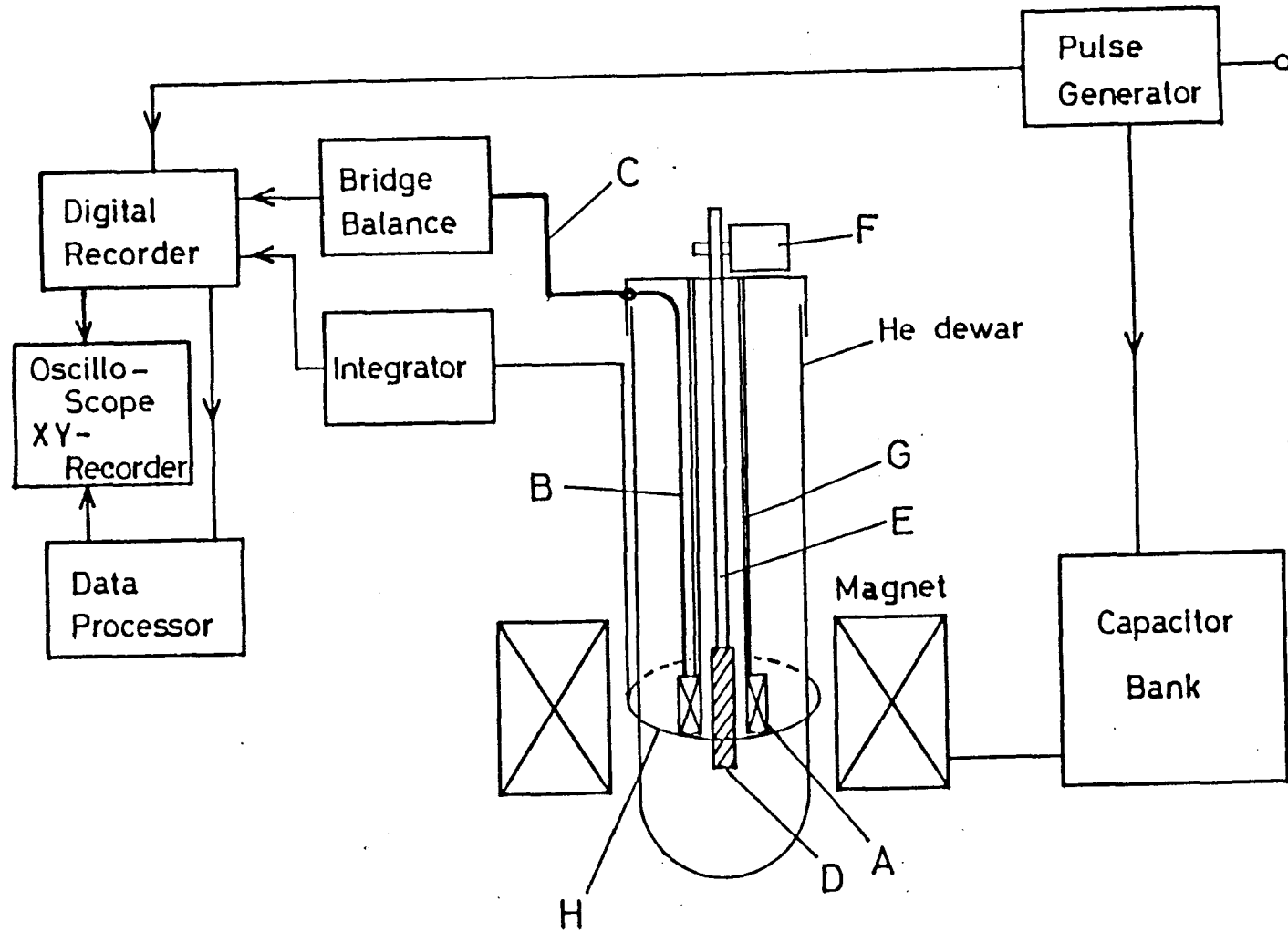


Fig.15 (a): Method of flux compensation. (b): Cut view of standard pick-up coil.

Fig.16 Block diagram of magnetization measurement system.



- |                   |                  |
|-------------------|------------------|
| A: Pick up Coil   | E: Glass Rod     |
| B: Cu Capillary   | F: Motor Drive   |
| C: Shielded Cable | G: Quartz Pipe   |
| D: Specimen       | H: Field Pick up |

the pick-up coil (A) are shielded by a copper capillary (B) in the cryostat and are connected to double shield cable (C) and transmitted to the bridge balance circuit. The balance signal is then stored in a digital recorder ( IWATSU, DM-901 ). Usual measurements are done at the time resolution of 200 ~ 500 ns. A specimen (D) is mounted on the tip of glass rod (E) by a teflon tube and driven by a miniature motor (F) for insertion and adjustment at the right position. Usually, a specimen whose length is 10 ~ 15 mm and diameter of 2.5 ~ 3.2 mm is used. The pick-up coil is found to be very sensitive to the axial displacement so that it is suspended by a quartz pipe (G) that has small coefficient of thermal expansion. A magnetic field is monitored by a single loop field pick-up coil (H). The output signal which is proportional to  $dH/dt$  is integrated by a high speed operational amplifier and also stored in the digital recorder. The time constant of the integrator is taken as 300 times longer than the field duration time.

The output signal of the bridge balance circuit is proportional to  $dM/dt$  but still contains background noise. Further noise reduction is done by Data Processor SM-1330, IWATSU. Using two shots of pulsed field generation, two sets of data with and without the specimen are taken. These are transferred to the Data Processor, where the subtraction of the background and the integration of  $dM/dt$  are done. The Data Processor enables one to analyze and check the data immediately and improves the efficiency of the experiment greatly. In this manner, sufficiently high sensitive measurement can be done under the final effective flux compensation of  $10^{-6}$ . This corresponds to the sensitivity of  $5 \times 10^{-6}$  emu/cc



in a susceptibility measurement.

The calibration of magnetization value is done by single crystalline  $\text{CuCl}_2 \cdot 2\text{H}_2\text{O}$  or  $\text{MnF}_2$ <sup>34)</sup> as the standard specimen. An integrated output signal is proportional to a magnetization, cross sectional area and demagnetization correction factor of a specimen. Magnetization value is determined by comparing these values with those of the standard specimen. So, the accuracy of the measurement depends on these geometrical conditions of the specimen.

The high field magnetization below 1 K was measured by introducing a conventional single-shot type  $^3\text{He}$  cryostat in the large-bore-magnet system.<sup>35)</sup> Cut view of the cryostat with the magnet location is illustrated in Fig.17. Dewar vessels, exchange gas chamber and liquid  $^3\text{He}$  chamber are made of glass to avoid the skin effect and eddy current heating due to the pulsed field. They are silvered along the inside wall with two vertical slits of 5 mm wide. The slits are necessary to cut the current loop along the wall though they cause heat inflow of about 100  $\mu\text{W}$  to the liquid  $^3\text{He}$  due to the radiation. As shown in Fig.17(A), the sample is mounted on the end of teflon rod of 3 mmD with a teflon holder. The bakelite bobbin on which the pick-up coils are wound is supported by a bakelite pipe and separated from the  $^3\text{He}$  chamber. The pipe is connected to the bottom of the exchange gas chamber. Gas handling system is similar to that of conventional  $^3\text{He}$  cryostat. Temperature of  $^3\text{He}$  bath is controlled by regulating the vapor pressure which is measured by the McLeod gauge. The measurement system for magnetization is the same as mentioned above. Experiment can be done for 3 hours under usual conditions.

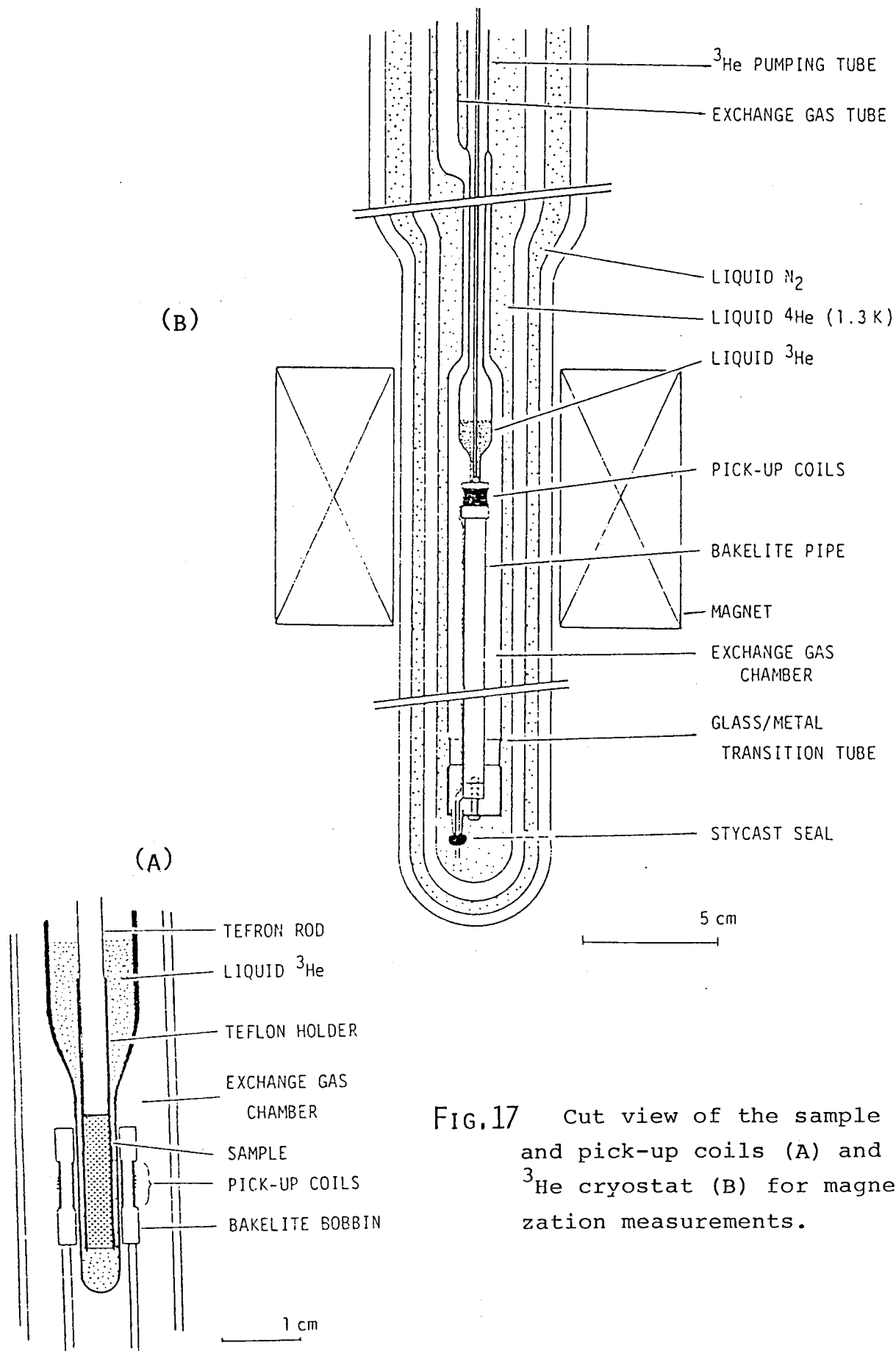


FIG.17 Cut view of the sample and pick-up coils (A) and  $^3\text{He}$  cryostat (B) for magnetization measurements.

## § 4. RESULTS AND DISCUSSIONS

### 4.1. Superconducting and Structural Phase Transitions

Typical results on the temperature dependent resistance of  $\text{Pb}_{1.2-x}\text{Eu}_x\text{Mo}_6\text{S}_8$  are shown in Fig.18. The resistance for low Eu concentrations ( $x \leq 0.6$ ) decreases monotonically with decreasing temperature and becomes superconducting at  $T_c$ . The resistance for Eu rich samples ( $x \geq 0.8$ ), on the other hand, shows anomalous behavior at low temperatures: for  $x = 1.2$  and  $1.0$  it increases sharply below 100 K with decreasing temperature, showing a qualitative agreement with the data obtained by Maple et al.<sup>36)</sup>

Fig.19 shows details of the resistance for  $\text{Eu}_{1.2}\text{Mo}_6\text{S}_8$  around the temperature where the resistance anomaly appears. As is seen in the figure, a clear hysteresis is found and the greatest change in slope, found by the intercept of two tangential lines, takes place at  $T_s = 110 \pm 10$  K. This temperature coincides with that for the structural transformation from the high temperature rhombohedral structure to the low temperature triclinic distortion<sup>37)</sup>. Thus we identify  $T_s$  in Fig.19 as a structural transformation temperature.

To analyze an anomalous increase of the resistance at low temperatures for Eu rich samples, we plot a logarithmic resistance as a function of inverse temperature, i.e.  $\log R$  versus  $1/T$ , in Fig.20. Two linear regions, a steep linear increase just below  $T_s$  and a weakly temperature dependent region at low temperatures, are found in the figure for each composition with  $x = 1.2, 1.0$  and  $0.8$ .

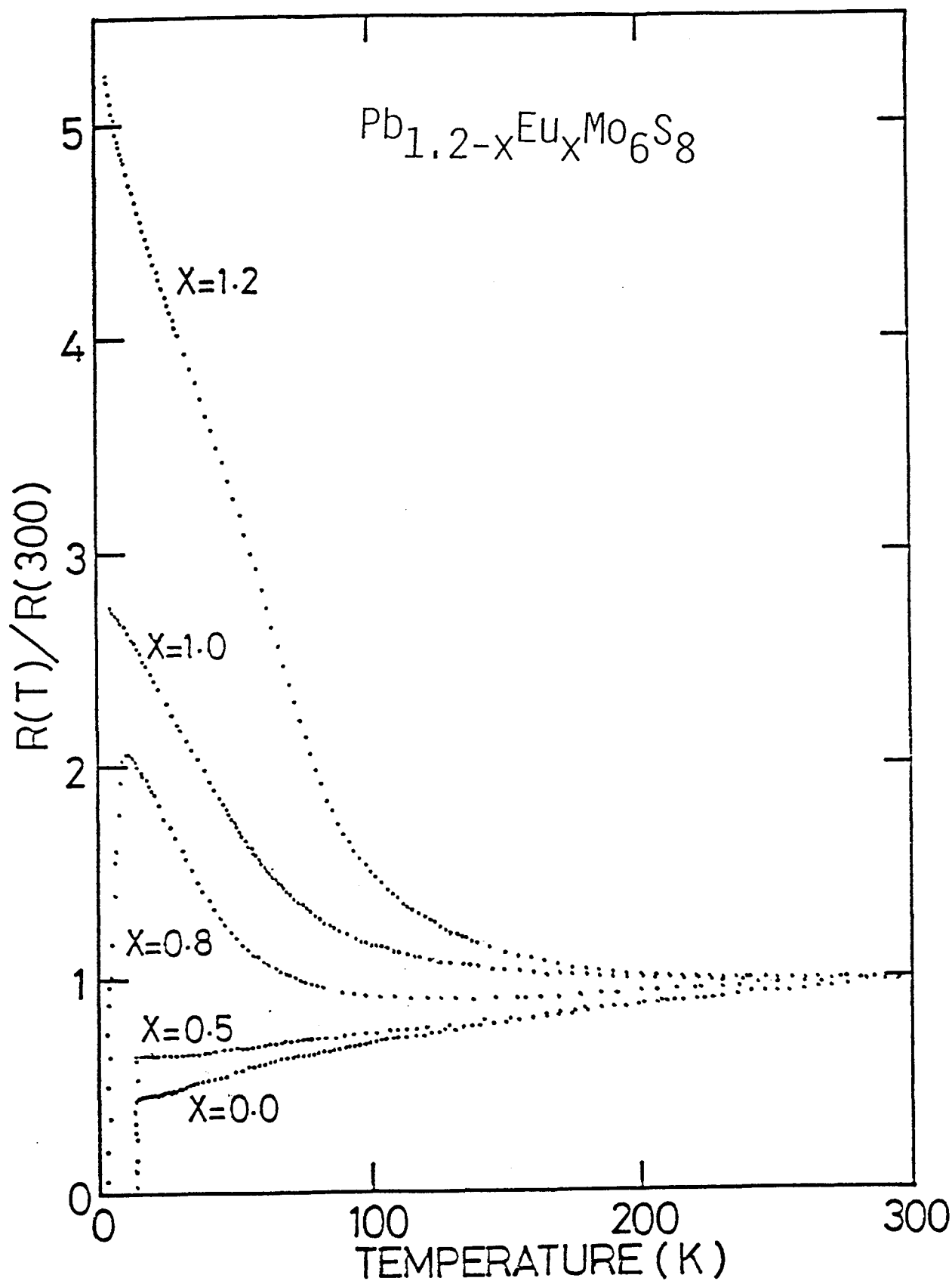


FIG.18 Temperature dependence of electrical resistance in  $\text{Pb}_{1.2-x}\text{Eu}_x\text{Mo}_6\text{S}_8$ . The resistance is normalized by the room temperature value.

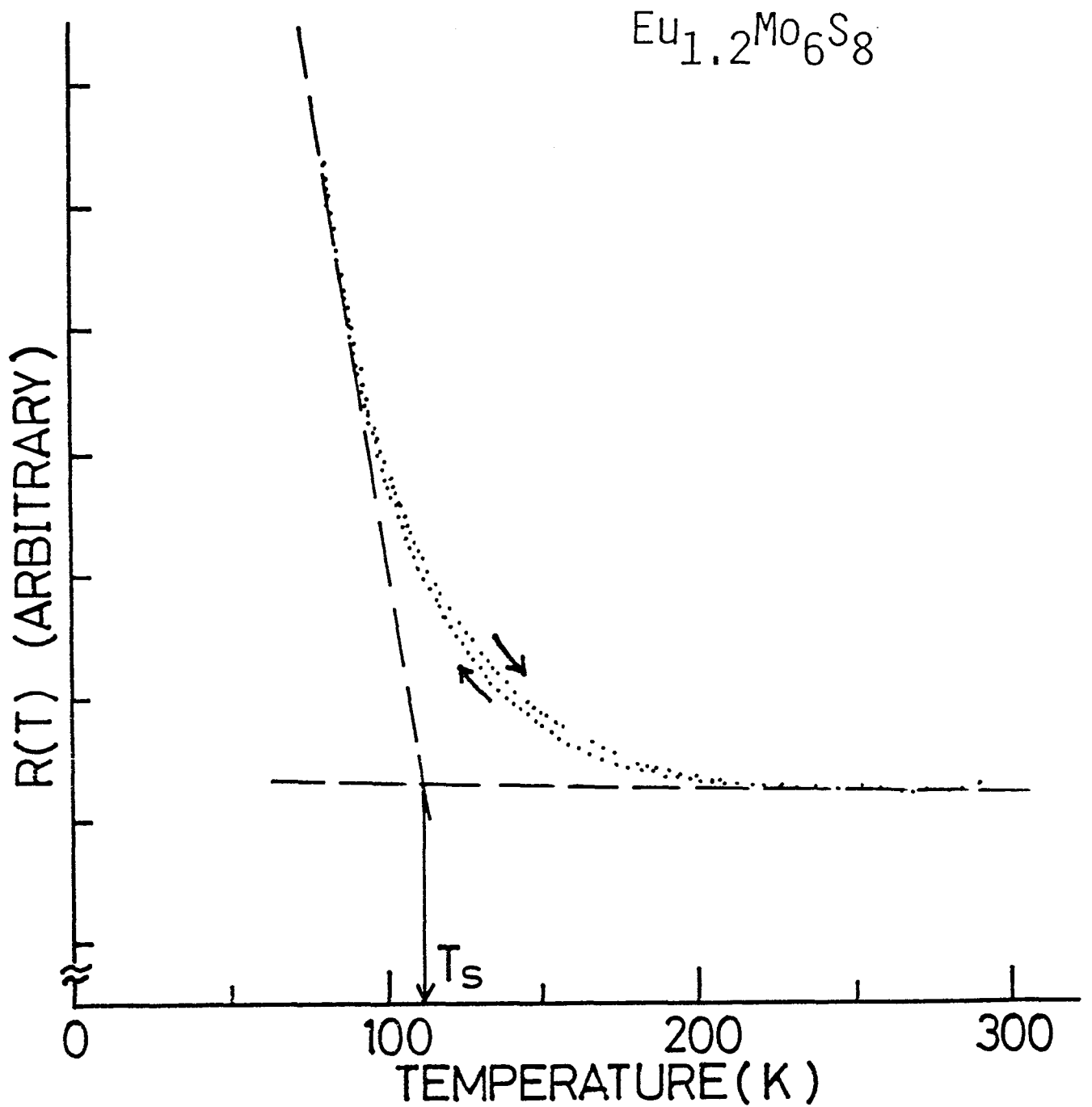


FIG.19 Temperature dependence of the electrical resistance around the structural transformation temperature  $T_s$  in  $\text{Eu}_{1.2}\text{Mo}_6\text{S}_8$ .

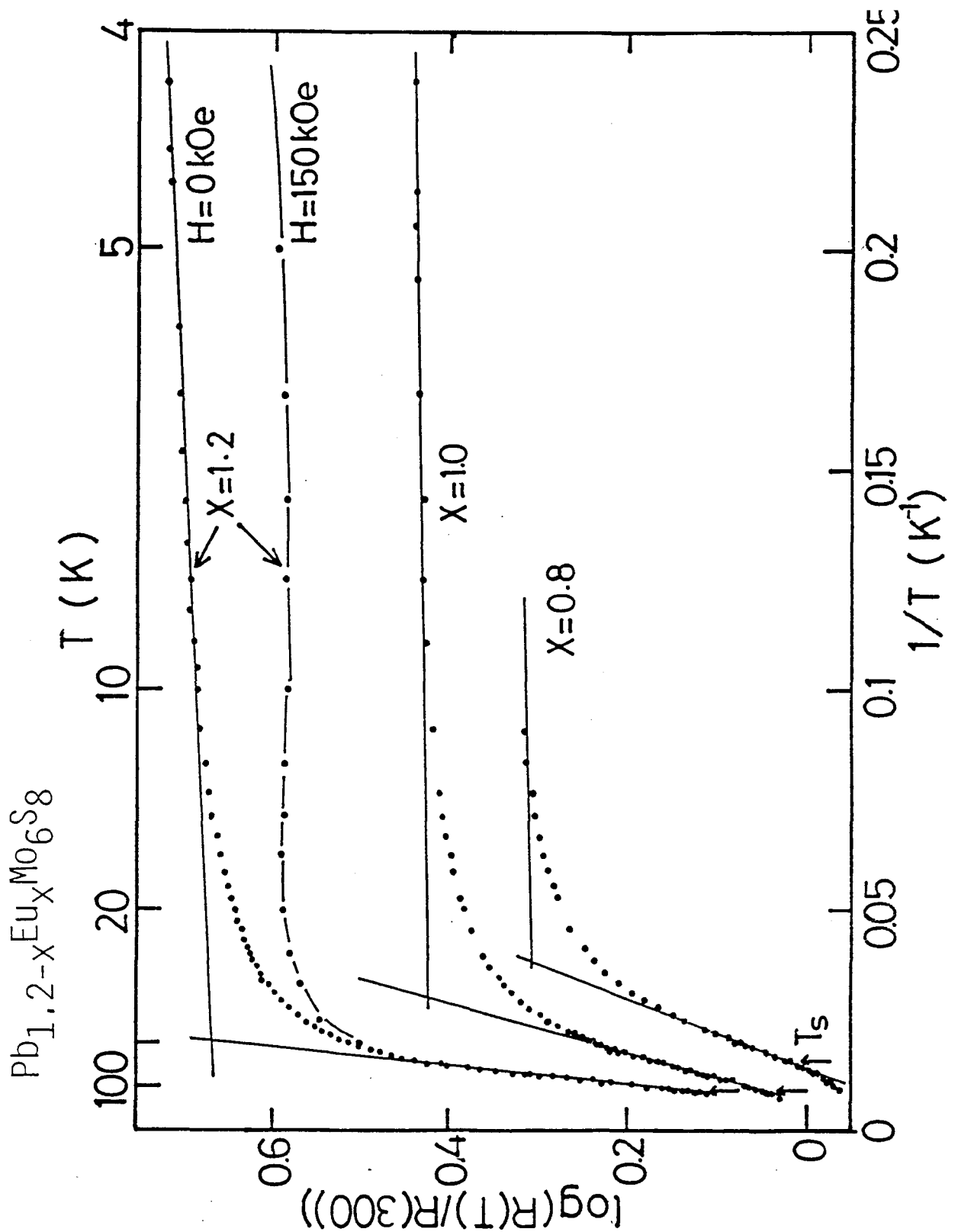


FIG.20 Logarithmic resistance  $\log[R(T)/R(300)]$  as a function of  $1/T$  for  $\text{Pb}_{1.2-x}\text{Eu}_x\text{Mo}_6\text{S}_8$  with  $x \geq 0.8$ .  $T_s$  is indicated by an arrow for each concentration. Solid lines are those fitted by the relation  $R \propto \exp(\Delta E^\pm/kT)$  with values of  $\Delta E^\pm$  in Table 1. Temperature dependence of the resistance in the magnetic field  $H = 150 \text{ kOe}$  is shown for  $x=1.2$ . A clear negative magnetoresistance is found below 50 K.

The result is analyzed in terms of the activation energy as usually done in semiconductors and two activation energies  $\Delta E^+$  and  $\Delta E^-$  are obtained as given in Table 1. The solid lines in Fig.20 are drawn by using these values  $\Delta E^\pm$ .  $\Delta E^+$  is two orders larger than  $\Delta E^-$  and decreases with increasing Pb content. The crossing region of two tangential lines in Fig.20 almost coincides with the temperature at which the Hall coefficient changes the sign, which was found by Harrison et al.<sup>38)</sup>. The temperature decreases by adding Pb as is seen in Fig.20. Considering these experimental facts and theoretical expectation of narrow and high DOS in  $\text{EuMo}_6\text{S}_8$  at high temperature crystal phase, it is suggested that a small energy gap corresponding to the order of  $\Delta E^+$  is introduced by the band Jahn-Teller effect.

Of particular interest is the composition  $\text{Pb}_{0.4}\text{Eu}_{0.8}\text{Mo}_6\text{S}_8$  which exhibits both the resistance anomaly and superconductivity. In Fig.21, the resistance for  $\text{Pb}_{0.4}\text{Eu}_{0.8}\text{Mo}_6\text{S}_8$  is shown as a function of temperature for several different applied magnetic field. It has a resistance peak at 10 K and becomes superconducting below 2.5 K in zero field. The peak value of the resistance is about two times of the resistance at room temperature. The resistance at low temperatures below 10 K is strongly field dependent. In low fields the compound remains completely superconducting down to the lowest temperature of 80 mK. However, a finite resistance reappears at 0.55 K in the field of 2.5 kOe. This behavior of the resistance depending on the temperature and magnetic field is quite similar to that found in  $\text{Er}_{1.2}\text{Mo}_6\text{S}_8$  and  $\text{Dy}_{1.2}\text{Mo}_6\text{S}_8$  by Ishikawa et al.<sup>39)</sup>. These facts suggest that some kind of magnetic order may appear at 0.8 K and coexist with the superconductivity in low field.

TABLE I The activation energy  $\Delta E^\pm$  obtained from the tangential lines in Fig.21.  $\Delta E^+$  and  $\Delta E^-$  are the energy in a high and low temperature region, respectively. \*Only the maximum value is estimated because of a rapid decrease of the resistance below 10 K.

X	$\Delta E^+$ ( meV )	$\Delta E^-$ ( meV )
1.2	$9.5 \pm 0.1$	$0.05 \pm 0.01$
1.0	$3.7 \pm 0.1$	$0.03 \pm 0.01$
0.8	$2.6 \pm 0.1$	$\leq 0.05^*$



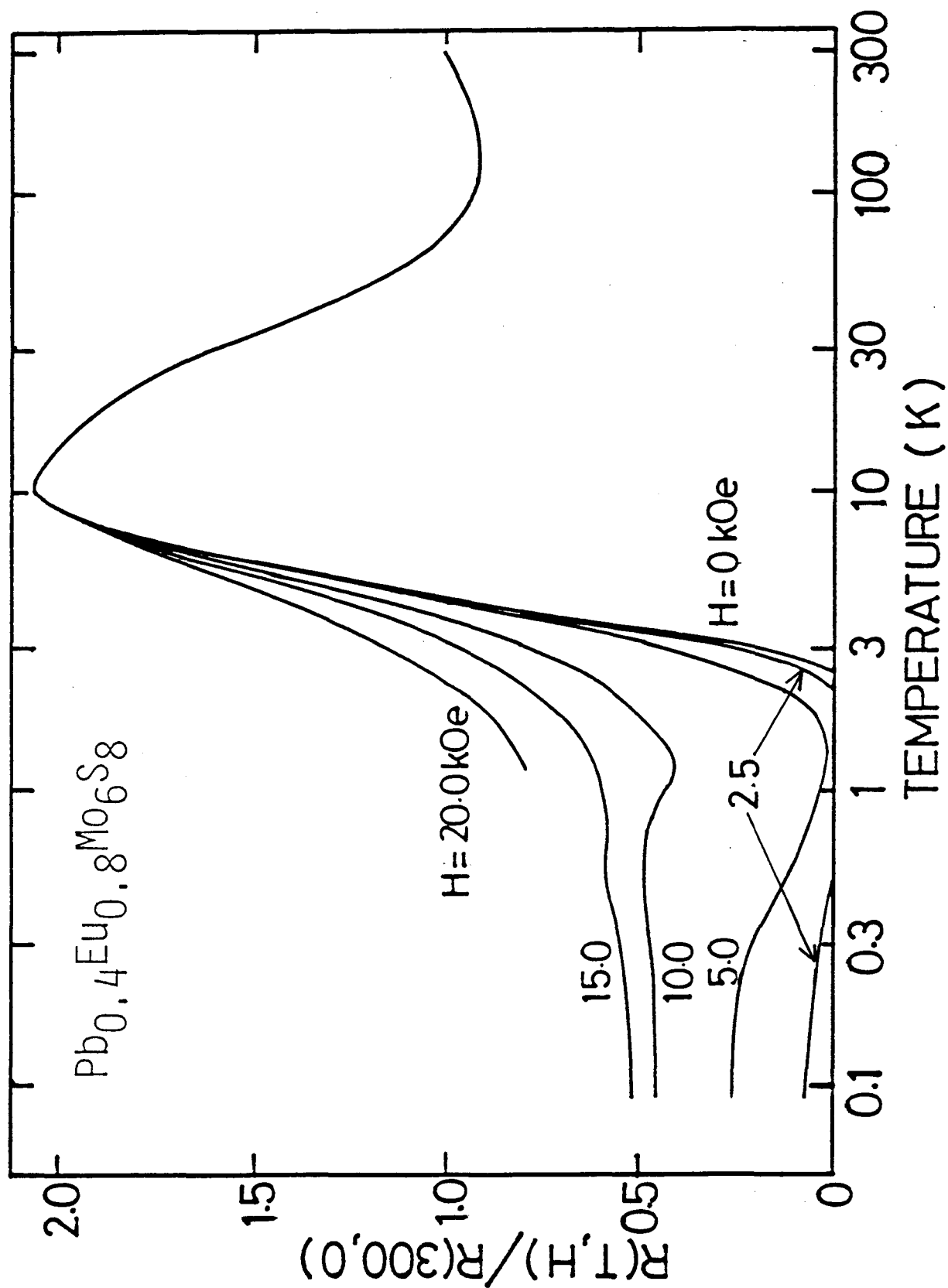


Fig.21 Temperature dependence of the magnetoresistance for  $\text{Pb}_{0.4}\text{Eu}_{0.8}\text{Mo}_6\text{S}_8$ . The resistance below 10 K is strongly field-dependent.

The electrical resistance for low Eu concentrations ( $x \leq 0.6$ ) decreases monotonically with decreasing temperature and becomes superconducting at  $T_c$ .  $T_c$  is determined from the midpoint of the transition. The concentration dependence of  $T_c$  and  $T_s$  are shown in Fig.22.  $T_s$  is strongly suppressed by substituting Pb for Eu. The extrapolated  $T_s(x)$  curve shows that the structural transformation disappears at  $x \approx 0.7$  and the rhombohedral structure is stable in a region  $0 \leq x \leq 0.7$ . On the other hand, the superconducting transition temperature  $T_c$  decreases abruptly for the concentrations  $x \geq 0.6$  and the superconductivity disappears at  $x \approx 0.82$ , as is seen in Fig.22. Thus, in a narrow region  $0.7 \leq x \leq 0.82$  the superconductivity coexists with the transformed triclinic structure.

$T_c(x)$  in a region  $0 \leq x \leq 0.7$  is compared with Maekawa-Tachiki theory ( MT )<sup>22)</sup>. As will be shown later, the present compounds have antiferromagnetic exchange interaction between the nearest-neighbor Eu spins. So, we apply the relation ( MT-4.10, refer to APPENDIX ) for the antiferromagnetic case. The nearest-neighbor number  $z$ , Eu spins  $S$  and BCS parameter  $g_{BCS}N(0)$  are taken to be 6,  $7/2$  and 0.3, respectively, as in their paper. The exchange interaction parameter  $J'$ , which is defined by  $J' = 3/4 \cdot S(S+1)J$  with the nearest-neighbor exchange interaction  $J$ , is taken as  $J' = -0.13$  K.  $J$  is obtained from the observed Currie-Weiss constant of  $\theta = -0.4$  K. Exchange interaction parameter  $I^2N(0)$  between the conduction electrons and Eu spins and superconducting transition temperature  $T_{c0}$  without magnetic ions are adjusted so as to get a best fit with the observed  $T_c(x)$ . The fitting is mainly done in the region  $x = 0.4 \sim 0.6$  because their theory is quantitatively applicable to

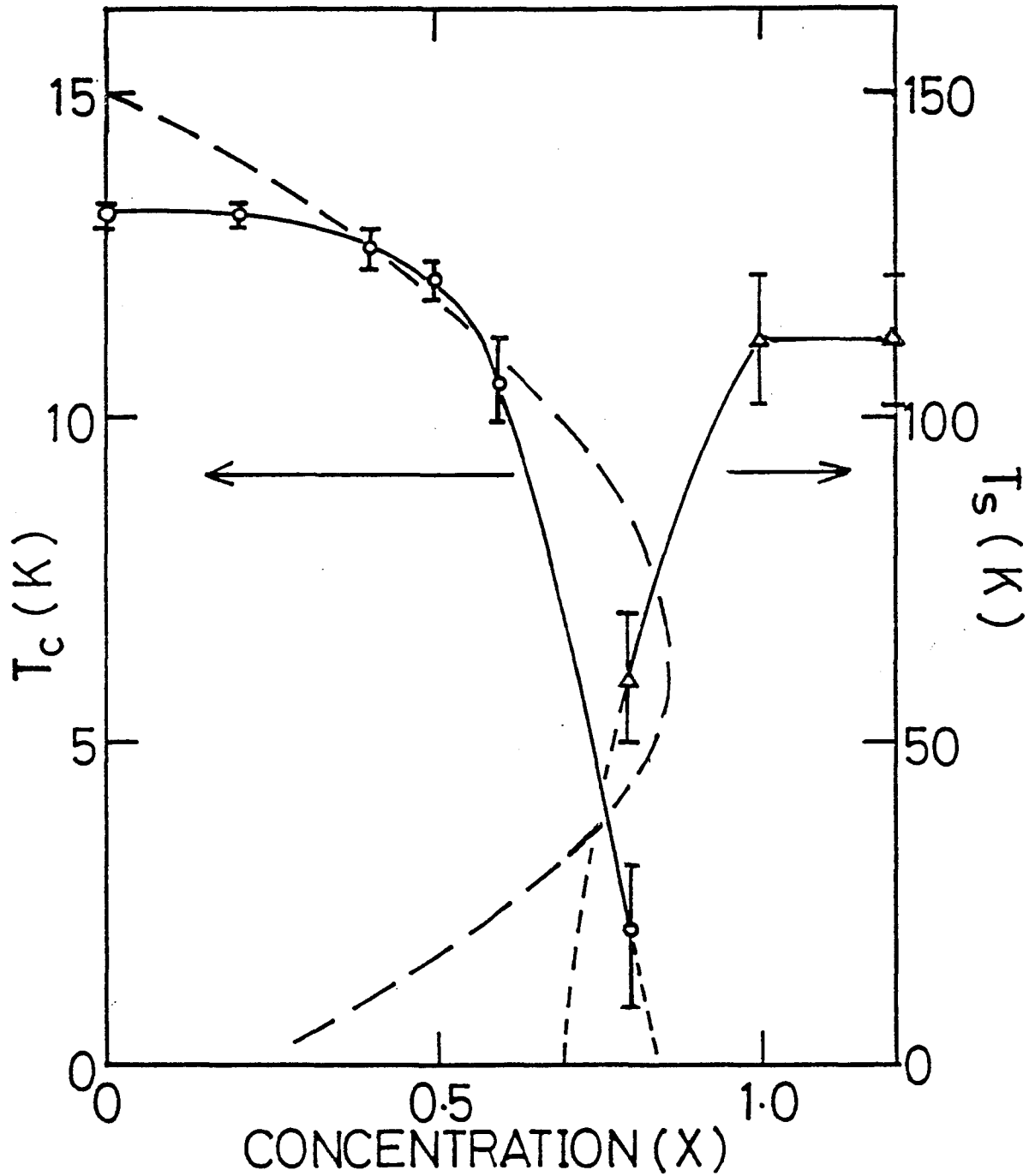


FIG.22 Eu concentration dependence of superconducting transition temperature  $T_c$  and structural transformation temperature  $T_s$ . A broken line is the theoretical curve of  $T_c(x)$ .

high  $x$ . The equations used in the calculation of  $T_c(x)$  are shown in APPENDIX. Obtained values are given as

$$\left. \begin{aligned} I^2 N(0) &= 3.0 \times 10^{-2} \text{ K} , \\ T_{c0} &= 15 \text{ K} . \end{aligned} \right\} \quad ( 1-5 )$$

Theoretical curve of  $T_c(x)$  is drawn by a broken line in Fig.22 using these values. An abrupt decrease in  $T_c$  for  $x > 0.6$  may be attributed to the effect of structural transformation. For the concentration  $x = 0.3 \sim 0.7$ , reentrant transition to the normal state is expected at low temperatures from the theoretical curve in Fig.22. However, no such a transition was observed in our measurements down to 0.4 K.

## 4.2. Upper Critical Field $H_{c2}$

An example of the magnetoresistance curve in the  $H_{c2}$  measurements is shown in Fig.23 for the composition  $Pb_{0.8}Eu_{0.4}Mo_6S_8$  at 1.3 K. The noise appeared at the start of increasing curve is due to switching for capacitor bank. Gradual increase in the resistance is found as the field increases and the resistance comes to the normal value around 540 kOe. Fig.24 shows magnetoresistance curves for  $Pb_{0.8}Eu_{0.4}Mo_6S_8$  at several temperatures from  $T_c$  to 1.3 K. Abrupt increase of the transition field is observed between 4.2 K and 5.5 K. The observed transitions are rather broader than that expected from the anisotropic  $H_{c2}$  which is about 20 % in  $PbMo_6S_8$ . We find that the transition width is proportional to the transition field and the magnetoresistance curves are almost reduced to a single curve by normalizing the field with a maximum critical field. It is shown in Fig.25 with the solid line.

The origin of observed gradual transition may come from three sources. One of them is the anisotropy in  $H_{c2}$ . The others are the imperfection of the crystal and the dynamical effect appeared in the pulsed field measurements. The first one was found by Decroux et al.<sup>40)</sup> on a single crystal of  $PbMo_6S_8$ . According to them, the  $H_{c2}$  has a uniaxial symmetry expressed as

$$H_{c2}(\theta) = H_{c2\parallel} (\cos^2\theta + \epsilon^2 \sin^2\theta)^{-1/2}, \quad (1-6)$$

where  $H_{c2\parallel}$  is the critical field parallel to the ternary axis,  $\epsilon = H_{c2\parallel}/H_{c2\perp} \approx 0.843$  and  $\theta$  being the angle between the ternary axis

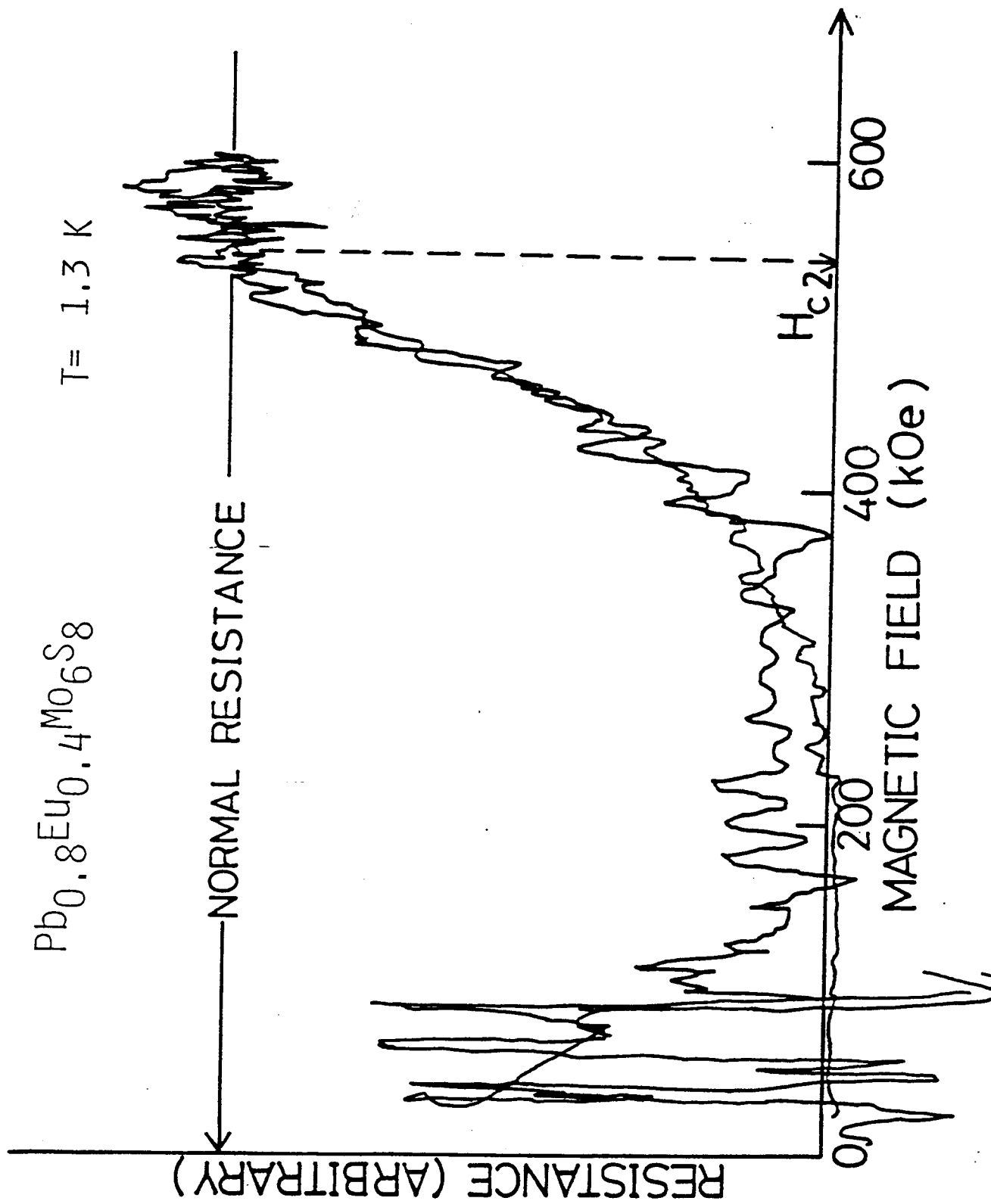


FIG.23 Magnetoresistance curve for  $\text{Pb}_{0.8}\text{Eu}_{0.4}\text{Mo}_6\text{S}_8$ . Our defined  $H_{c2}$  is indicated by an arrow.

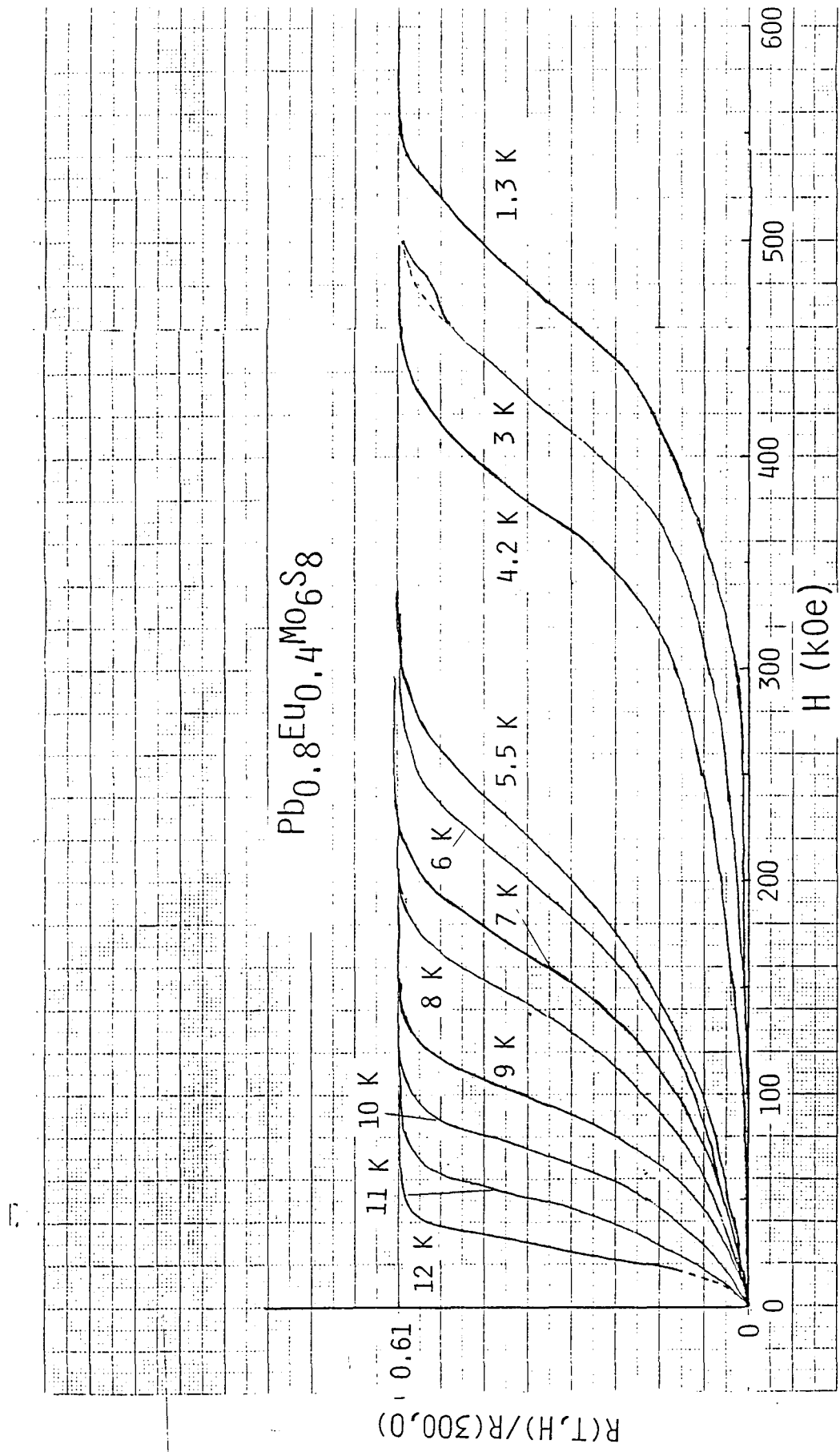


FIG.24 Magnetoresistance curves for  $\text{Pb}_{0.8}\text{Eu}_{0.4}\text{Mo}_6\text{S}_8$  as a parameter of temperature.

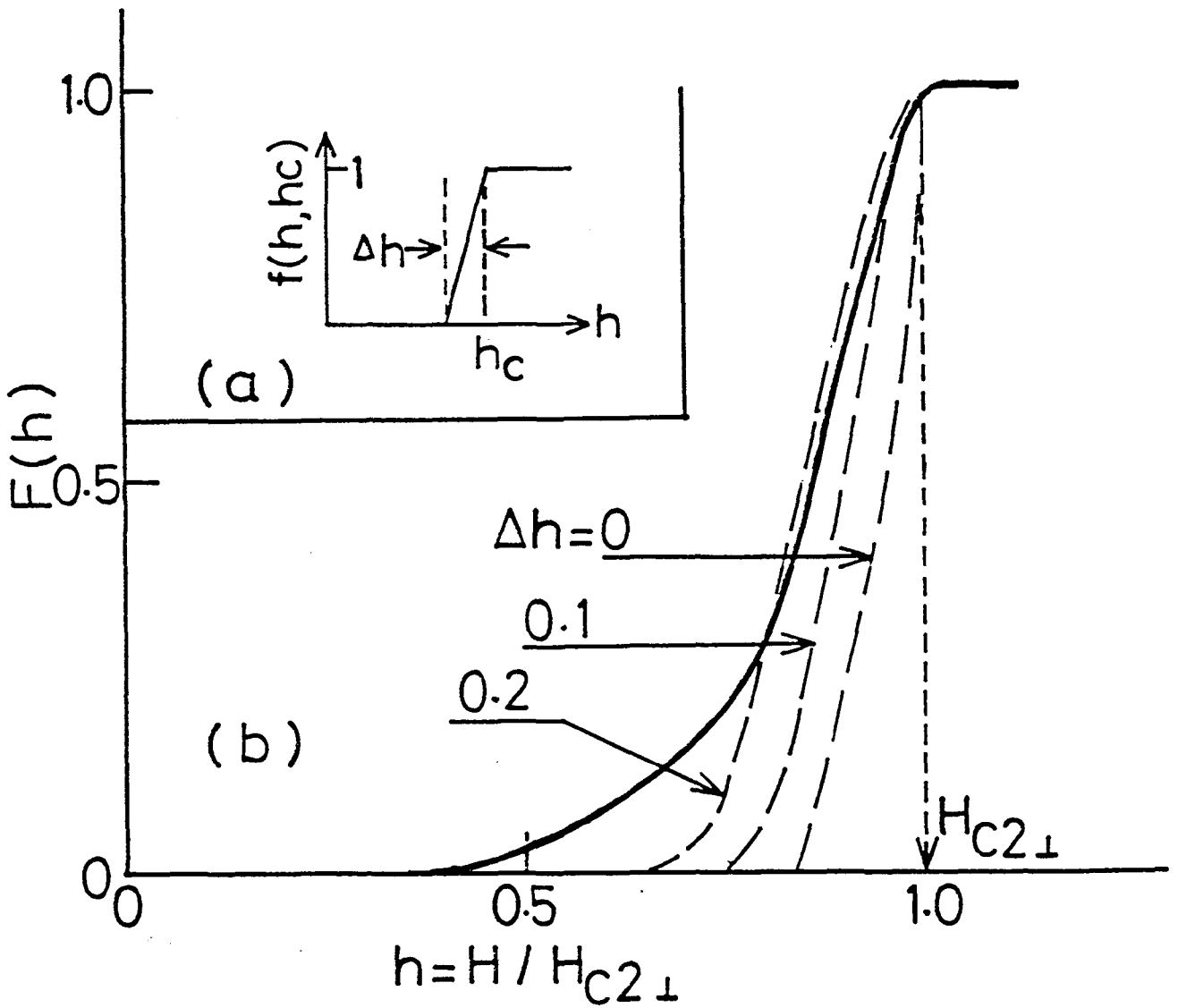


FIG.25 (a) Assumed transition curve of single crystal.  $h_c$  means  $H_{C2}(\theta)/H_{C2\perp}$ . (b) Powder average of the transition curve as a parameter of  $\Delta h$ , which is drawn with dashed line. A solid line is the experimental curve shown in Fig.24.



and  $H$ . The effect of crystal imperfection on  $H_{c2}$  is phenomenologically taken into account by introducing a broadening parameter  $\Delta h$  as shown in Fig.25(a).  $h$  is the reduced field defined in Fig. 25(b) and  $\Delta h$  is inhomogeneous broadening of the critical field due to imperfections.  $h_c$  means the reduced critical field,  $h_c = H_{c2}(\theta)/H_{c2\perp}$  and  $f(h, h_c)$  is an assumed function of the reduced magnetoresistance of single crystal. Then, the powder average of the transition curve is calculated using the relation ( 1-6 ) and  $\Delta h$  as follows:

$$F(h) = \int_{\epsilon}^1 f(h, h_c) P(h_c) dh_c \quad ( 1-7 )$$

where  $P(h_c) = |d\cos\theta/dh_c|$  is the probability of having the appropriate spatial orientation that would satisfy the relation ( 1-6 ) at a given field  $h_c$ . The calculated curves are shown by broken lines in Fig.25(b) as a parameter of  $\Delta h$ , together with the experimental curve of Fig.24. Except for a tail of the curve, the experimental curve is well fitted for  $\Delta h = 0.1 \sim 0.2$ , which is in agreement with the observed width in single crystal<sup>40)</sup>.

Deviation from the theoretical curve found in the low field region may be attributed to the dynamical effect such as flux-flow resistance. In fact, the low field part of the curve depends on the experimental conditions such as the electrical current density and the geometrical arrangement between the field and current direction. The magnetoresistance curves for both configurations, the applied field parallel ( $H_{\parallel}$ ) and perpendicular ( $H_{\perp}$ ) to the currents are checked for  $\text{LaMo}_6\text{S}_8$  with  $T_c = 5.6$  K. As is shown in Fig.26 the magnetoresistance curves in a high field region are

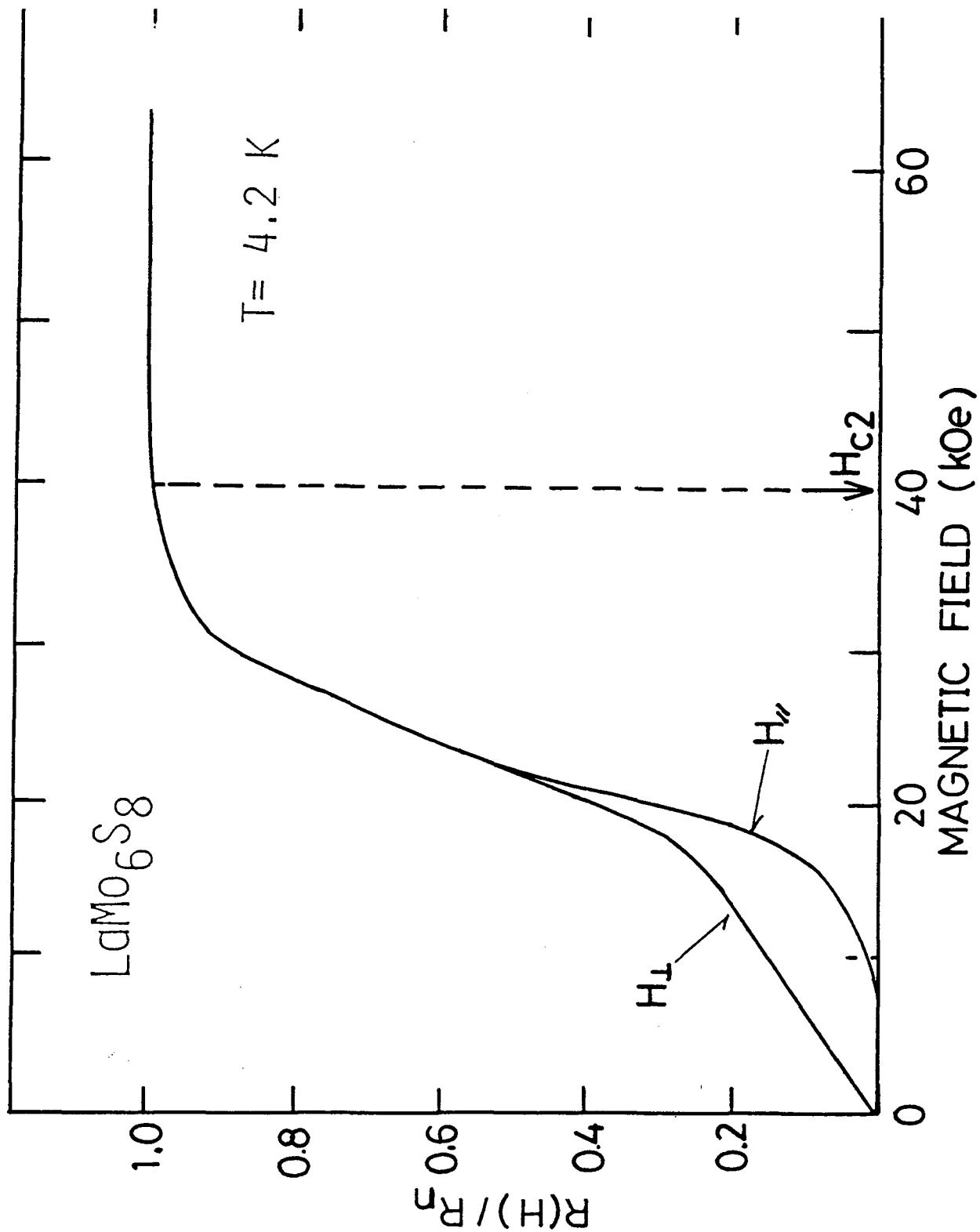


FIG.26 The magnetoresistance curves for  $\text{LaMo}_6\text{S}_8$  at 4.2 K.  $H_{||}$  and  $H_{\perp}$  mean the experimental configurations, the applied field parallel and perpendicular to the current along a long axis of the sample, respectively. A bold arrow indicates our defined  $H_{c2}$  which is quite near the field for the complete suppression of the superconductivity.  $R_n$  is the normal resistance well above  $H_{c2}$ .

almost coincident for both directions. The linear increase in low fields for the perpendicular case is explained by the effect of flux-flow as in general texts of superconductivity<sup>41)</sup>. The effect of  $H_{c3}$ , which is important for a single crystal with clean surfaces, does not appear in the present sintered materials. Therefore, the most reliable data for the  $H_{c2}$  could be obtained by defining the field indicated by an arrow in Fig.23 and Fig.25 as  $H_{c2}^{5)}$ . Thus, our defined  $H_{c2}$  means a " maximum critical field " in the anisotropic  $H_{c2}$  as is seen in Fig.25.

The obtained results on the temperature dependence of  $H_{c2}$  are summarized in Fig.27(a) to (d) for the Eu concentrations  $x = 0.2, 0.4, 0.5$  and  $0.6$ , respectively, together with that for  $x = 0$  which was obtained in our group six years ago<sup>5)</sup>. They show a positive curvature: near  $T_c$  they increase slowly with decreasing temperature but steeply increase at low temperatures. In particular, the  $H_{c2}$  for the composition  $x = 0.5$  exceeds that of  $x = 0$  at 3.5 K and becomes  $H_{c2}(0) \simeq 630$  kOe at 0 K. These particular dependence of  $H_{c2}$  on the temperature and the concentration of magnetic ions are attributed to the effect of magnetic ions with the antiferromagnetic exchange interaction between the conduction electrons and local magnetic moments.

Quantitative explanation for them is given by the MT theory. In order to compare the present results with their theory, we use the equation ( MT-5.18, see APPENDIX ) for the case with a general value of spin-orbit scattering parameter  $\lambda_{so}$ . The following parameters,  $I^2N(0)/T_{c0}$ ,  $|J'|/T_{c0}$ ,  $I/T_{c0}$ ,  $\lambda_{so}$  and  $\alpha$ , where  $\alpha$  is non-magnetic scattering parameter which is proportional to inverse of

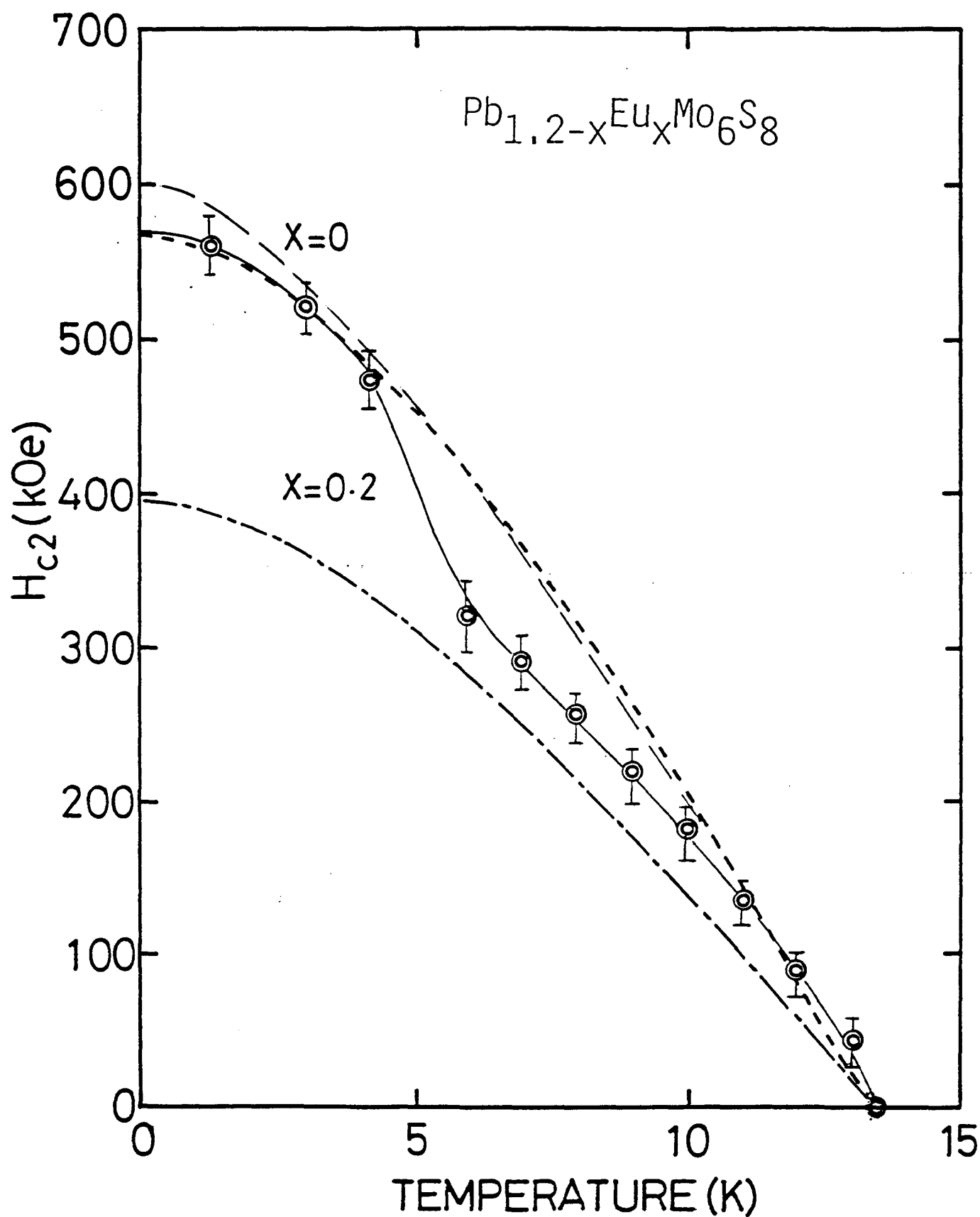


FIG.27(d) Temperature dependence of  $H_{c2}$  in  $Pb_{1.2-x}Eu_xMo_6S_8$  for  $x = 0.2$ . A dashed line is for  $x = 0$ . Broken line and dash-dotted line are the theoretical curves as given in the text.

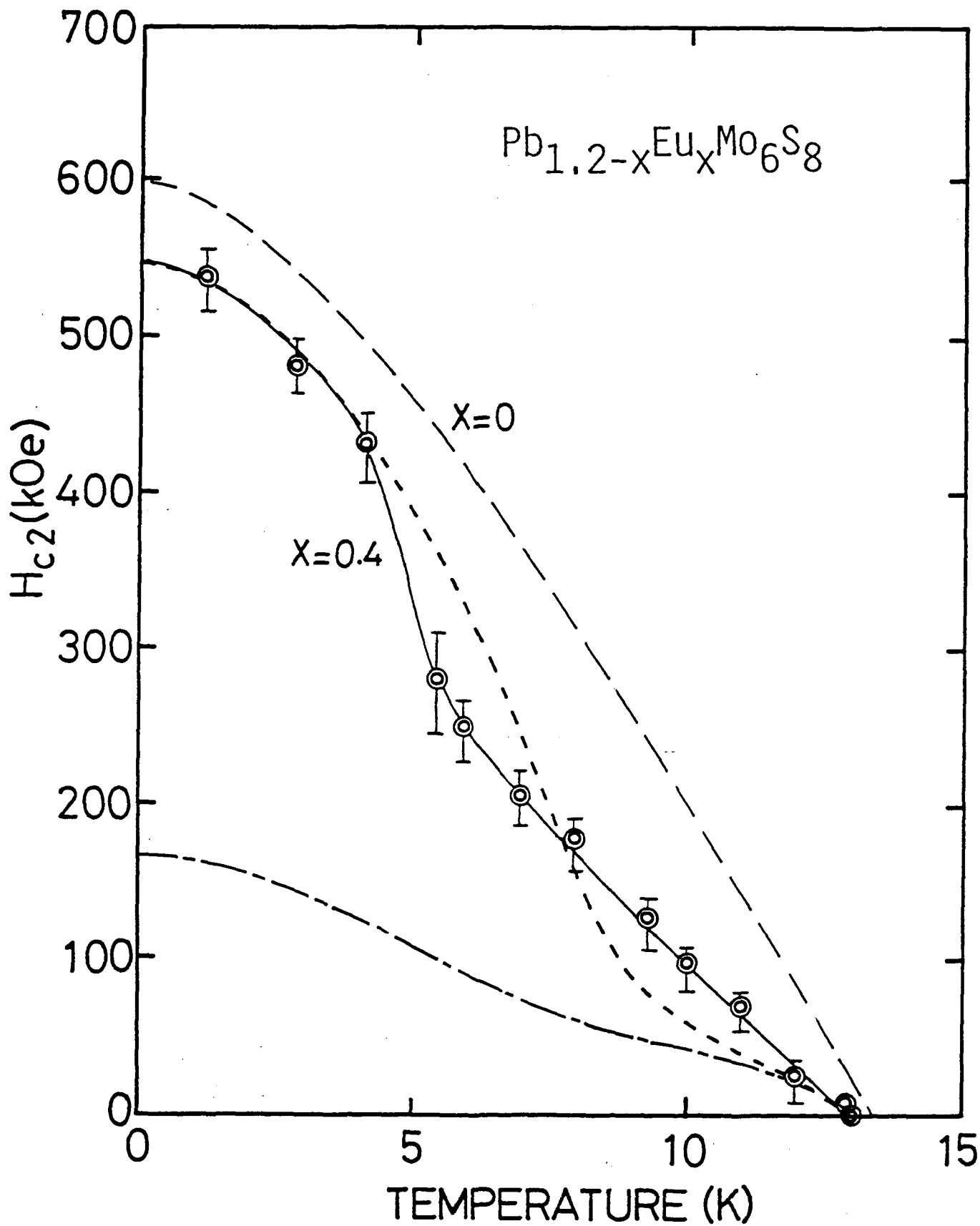


FIG.27(b)  $H_{c2}(T)$  for  $x = 0.4$ .

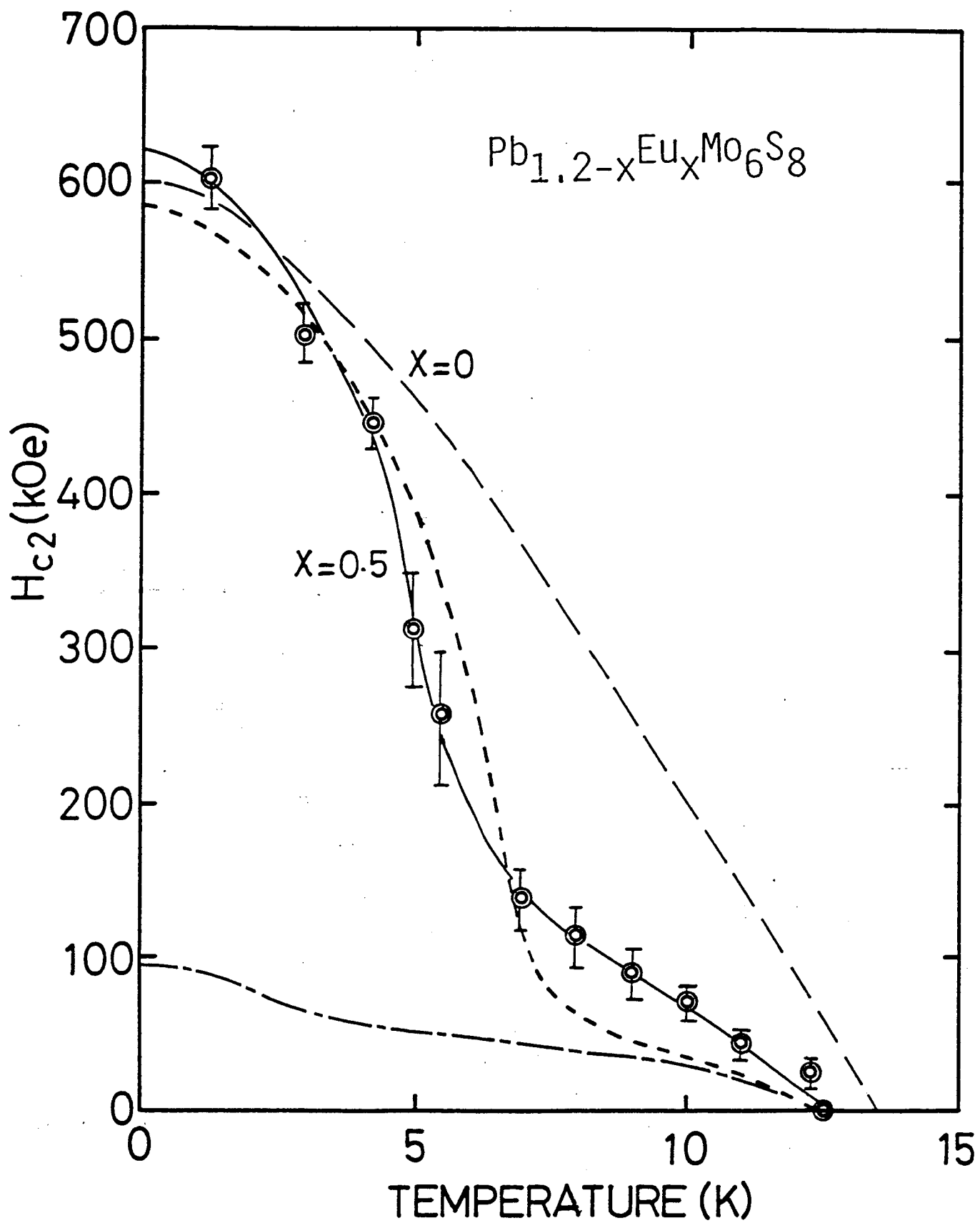


FIG.27(c)  $H_{c2}(T)$  for  $x = 0.5$ .

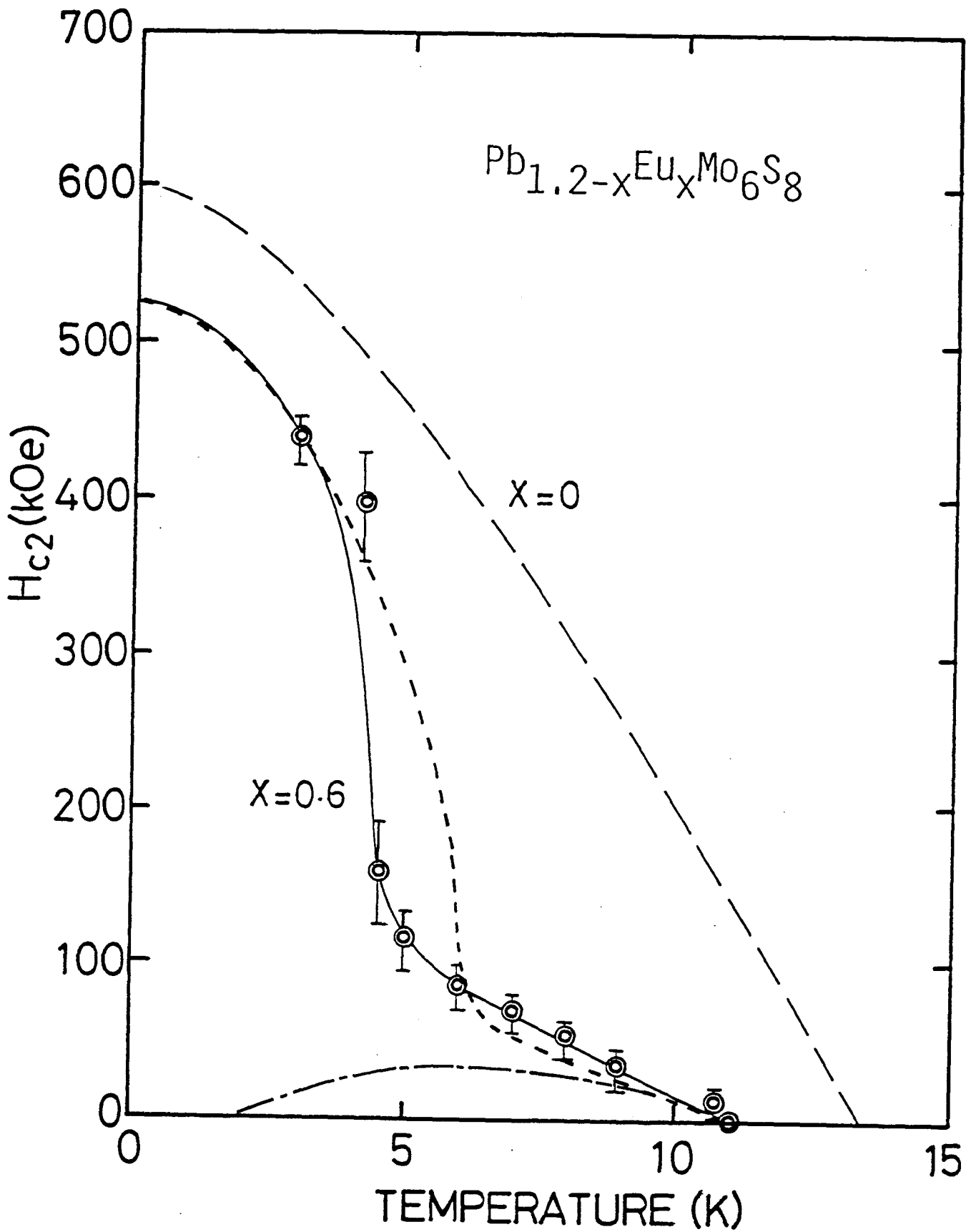


FIG.27 (d)  $H_{c2}(T)$  for  $x = 0.6$ .

initial slope of  $H_{c2}$ , are adjusted so as to obtain a good fitting with the experimental  $H_{c2}(T)$  curve by using a mini-computer ECLIPSE S/20. The relations used in the calculation of  $H_{c2}$  are shown in APPENDIX. The calculated curves are shown in Figs.27(a) to (d) by a broken line, which is normalized at  $T_c$ , and the adjusted parameters are listed in Table 2. Better fit is obtained in higher Eu concentrations. It is consistent with the theoretical treatment that the inelastic scattering of conduction electrons with the interacting magnetic spin system plays an important role and the effect of isolated spins is neglected. The exchange interaction,  $I$ , between the conduction electrons and magnetic spins is obtained by Eq.( 1-5 ) and the value in Table 2 as

$$I = -3.2 \pm 0.6 \text{ meV} . \quad ( 1-8 )$$

Here, it is noted that the exchange interaction,  $I$ , is antiferromagnetically. If we assume the sign of  $I$  is positive, the  $H_{c2}$  is strongly suppressed as shown in Figs.27(a) to (d) by a dash-dotted line. This means that the peculiar behavior of  $H_{c2}(T)$  is mainly attributed to the compensation of the external field by the exchange field acting on the conduction electron spins. The spin-orbit scattering parameter  $\lambda_{so}$  decreases with decreasing the Pb content and it suggests that Pb atoms are effective to the spin-orbit scattering of the conduction electrons. The parameter  $\alpha$  has a minimum value at  $x = 0.5$ . It may be attributed to the combined effect of an increase in non-magnetic scattering and Fermi velocity due to broadening the band width with substitution of Eu.



TABLE 2 The parameters used for the theoretical  $H_{c2}(T)$  curves in Fig.27(a) ~ (d) for  $Pb_{1.2-x}Eu_xMo_6S_8$ . The parameters are defined as  $\lambda_{so} = (3\pi T_{c0}\tau_{so})^{-1}$  and  $\alpha = e\tau_0 v_F^2 / T_{c0}$  where  $\tau_{so}$  and  $\tau_0$  are the relaxation time for spin-flip and non-spin-flip scattering, respectively.

X	$I^2 N(0) / T_{c0}$	$ J'  / T_{c0}$	$I / T_{c0}$	$\lambda_{so}$	$\alpha$ [1/kOe]
0.2	$2.0 \times 10^{-3}$	$8.88 \times 10^{-3}$	- 3.0	10	$4.64 \times 10^{-3}$
0.4			- 3.0	6	$4.35 \times 10^{-3}$
0.5			- 2.5	5	$4.00 \times 10^{-3}$
0.6			- 2.0	4.5	$4.32 \times 10^{-3}$

A disagreement with the theory in low concentrations of Eu may be due to the effect of random distribution of magnetic ions and the multi-band effect might be also included in the  $H_{c2}(T)$ . Anyway, the main part of the present results could be explained by the MT theory.

The magnetoresistance curve for  $Pb_{0.4}Eu_{0.8}Mo_6S_8$  is shown in Fig.28 as a parameter of temperature. The transition between superconducting and normal state due to magnetic field is considerably broad. The resistance increases monotonically with increasing field even at 4.22 K where the finite resistance appears in zero field. This fact suggests that partial superconductivity due to some kind of inhomogeneity remains. In the case it is difficult to determine the  $H_{c2}$ . So, the magnetic field at which the finite resistance just appears is taken as the upper critical field of the compound. It is plotted in Fig.29 as the function of temperature. The  $H_{c2}(T)$  obtained in this way has a broad peak around 1.3 K and decreases with decreasing temperature. Magnetoresistance of  $Pb_{0.4}Eu_{0.8}Mo_6S_8$  was measured up to 400 kOe at 1.3 K with expectation of the field-induced superconductivity which is reported by several groups in  $Eu_xSn_{1-x}Mo_6S_8$  with  $x \sim 0.8$ <sup>42)</sup>. The result is shown in Fig.30. Increasing the field, the resistance appears with abrupt slope in the low field region below 30 kOe, slowly increases in the region between 30 kOe and 280 kOe and saturates above 280 kOe. The saturation value of the magnetoresistance which is reduced by the resistance at 300 K is almost coincident with the peak value of the temperature dependent resistance as is shown in Fig.21. Anyway, no reentrant transition

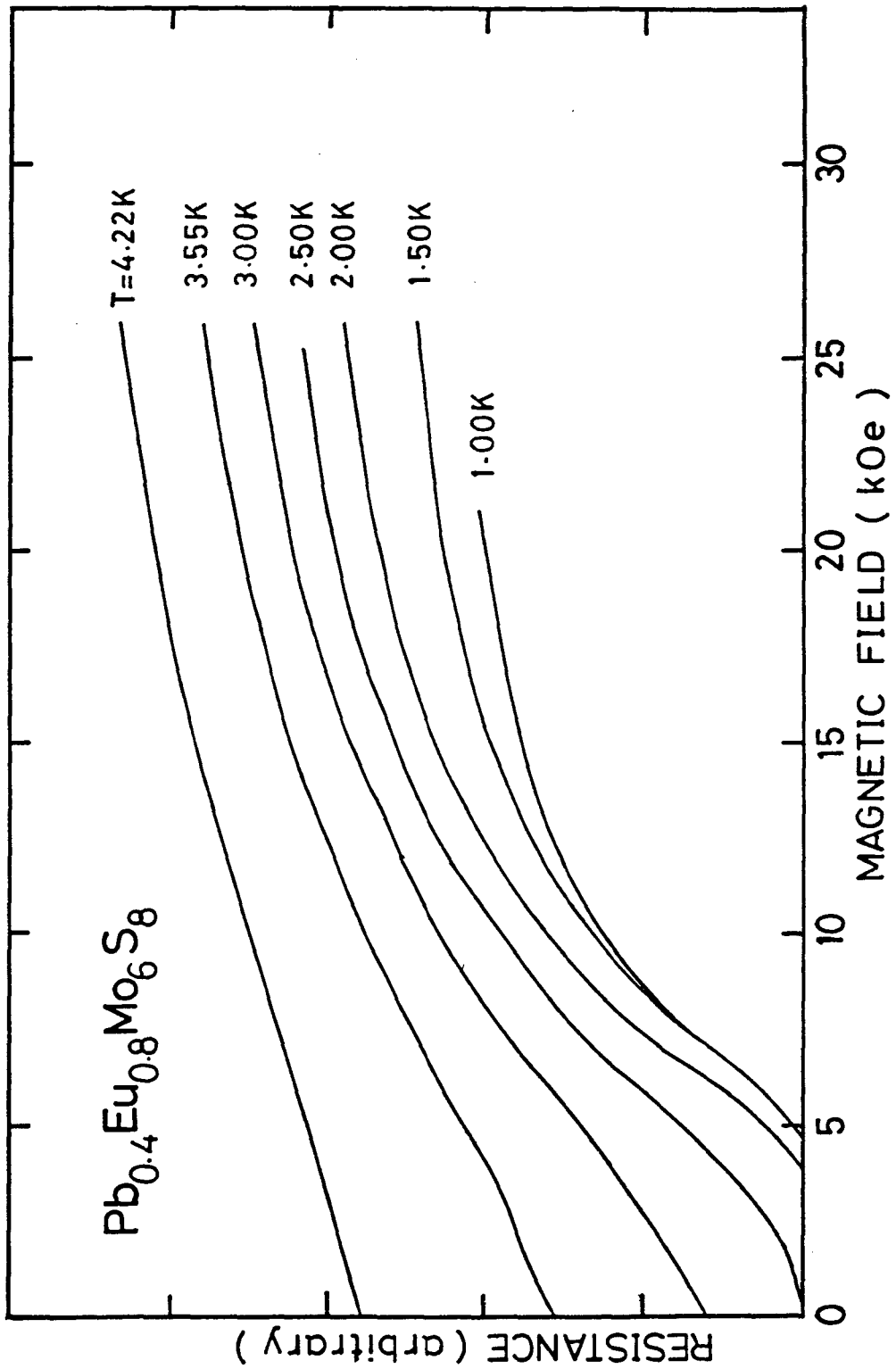


FIG.28 Magneto-resistance curves for  $\text{Pb}_{0.4}\text{Eu}_{0.8}\text{Mo}_6\text{S}_8$  as a parameter of temperature.

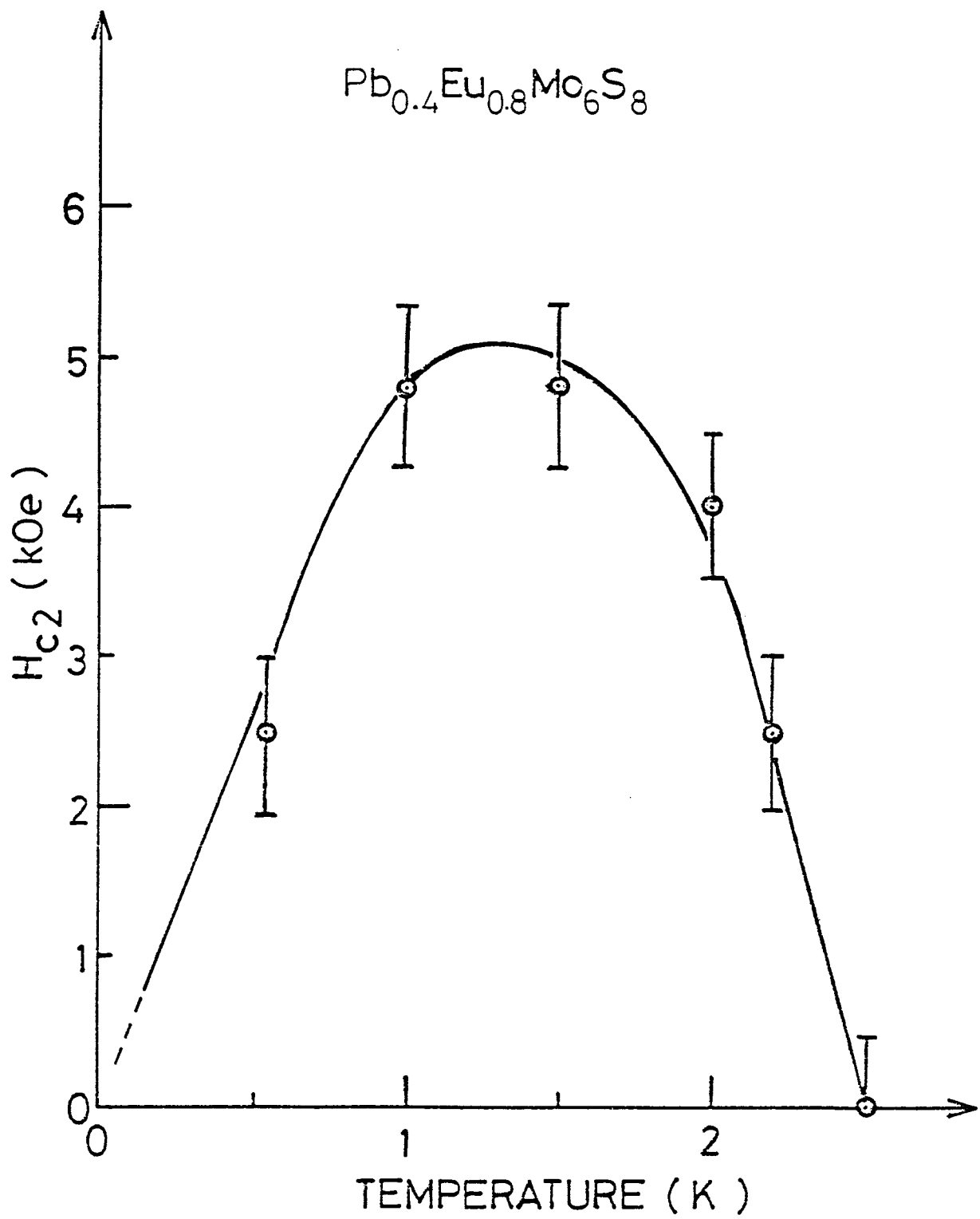
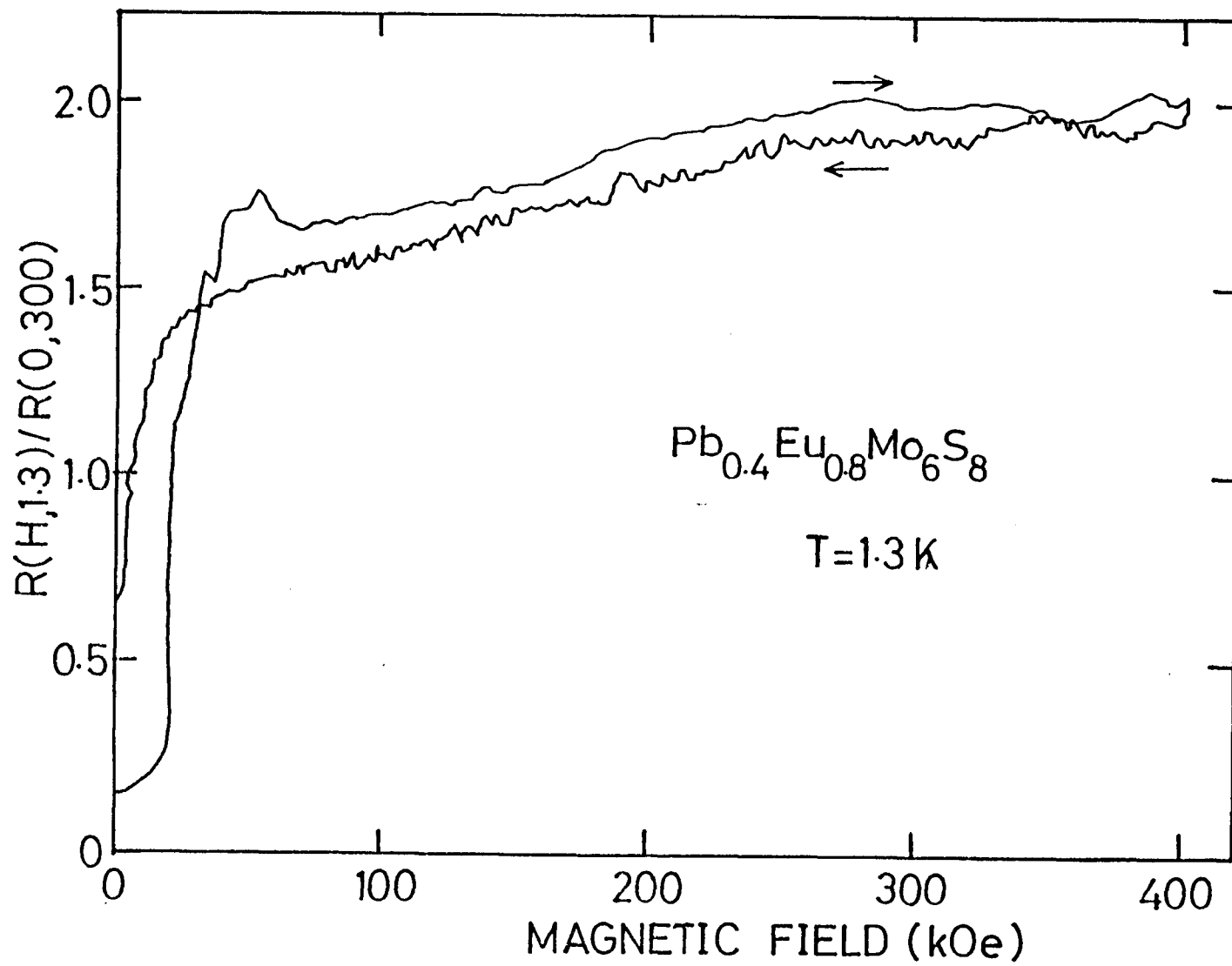


FIG.29 Temperature dependence of  $H_{c2}$  in  $\text{Pb}_{0.4}\text{Eu}_{0.8}\text{Mo}_6\text{S}_8$ .

Fig.30 Magneto-resistance curve of  $\text{Pb}_{0.4}\text{Eu}_{0.8}\text{Mo}_6\text{S}_8$ .



from normal to superconducting state was found at the present time. High field magnetoresistance measurement below 1 K is required.

#### 4.3. Magnetic Properties of $\text{Eu}_{1.2}\text{Mo}_6\text{S}_8$

Magnetic susceptibility of  $\text{Eu}_{1.2}\text{Mo}_6\text{S}_8$  and  $\text{Pb}_{0.4}\text{Eu}_{0.8}\text{Mo}_6\text{S}_8$  follows the Curie-Weiss law  $\chi_g = C/(T-\theta)$  with  $C = 5.88 \times 10^{-3}$  and  $3.88 \times 10^{-3} \text{ cm}^3\text{K/g}$  and  $\theta = -0.4$  and  $-0.1$  K, respectively down to 1.4 K as shown in Fig.31(a) and (b). From the Curie constant the effective magnetic moment is estimated to be  $\mu_{\text{eff}} = 6.3 \mu_B/\text{Eu}$  for both compositions  $x = 0.8$  and  $1.2$ , which is about 80 % of  $\text{Eu}^{2+}$  value. The result suggests that about 20 % of  $\text{Eu}^{3+}$  is mixed in accord with the results in Mössbauer study by Dunlap et al.<sup>43)</sup>. The contribution of the corresponding amount of  $\text{Eu}^{3+}$  to the linearity of  $1/\chi$  curve is negligibly small.  $\text{Eu}^{3+}$  is non magnetic in the ground state and the excited multiplet is  $255 \text{ cm}^{-1}$  above the ground state. Therefore,  $\text{Eu}^{3+}$  gives negligible contribution to the susceptibility.

The magnetization process of  $\text{EuMo}_6\text{S}_8$  is measured in the field up to 300 kOe at 0.6 K as is shown in Fig.32. Any hysteresis is not seen in the compound. The magnetization curve saturates in the high field region with the saturation moment of  $5.9 \pm 0.3 \mu_B$ . This is consistent with a spin 7/2 paramagnetic behavior of  $\text{Eu}^{2+}$  ions assuming the presence of 20 % non magnetic ( $J = 0$ )  $\text{Eu}^{3+}$  ions as determined from the susceptibility measurement. The theoretical curve given by the broken line is drawn by using the Brillouin function with the exchange interaction  $J'$  of  $-0.13$  K which is determined from the Curie-Weiss constant of  $\theta = -0.4$  K. The Van Vleck contribution of the  $J = 1$  first excited state of  $\text{Eu}^{3+}$  represents only a 3 ~ 4 % correction to the number of paramagnetic ions. These

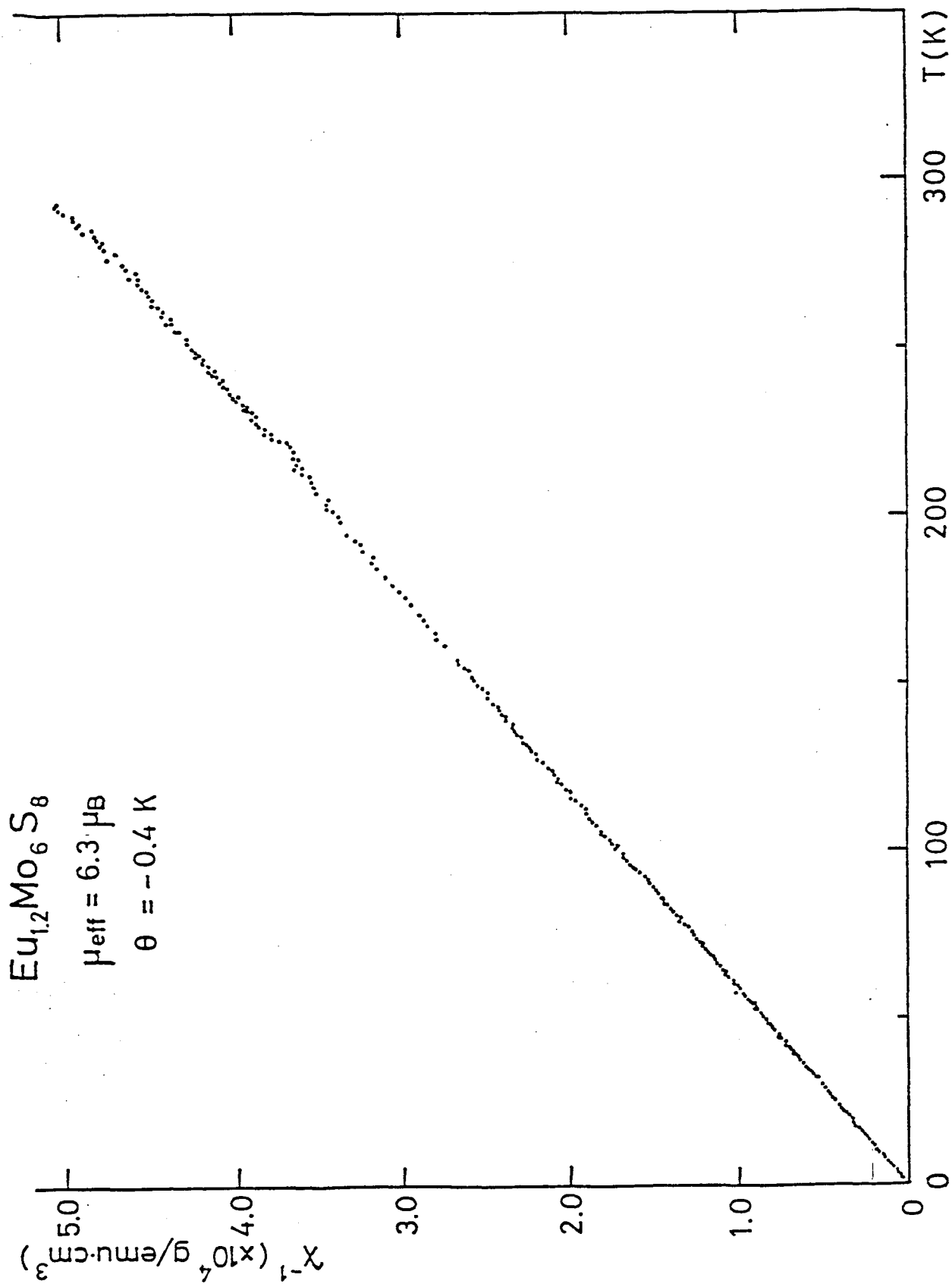


FIG.31(a) Temperature dependence of magnetic susceptibility of  $\text{Eu}_{1.2}\text{Mo}_6\text{S}_8$ .



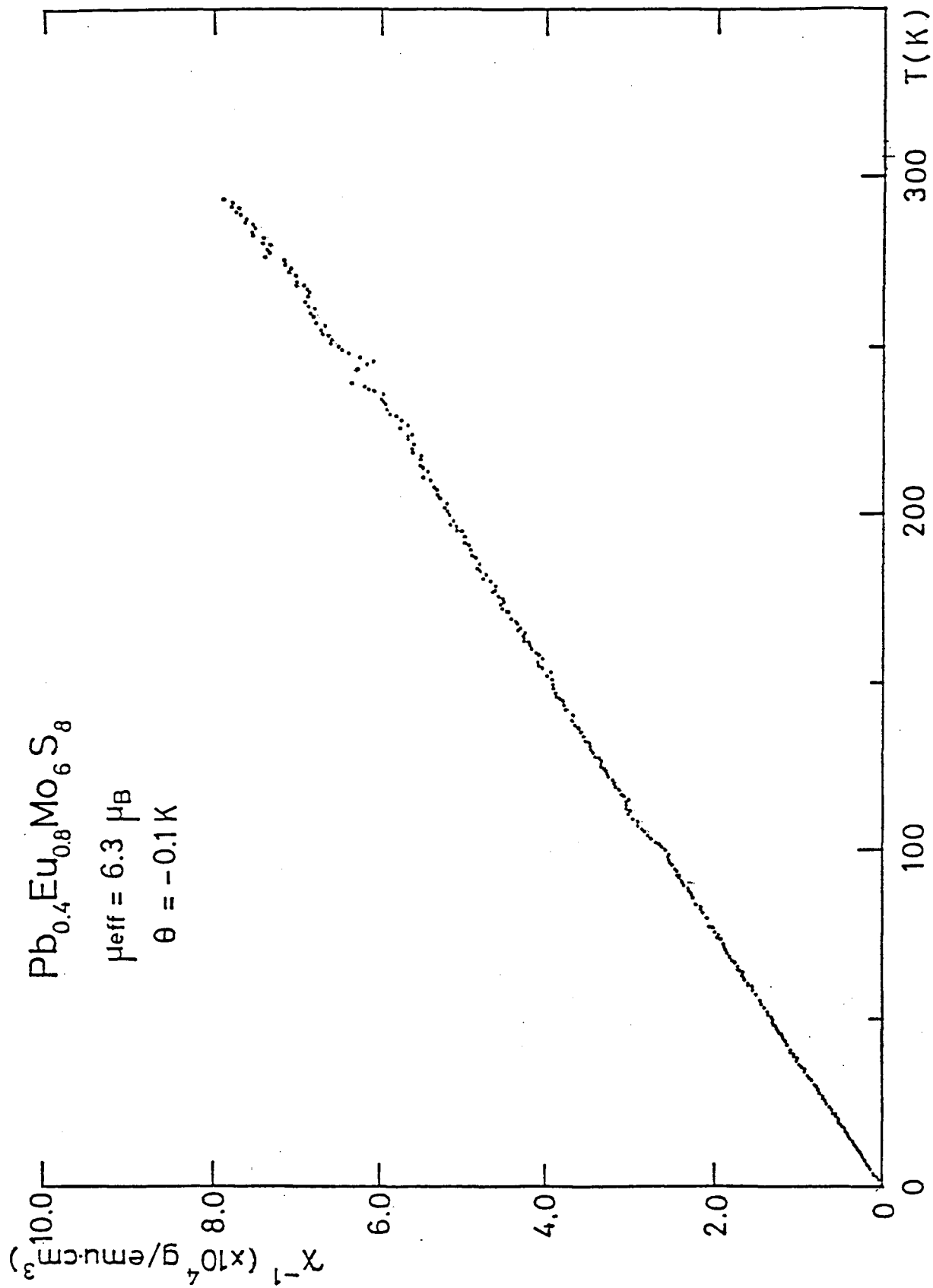


FIG.31(b) Temperature dependence of magnetic susceptibility of  $\text{Pb}_{0.4}\text{Eu}_{0.8}\text{Mo}_6\text{S}_8$ .

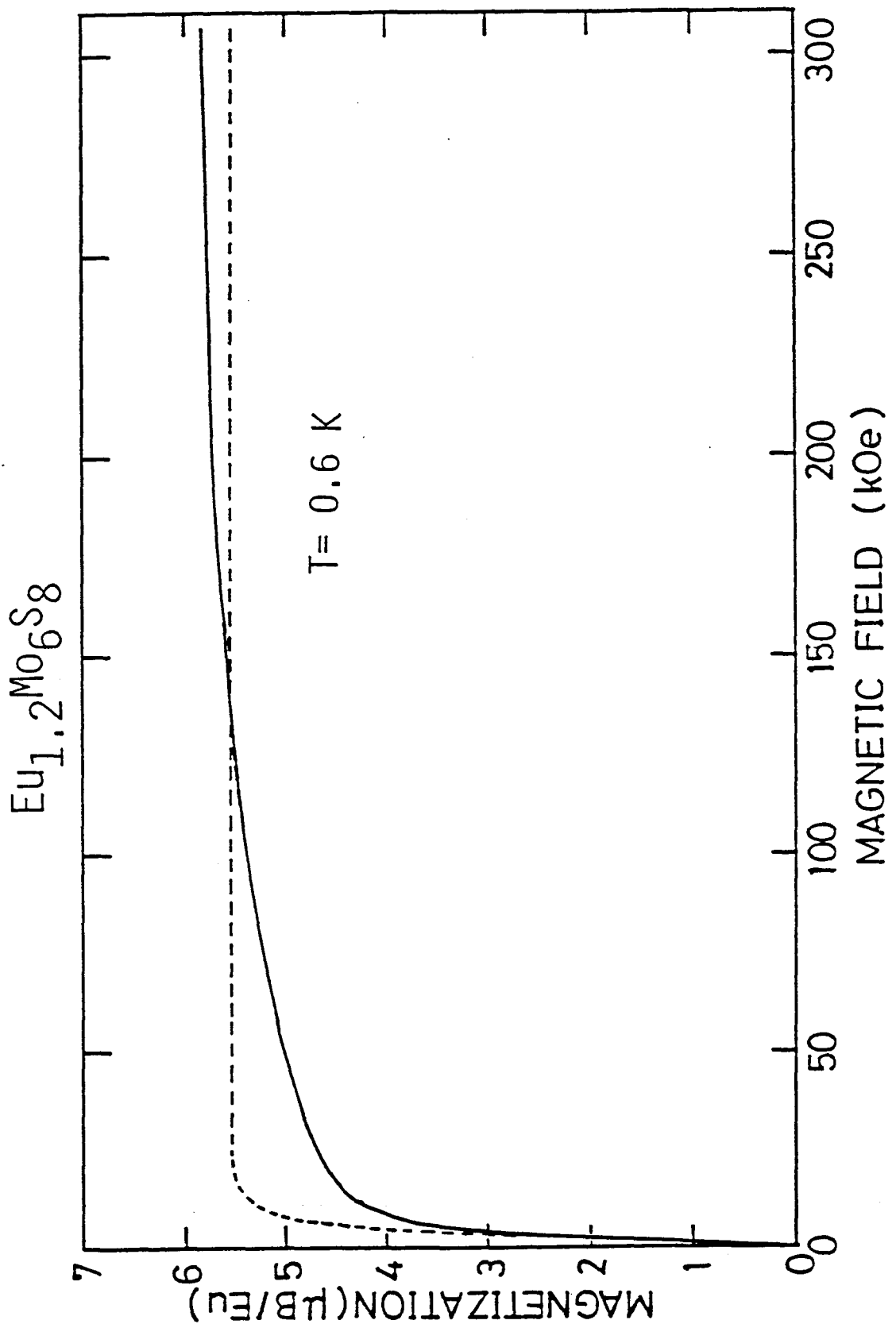


FIG.32 Magnetization curve of  $\text{Eu}_{1.2}\text{Mo}_6\text{S}_8$ . A solid line is the experimental curve. A broken line is the theoretical curve as given in the text.

results show a good agreement with the data obtained by Thompson et al.<sup>44)</sup>. The origin of deviation in the low field region is not clear.

The longitudinal magnetoresistance is measured up to 300 kOe as is shown in Fig.33. The resistance is strongly suppressed by the field up to 100 kOe in accord with the results by Thompson et al.<sup>44)</sup> while it is almost constant above 100 kOe. As one of the origin for the negative magnetoresistance at low temperatures, the effect of spin fluctuation is considered because the spin fluctuation is suppressed by applying magnetic field so that the resistivity decreases as the field increases. Fig.34 shows a temperature dependent magnetoresistance. It is noted that the magnetic order arises at 0.3 K which is inferred from the peak of ac-susceptibility by Willis et al.<sup>45)</sup> and the spin fluctuation will be enhanced around the temperature.

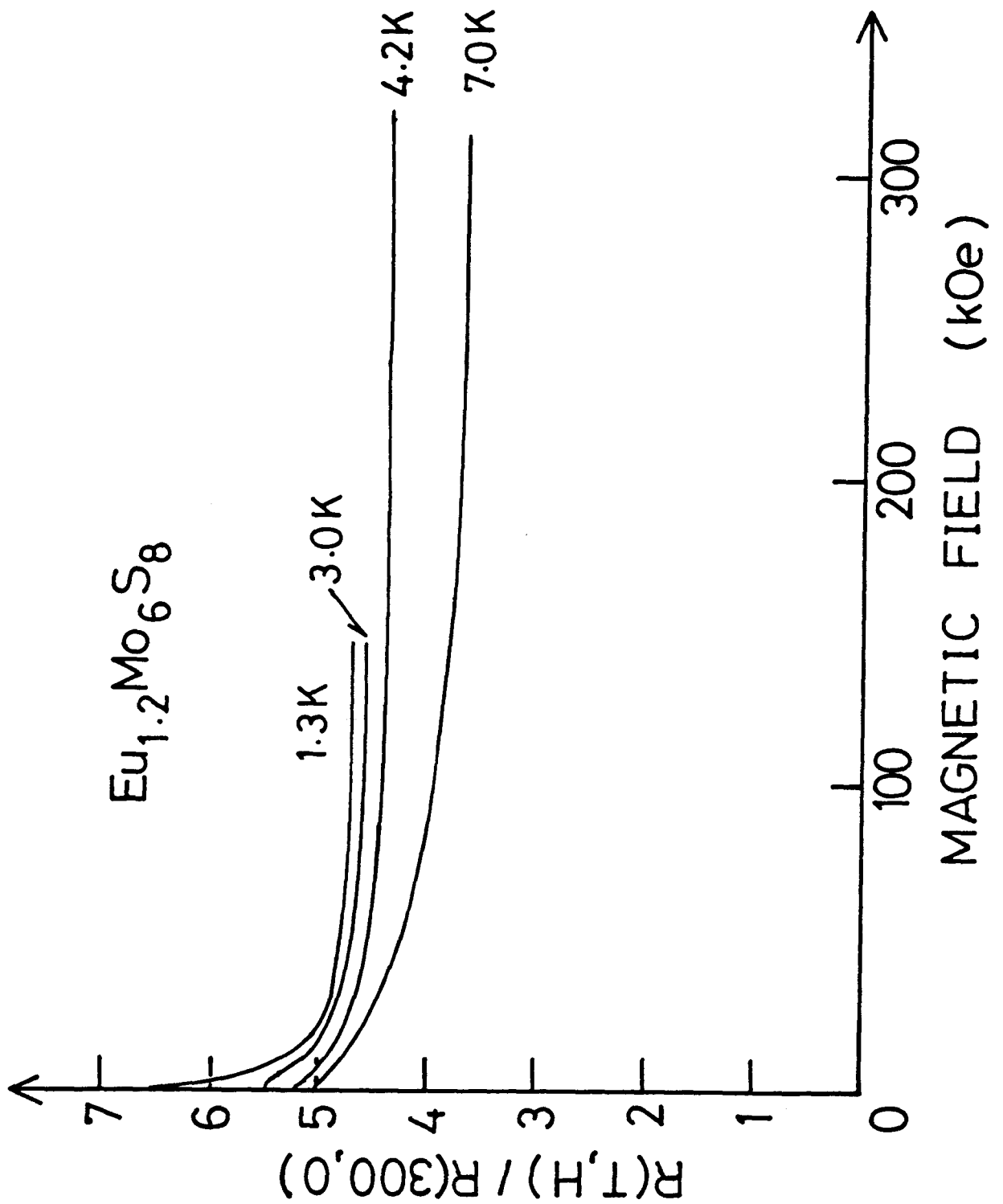


FIG.33 Magnetoresistance curves for  $\text{Eu}_{1.2}\text{Mo}_6\text{S}_8$  as a parameter of temperature.

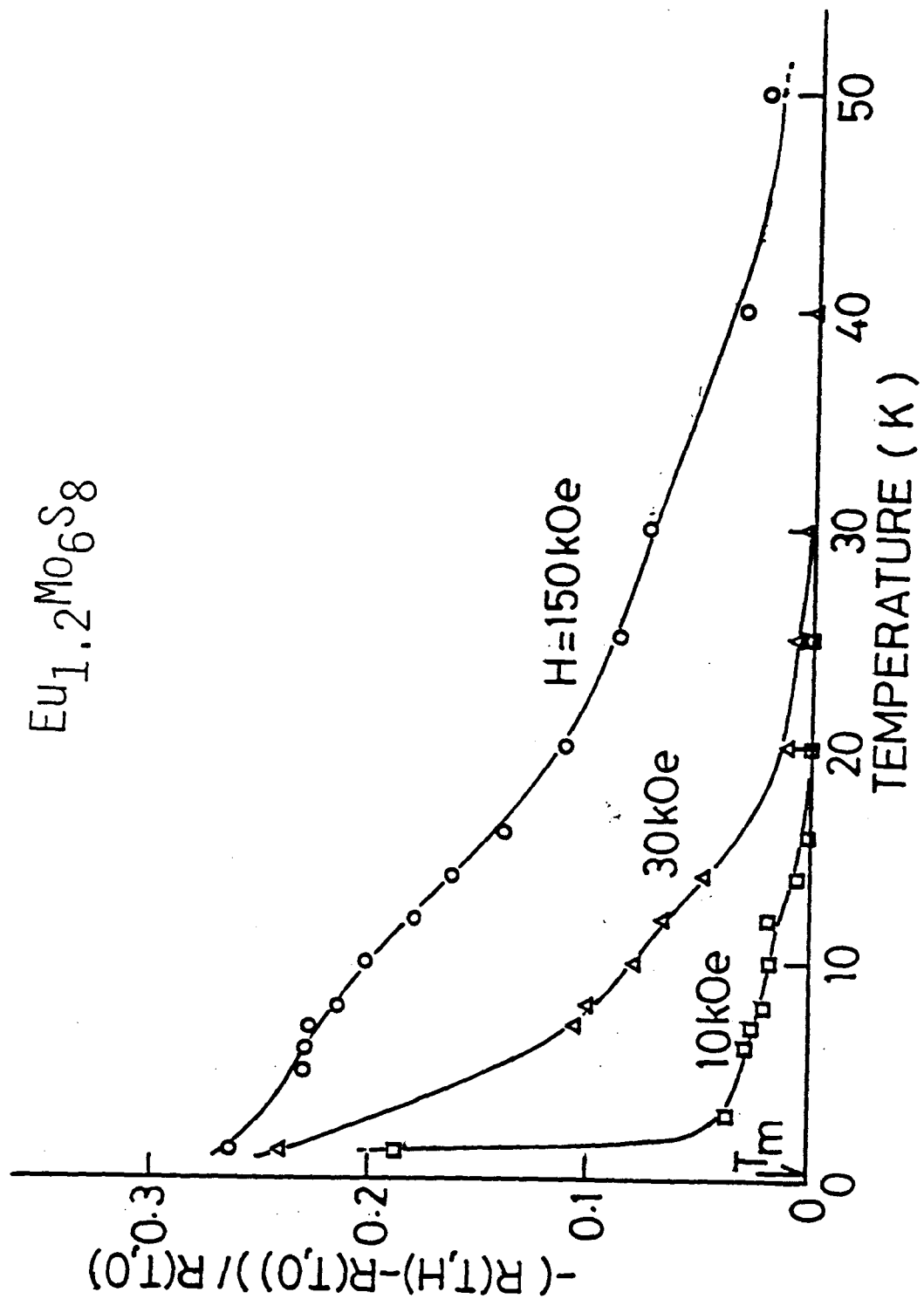


FIG.34 Temperature dependence of the magnetoresistance of  $\text{Eu}_{1.2}\text{Mo}_6\text{S}_8$  as a parameter of applied magnetic field.

## § 5. CONCLUDING REMARKS

The results of the  $H_{c2}$  measurements in the  $Pb_{1.2-x}Eu_xMo_6S_8$  compounds for  $x \leq 0.6$  are successfully explained by the MT theory with the antiferromagnetic exchange coupling of  $-3.2 \pm 0.6$  meV between the conduction electrons and Eu-spins. Particularly, the  $H_{c2}(0)$  for  $x = 0.5$  is found to be 630 kOe which is higher than that of  $Pb_{1.2}Mo_6S_8$ . This concentration appears to be the most favourable for the compensation of applied field by the negative exchange field and to enhance the  $H_{c2}$ .

For Eu rich compounds, on the other hand, the structural transformation is observed around 100 K. The resistance anomaly below 100 K in Eu rich samples is speculated due to a small gap at the Fermi energy resulting from the structural transformation. High field magnetization and temperature dependent susceptibility for  $Eu_{1.2}Mo_6S_8$  shows free-spin paramagnetic behavior characteristic of the  $S = 7/2$  ground state of  $Eu^{2+}$  with a small Van Vleck contribution from 20 %  $Eu^{3+}$  ions. A large negative magnetoresistance is found near the magnetic ordering temperature  $T_m$ . This fact indicates that the spin fluctuation effect is large in these compounds. It is noted that these behaviors are quite similar to those found in  $SmB_6$ <sup>46)</sup> or  $YbB_{12}$ <sup>47)</sup>.

APPENDIX -- CALCULATION OF  $T_c$  AND  $H_{c2}$  BY MT THEORY --

In this section, the calculation of  $T_c$  and  $H_{c2}$  by applying the Maekawa and Tachiki theory is reviewed.

According to their theory,  $T_c$  is given by the relation ( MT-4.10 ) in antiferromagnetic case with nearest-neighbor exchange interaction. ( MT-4.10 ) is represented as follows:

$$T_c = 1.14\omega_D \exp\left[-1/\left(g_{BCS}N(0) - \frac{2c'S(S+1)I^2N(0)\beta_c}{2-\frac{1}{2}z'(1-\exp(2\beta_c|J'|))}\right)\right], \quad (A-1)$$

with

$$\left. \begin{aligned} J' &= 4/3 \cdot S(S+1)J, \\ c' &= c[1 - (1-c)^z], \\ z' &= 1 + (z-1)c', \\ \beta_c &= 1/T_c, \end{aligned} \right\} \quad (A-2)$$

where  $\omega_D$  is the phonon Debye energy,  $g_{BCS}$  the BCS interaction,  $N(0)$  the density of states at the Fermi level in the normal state,  $c$  the magnetic-ion concentration,  $z$  the number of nearest-neighbor sites and  $S$  being the spin number.  $J$  is the parameter of the nearest-neighbor exchange interaction.  $I$  is the exchange interaction parameter between the conduction electrons and local spins. Superconducting transition temperature  $T_{c0}$  without magnetic ions is given by

$$T_{c0} = 1.14\omega_D \exp[-1/g_{BCS}N(0)]. \quad (A-3)$$

Now, we can calculate the concentration dependence of  $T_c$  by using the relations and parameters given in the text.

In the temperature dependence of  $H_{c2}$ , we use the equation ( MT-5.18 ) for the case with a general value of spin-orbit scattering parameter  $\lambda_{so}$  as follows:

$$\ln \frac{T}{T_{c0}(H)} + \frac{1}{2} \left[ \left( 1 + \frac{b_s}{(b_s^2 - I_s^2)^{1/2}} \right) \psi \left( \frac{1}{2} + \rho_- \right) + \left( 1 - \frac{b_s}{(b_s^2 - I_s^2)^{1/2}} \right) \psi \left( \frac{1}{2} + \rho_+ \right) \right] - \psi \left( \frac{1}{2} \right) = 0 ,$$

( A-4 )

with

$$\left. \begin{aligned} b_s &= (3\tau_{so})^{-1} , \\ I_s &= \sigma h , \\ \rho_{\pm} &= (1/2\pi T) \left[ a_s \pm (b_s^2 - I_s^2)^{1/2} \right] , \\ a_s &= b_s + 1/3 \cdot e\tau_0 v_F^2 B , \\ \lambda_{so} &= 1/3\pi T_{c0} \tau_{so} , \\ \alpha &= e\tau_0 v_F^2 / T_{c0} , \\ B &= H + 4\pi M , \\ \sigma &= + \text{ or } - , \\ h &= -\mu_B B + I_c \langle S_z \rangle , \end{aligned} \right\} \quad ( A-5 )$$

where  $\lambda_{so}$  is the spin-orbit coupling parameter,  $\alpha$  the non-magnetic scattering parameter,  $B$  the magnetic induction,  $\mu_B$  the Bohr magneton and  $\langle S_z \rangle$  being the local spin polarization induced by the field. The magnetization  $M$  is neglected in the calculation.  $\langle S_z \rangle$  is assumed to be Brillouin function with  $S = 7/2$ .  $\psi(x)$  is the digamma function.  $T_{c0}(H)$  is given by



$$T_{c0}(H) = 1.14\omega_D \exp[-1/g_{\text{eff}}(H)N(0)] . \quad (\text{A-6})$$

The effective coupling constant  $g_{\text{eff}}(H)$  is given in antiferromagnetic case as follows:

$$g_{\text{eff}}(H) = g_{\text{BCS}} - I^2 c \left[ \frac{S^2 B'_S(\beta Sa)}{T - 2cJ_0 S^2 B'_S(\beta Sa)} + \frac{2SB_S(\beta Sa)}{a - 2cJ_0 SB_S(\beta Sa)} \right] , \quad (\text{A-7})$$

where  $B_S(x)$  is the Brillouin function,  $B'_S(x) = (d/dx)B_S(x)$  and  $J_0$  is given from Curie Weiss temperature  $\theta$  [  $\theta = \frac{2S(S+1)J_0}{3}$  ].  
 $a$  is given by

$$\left. \begin{aligned} a &= -g' \mu_B H + 2cJ_0 \langle S_z \rangle , \\ g' &= g_J / (g_J - 1) , \end{aligned} \right\} \quad (\text{A-8})$$

where  $g_J$  is Landé g factor.

Now, we can calculate the temperature dependence of  $H_{c2}$  by using the relations and parameters given in the text.

## REFERENCES

- 1) For instance, J.Muller: Rep. Prog. Phys. 43 (1980) 641.
- 2)  $\phi$ .Fischer: Appl. Phys. 16 (1978) 1.
- 3) S.Foner, E.J.McNiff Jr. and E.J.Alexander: Phys. Lett. 49A (1974) 269.
- 4)  $\phi$ .Fischer, H.Jones, G.Bongi, M.Sergent and R.Chevrel: J. Phys. C (Solid State Phys.) 7 (1974) L450.
- 5) K.Okuda, M.Kitagawa, T.Sakakibara and M.Date: J. Phys. Soc. Jpn. 48 (1980) 2157.
- 6) C.Rossel and  $\phi$ .Fischer: J. Phys. F (Met. Phys.) 14 (1984) 455.
- 7) E.Cruceanu and L.Miu: "Proceedings of the LT-17" eds. V.Eckern, A.Schmid, W.Weber and H.Wühl (North-Holland, Amsterdam, Oxford, New York, Tokyo, 1984) p.351.
- 8) K.Hamasaki, K.Hirata, T.Yamashita, T.Komata, K.Noto and K. Watanabe: IEEE Trans. on Mag.MAG-21 (1985) 471.
- 9) K.Okuda, S.Noguchi, T.Masuda, T.Miyatake and M.Ogawa: to be published.
- 10) D.St.James, G.Sarma and E.J.Thomas: "Type II Superconductivity" (Pergamon Press, 1969) p.46.
- 11) A.M.Clogston: Phys. Rev. Lett. 9 (1962) 266; B.S.Chandrasekhar: Appl. Phys. Lett. 1 (1962) 7.
- 12) N.R.Werthamer, E.Helfand and P.C.Hohenberg: Phys. Rev. 147 (1966) 295.
- 13) T.P.Orland and M.R.Beasley: Phys. Rev. Lett. 46 (1981) 1598.
- 14) R.Chevrel, M.Sergent and J.Prigent: J. Solid State Chem. 3 (1971) 515.

- 15) B.T.Matthias, M.Marezio, E.Corenzwit, A.S.Cooper and H.E.Bartz:  
Science 175 (1972) 1465.
- 16)  $\phi$ .Fischer, A.Treyvaud, R.Chevrel and M.Sergent: Solid State  
Comm. 17 (1975) 721.
- 17) W.A.Fertig, D.C.Johnston, L.E.DeLong, R.W.McCallum, M.B.Maple  
and B.T.Matthias: Phys. Rev. Lett. 38 (1977) 987.
- 18) "Ternary Superconductors" eds. G.K.Shenoy, B.D.Dunlap and F.Y.  
Fradin (North-Holland, New York, Amsterdam, Oxford, 1981).
- 19) V.Jaccarino and M.Peter: Phys. Rev. Lett. 9 (1962) 290.
- 20) F.Y.Fradin, G.K.Shenoy, B.D.Dunlap, A.T.Aldred and C.W.Kimball:  
Phys. Rev. Lett. 38 (1977) 719.
- 21) T.Jarlborg and A.J.Freeman: J. Magn. Magn. Mat. 27 (1982) 135.
- 22) S.Maekawa and M.Tachiki: Phys. Rev. B18 (1978) 4688.
- 23) K.Okuda, S.Noguchi, M.Honda, K.Sugiyama and M.Date: "High Field  
Magnetism" ed. M.Date (North-Holland Amsterdam New York Oxford,  
1983) p.143.
- 24)  $\phi$ .Fischer, M.Decroux, S.Roth, R.Chevrel and M.Sergent: J. Phys.  
C8 (1975) L474.
- 25) M.Date, M.Motokawa, K.Okuda, H.Hori and T.Sakakibara: "Physics  
in High Magnetic Fields" eds. S.Chikazumi and M.Miura (Springer-  
Verlag Berlin Heidelberg New York, 1981) p.44.
- 26) A.Yamagishi and M.Date: "High Field Magnetism" ed. M.Date  
(North-Holland Amsterdam New York Oxford, 1983) p.289.
- 27) K.Okuda, S.Noguchi, K.Sugiyama and M.Date: J. Magn. Magn. Mat.  
31-34 (1984) 517.
- 28) K.Okuda, S.Noguchi, M.Honda and M.Date: J. Phys. Soc. Jpn.  
54 (1985) 1560.

- 29) K.Okuda and M.Date: J. Phys. Soc. Jpn. 27 (1969) 839.
- 30) S.Kuroda, M.Motokawa and M.Date: J. Phys. Soc. Jpn. 44 (1978) 1797.
- 31) "Report on Research & Development in High Magnetic Field Laboratory Faculty of Osaka University" ed. M.Date No.1 (1979) p.20.
- 32) K.Okuda and M.Date: J. Phys. Soc. Jpn. 50 (1981) 3827.
- 33) T.Sakakibara: Thesis, Osaka University, 1983.
- 34) M.Motokawa: J. Phys. Soc. Jpn. 44 (1978) 1804.
- 35) T.Yosida: "High Field Magnetism" ed. M.Date (North-Holland Amsterdam New York Oxford, 1983) p.289.
- 36) M.B.Maple, L.E.DeLong, W.A.Fertig, D.C.Johnston, R.W McCallum and R.N.Shelton: "Valence Instabilities and Related Narrow-band Phenomena" ed. R.D.Parks (New York Plenum 1977) p.17.
- 37) R.Bailif, A.Dunand, J.Muller and K.Yvon: Phys. Rev.Lett. 47 (1981) 672.
- 38) D.W.Harrison, K.C.Lim, J.D.Thompson, C.Y.Huang, P.D.Hambourger and H.L.Luo: Phys. Rev. Lett. 46 (1981) 280.
- 39) M.Ishikawa and  $\phi$ .Fischer: Solid State Comm. 24 (1977) 747.
- 40) M.Decroux,  $\phi$ .Fischer, R.Flükiger, B.Seeber, R.Delesclafs and M.Sergent: Solid State Comm. 25 (1978) 393.
- 41) R.D.Parks: "Superconductivity" (Macel Dekker Inc. New York, 1969) Vol.2, p.1114, 1122; D.Saint-James, G.Sarma and E.J. Thomas: "Type II Superconductivity" (Pergamon Press, 1970) p.231.
- 42) M.Isino, N.Kobayashi, Y.Muto: "Ternary Superconductors" eds. G.K.Shenoy, B.D.Dunlap and F.Y.Fradin (North-holland New York Amsterdam Oxford, 1981) p.95; H.W.Meul, C.Rossel, M.Decroux,

- $\phi$ .Fischer, G.Remenyi and A.Briggs: Phys. Rev. Lett. 53 (1984) 497.
- 43) B.D.Dunlap, G.K.Shenoy, F.Y.Fradin, C.D.Barnet and C.W.Kimball: J. Magn. Magn. Mat. 13 (1979) 319.
- 44) J.D.Thompson, M.P.Maley, C.Y.Huang, J.O.Willis, J.L.Smith and H.L.Luo: J. Low Temp. Phys. 43 (1981) 243.
- 45) J.O.Willis, J.D.Thompson, C.Y.Huang and H.L.Luo: J. Appl. Phys. 52 (1981) 2174.
- 46) T.Kasuya, M.Kasaya, K.Takegahara, T.Fujita, T.Goto, A.Tamaki, M.Takigawa and H.Yasuoka: J.Magn. Magn. Mat. 31-34 (1983) 447.
- 47) M.Kasaya, F.Iga, K.Negishi, S.Nakai and T.Kasuya: J. Magn. Magn. Mat. 31-34 (1983) 437.

## PART II

### VALENCE OF Ce AND KONDO EFFECT IN $Ce_xLa_{1-x}Mo_6S_8$

#### ABSTRACT

Valence of Ce and Kondo effect in the Chevrel compound  $Ce_xLa_{1-x}Mo_6S_8$  was investigated by XPS, X-ray diffraction, electrical resistance, magnetoresistance and magnetic susceptibility measurements in a temperature range down to 0.4 K.

The concentration dependence of lattice constant follows the Vegard's law in a whole concentration region of Ce. The Ce 3d and 4d XPS spectra of  $CeMo_6S_8$  show strong peaks with the initial state of  $Ce^{3+}$  and no peaks due to  $Ce^{4+}$ . Superconducting properties with low x are well explained by the Matsuura-Ichinose-Nagaoka theory based on the Kondo effect with a range of  $T_K/T_{C0} = 0.01 \sim 0.001$ , where  $T_K$  and  $T_{C0}$  are the Kondo temperature and the superconducting transition temperature without magnetic ions, being  $T_{C0} \approx 6$  K, respectively. The magnetic susceptibility per mole Ce is independent of the Ce concentration and it is explained by the crystal field splitting and Kondo effect. A model of crystal field splitting which consists of three doublets with the excited energy of 10 K and 400 K in  $CeMo_6S_8$  is proposed. A large negative magnetoresistance was found below 10 K for  $CeMo_6S_8$ , which shows  $\log H$  dependence below 1.2 K. Magnetic and superconducting phase diagram of  $Ce_xLa_{1-x}Mo_6S_8$  was determined.

## § 1. INTRODUCTION

Rare earth compounds are important magnets as well as transition metal compounds. So far, magnetic properties of the compounds have been usually explained by the model of well localized 4f electrons of the rare earth ions. Recently, Ce or Yb intermetallic compounds have been intensively investigated by many researchers because of their peculiar behavior on magnetic or transport properties associated with the valence fluctuation and Kondo effect.<sup>1)</sup>

Cerium Chevrel compound  $\text{CeMo}_6\text{S}_8$  is known to be exceptionally lack of superconductivity among the rare earth Chevrel compounds  $\text{REMo}_6\text{S}_8$  which are all superconducting and coexist with antiferromagnetic ordering at low temperatures<sup>2)</sup>. The electronic energy band of Chevrel compounds is characterized by the high Mo d-band density of states (DOS) at  $E_F$  and the low conduction electron DOS at RE site<sup>3)</sup>. The specific heat of  $\text{CeMo}_6\text{S}_8$  was measured by Maple et. al.<sup>4)</sup>, which is shown in Fig.1. As is shown in the figure, the magnetic contribution to the specific heat  $C_m$  has a peak at 2.5 K suggesting the magnetic ordering and a relatively high value of  $\gamma$ ,  $\gamma \approx 100 \text{ mJ/mole}\cdot\text{K}^2$ , which is estimated from their data in a temperature region from 4.5 to 8 K. Temperature dependence of the magnetization was measured for  $\text{CeMo}_6\text{S}_8$  under several magnetic fields from 0.64 to 7.8 kOe by Pelizzone et. al.<sup>5)</sup>, which is shown in Fig.2. Their results show that the magnetization for the fields below about 3 kOe has a weak maximum and minimum at 2.3 and 1.6 K, respectively and followed by an increase with decreasing temperature. However, the magnetization for the fields above 4 kOe

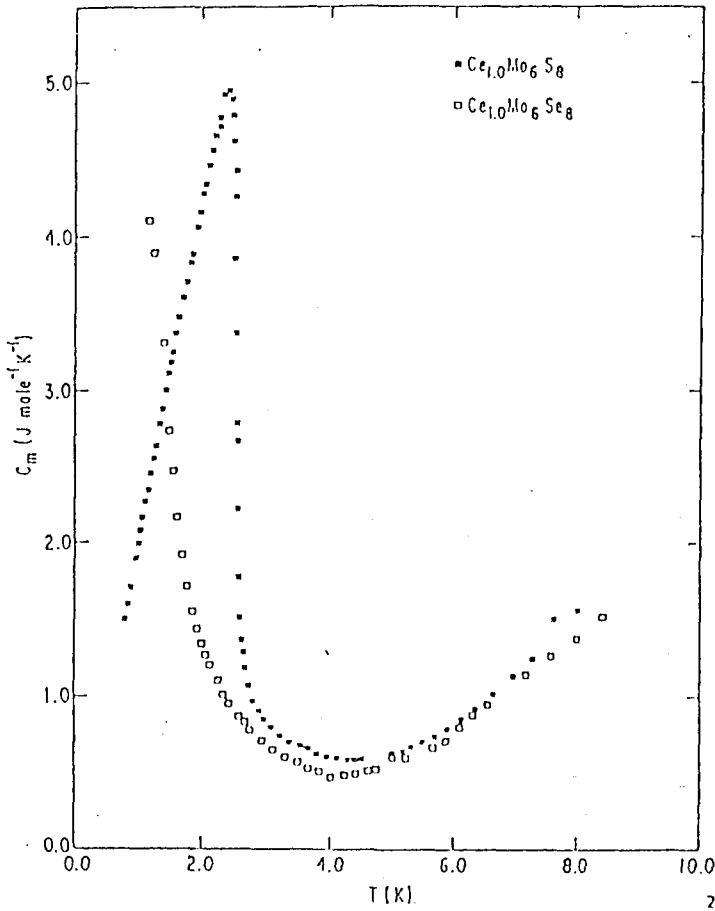
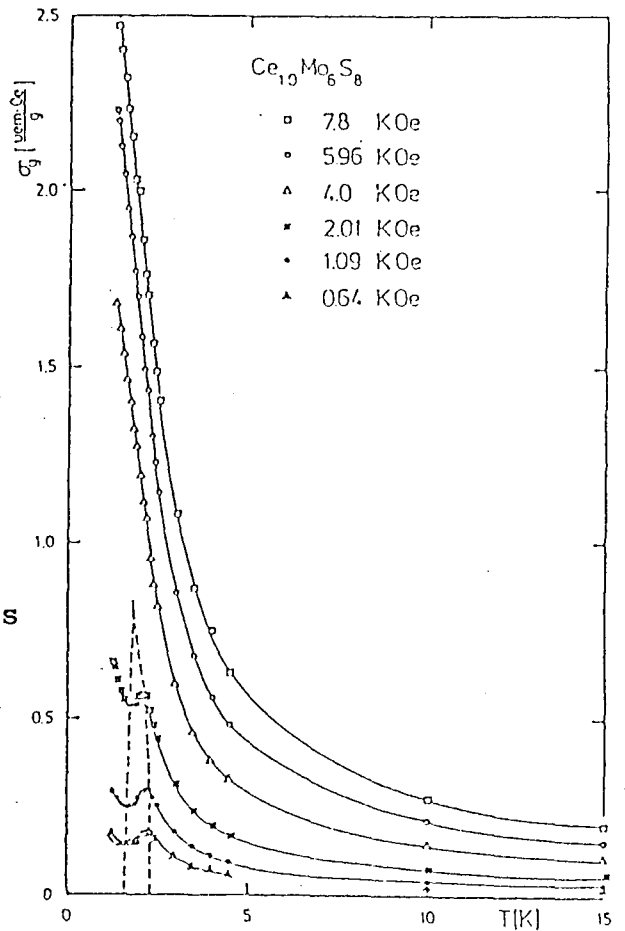


FIG.1

Magnetic heat capacity  $C_m$  versus temperature  $T$  for  $Ce_{1.0}Mo_6S_8$  and  $Ce_{1.0}Mo_6Se_8$ .<sup>4)</sup>

FIG.2

Specific magnetization  $\sigma_g(T)$  versus temperature between 1.28 and 15 K and for different constant values of the magnetic field for  $Ce_{1.0}Mo_6S_8$ .<sup>5)</sup>





shows no such an anomaly around 2 K but an increase as Curie-Weiss law. These results suggest that the compound is antiferromagnetically ordered near  $T_N \approx 2.4$  K and the critical field to the paramagnetic state is about 4 kOe.

The magnetic ordering temperature  $T_m$  and superconducting transition temperature  $T_c$  for  $RE_xMo_6Se_8$  and  $RE_xMo_6S_8$  compounds are summarized for RE constituent in Fig.3. The dashed lines are linear interpolations between the superconducting transition temperatures of the nonmagnetic endmember La and Lu molybdenum selenide and sulfide compounds which represent a first approximation to the transition temperatures of the RE compounds with partially-filled 4f electron shells in the absence of pair breaking interactions due to the magnetic moments of the RE ions. The depressions of  $T_c$  relative to these linear interpolations are also shown by  $\Delta T_c$  in Fig.3. Here it can be seen that the systematic variation of  $\Delta T_c$  with RE can be described qualitatively by the deGennes factor  $(g-1)^2 J(J+1)$  ( represented by the solid lines in Fig.3 ) where  $g$  is the Landé  $g$ -factor and  $J$  is the total angular momentum of the Hund's rule ground state. This follows from the AG theory<sup>6)</sup> for RE impurity ions in the limit of low impurity concentration  $n$  for which  $\Delta T_c \propto nN(0)J^2(g-1)^2J(J+1)$ , where  $N(0)$  is the density of states at the Fermi energy  $E_F$  which is presumed not to vary substantially with RE ions.  $J$  is the exchange interaction between conduction electrons and the RE ions, which is small, i.e.,  $J \sim 0.01$  eV in the compounds.  $CeMo_6S_8$  does not follow the general trends exhibited by the other RE ions. Similar situation is realized on the magnetic ordering temperatures of the compounds. The  $T_m$  of the rare earth

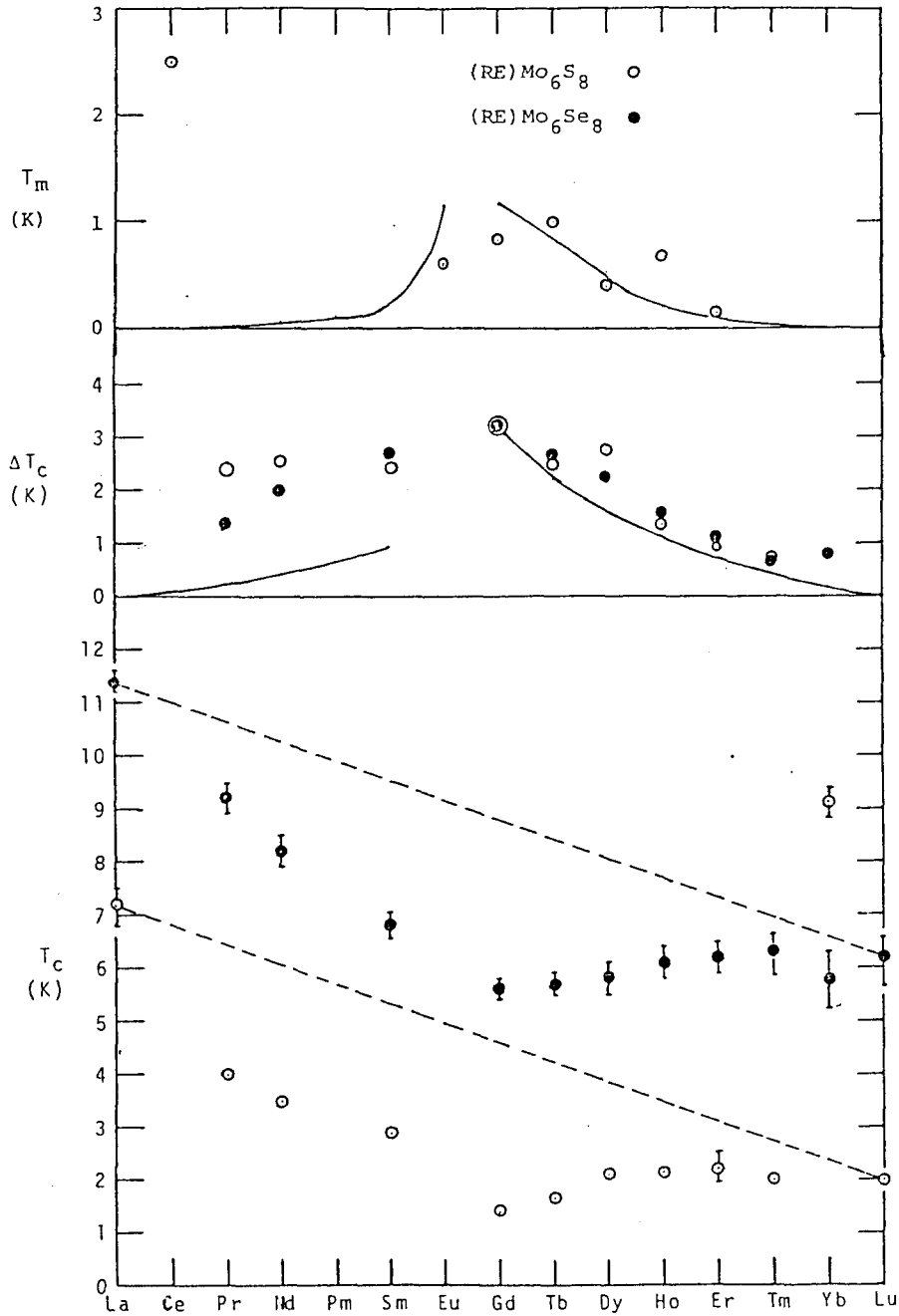


FIG.3 Magnetic ordering temperature  $T_m$ , superconducting transition temperature  $T_c$  and depression of  $T_c$  ( $\Delta T_c$ ) versus RE constituent for  $(RE)_xMo_6S_8$  and  $(RE)_xMo_6Se_8$  compounds. The dashed lines represent the interpolated  $T_c$ 's of the RE molybdenum chalcogenide compounds in the absence of magnetic pair breaking interactions. The solid lines are proportional to deGennes factor which is a parameter of the magnetic interaction.

Chevrel compounds are almost below 1 K and show a systematic variation with RE in proportion to the deGennes factor. However, the  $T_N$  of  $CeMo_6S_8$  is higher away from the systematic variation.

In the present work, to investigate these problems in  $CeMo_6S_8$ , a systematic study of XPS, X-ray diffraction, electrical resistance, magnetoresistance and magnetic susceptibility measurements was done in the system  $Ce_xLa_{1-x}Mo_6S_8$ .<sup>7-10)</sup> The results on the valence of Ce in  $CeMo_6S_8$  are given in Section 3. The superconducting properties of  $Ce_xLa_{1-x}Mo_6S_8$  with  $x \leq 0.14$  and the magnetic properties of  $Ce_xLa_{1-x}Mo_6S_8$  with  $x > 0.2$  are discussed in Section 4 and 5, respectively.

## § 2. EXPERIMENTAL

Samples of  $Ce_xLa_{1-x}Mo_6S_8$  were prepared by sintering from  $Ce_2S_3$ ,  $La_2S_3$ ,  $MoS_2$  and Mo powders. The procedure is shown in Fig.4. The rare-earth sulfides used in the sintering were obtained by the chemical reaction between  $(RE)Cl_3$  and  $H_2S$  at 1000 °C for 2 hours, where RE = Ce or La. The sulfides  $MoS_2$ ,  $Ce_2S_3$  and  $La_2S_3$  were heated to dehydrate at 200 °C for 24 hours with pumping. Mo powder was deoxidized under a flow of hydrogen gas at 1000 °C for 10 hours. Appropriate amounts of these powders were well ground together, pressed into tablets of 10 mmD x 1 mmT and reacted at 1350 °C for 3 hours under an argon atmosphere of 40 kg/cm<sup>2</sup> in a high pressure furnace after preheating at 400 °C for 24 hours. Subsequently, they were crushed, reground, pressed again into tablets and annealed at 1350 °C. To get a homogeneous phase, the samples with low concentration of Ce were prepared by dilution in cascade from the concentrated samples. The crystal structure was checked at each step by the X-ray diffraction and the Chevrel phase was confirmed with no trace of the other phase. The ratio of constitutional elements was checked by EPMA analysis.

The compounds  $Ce_xLa_{1-x}Mo_6S_8$  crystallize in a hexagonal rhombohedral unit cell. The lattice constant  $a_r$  and the angle  $\alpha$  in the rhombohedral unit cell were determined by a standard X-ray diffraction method at room temperature. The angle of the powder diffraction pattern is calibrated by a standard sample of Si.

XPS measurements were done on the compound  $CeMo_6S_8$  at room temperature by using a standard photoelectron spectrometer ( SHIMAZU

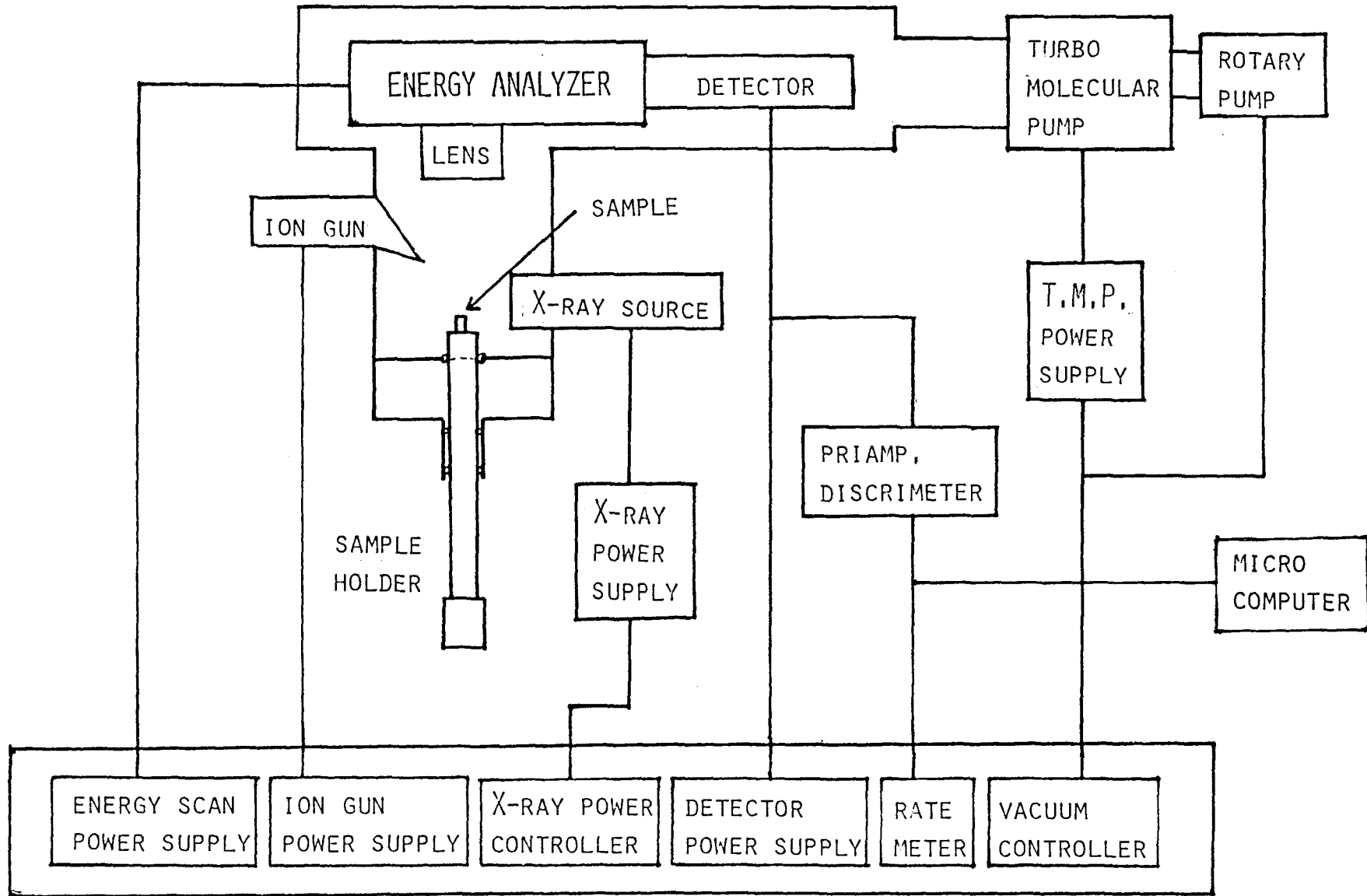
FIG.4. Sample Preparation Procedure of  $Ce_xLa_{1-x}Mo_6S_8$

- 1)  $LaCl_3 \cdot nH_2O \longrightarrow LaCl_3 + nH_2O$   
 $CeCl_3 \cdot nH_2O \longrightarrow CeCl_3 + nH_2O$  ) at 200 °C for 2 hours
- 2)  $2LaCl_3 + 3H_2S \longrightarrow La_2S_3 + 6HCl \uparrow$   
 $2CeCl_3 + 3H_2S \longrightarrow Ce_2S_3 + 6HCl \uparrow$  ) at 1000 °C for 1.5 hours
- 3)  $MoS_2, Ce_2S_3, La_2S_3$  : dehydrated at 200 °C for 24 hours  
 Mo : deoxidized at 1000 °C for 10 hours with  $H_2$  gas
- 4)  $0.5xCe_2S_3 + 0.5(1-x)La_2S_3 + 3.25MoS_2 + 2.75Mo$   
 mixed powder is pressed into tablet at 10 t/cm<sup>2</sup>  
 $\longrightarrow Ce_xLa_{1-x}Mo_6S_8$   
 sintered at 400 °C for 24 hours and 1350 °C  
 for 3 hours at 40 kg/cm<sup>2</sup> Ar gas atmosphere
- 5)  $Ce_xLa_{1-x}Mo_6S_8$  : X-ray check
- 6) Annealed at 1350 °C for 3 hours at 40 kg/cm<sup>2</sup> Ar gas
- 7)  $Ce_xLa_{1-x}Mo_6S_8$  : X-ray check and EPMA analysis

ESCA 750 ) with the Mg-K $\alpha$  line ( 1253.6 eV ) as an exciting source. The block diagram is shown in Fig.5. The sample was prepared by cutting into a small tablet of 5 mmD x 1 mm from the sintered materials and polishing the surface. In order to obtain signals from the inside of tablet, the surface of the sample on the mount piece was sputtered with argon ion beam of 15  $\mu$ A accelerated with 2 kV during 5 minutes under argon atmosphere of  $10^{-6}$  Torr. After that, the chamber was evacuated below  $10^{-8}$  Torr by turbo molecular pump and spectra of XPS were obtained. Excited voltage of Mg-K $\alpha$  and emission current were 8 kV and 30 mA, respectively. The measurements were done automatically by connecting the micro-computer where the data were processed and stored. The binding energy of the XPS spectra was calibrated with the Au 4f $_{7/2}$  level ( 83.8 eV ).

Superconducting transition temperature  $T_c$  was determined by using conventional four probe dc electrical resistance method down to 0.4 K by  $^3\text{He}$  refrigerator. The upper critical magnetic field  $H_{c2}$  was measured by the magnetoresistance method. Temperature dependence of the magnetic susceptibility was measured by using the Faraday type magnetometer ( CAHN 2000 ). High field magnetization and magnetoresistance measurements were done in High Field Laboratory of Osaka University. Details of the measurement systems are mentioned at Section 3 in PART I.

MEASUREMENT CHAMBER  $\sim 10^{-8}$  TORR



OPERATION CONTROLLER

FIG. 5 Block diagram of XPS measurement (ESCA 750)

### § 3. VALENCE OF Ce IN $\text{CeMo}_6\text{S}_8$

Valence of Ce in the Chevrel compound  $\text{CeMo}_6\text{S}_8$  was investigated by lattice constant and XPS measurements at room temperature.<sup>7)</sup>

The lattice constant  $a_r$  and the angle  $\alpha$  in the rhombohedral unit cell were determined by the X-ray diffraction method. Obtained values are shown in Fig.6 as a function of Ce concentration in the system  $\text{Ce}_x\text{La}_{1-x}\text{Mo}_6\text{S}_8$ . The lattice constant  $a_r$  decreases linearly with increasing Ce concentration as in Fig.6(a), following the Vegard's law<sup>11)</sup> in a whole concentration region of Ce within our experimental errors. The concentration dependence of  $a_r(x)$  is given by a following experimental formula

$$a_r(x) = ( 6.521 - 0.014 \cdot x ) \pm 0.001 \text{ \AA} , \quad ( 2-1 )$$

where  $x$  is the Ce concentration. The angle  $\alpha$  has almost constant value of  $( 88.77 \pm 0.02 )^\circ$  as shown in Fig.6(b).

Fig.7 shows the Ce 3d XPS spectrum in  $\text{CeMo}_6\text{S}_8$ . Two strong peaks with binding energies 904.5 and 885.9 eV are assigned to the  $3d_{3/2}$  and  $3d_{5/2}$  transitions with a  $4f^1$  final state of  $\text{Ce}^{3+}$ , labelled by  $\text{Ce}^{3+}(4f^1)$  in the figure. Two weak shoulders, whose binding energies are approximately 3.3 eV lower than main peaks, are their shake-down satellites with a  $4f^2$  final state of  $\text{Ce}^{3+}$ , labelled by  $\text{Ce}^{3+}(4f^2)$  in Fig.7. The peak associated with  $\text{Ce}^{4+}(4f^0)$  expected near 915 eV<sup>12,13)</sup> does not appear above the noise level which is about 1.7 % of the peak intensity of  $\text{Ce}^{3+}$ . Fig.8 shows the Ce 4d XPS spectrum in  $\text{CeMo}_6\text{S}_8$ . A single broad peak is found near 111.9



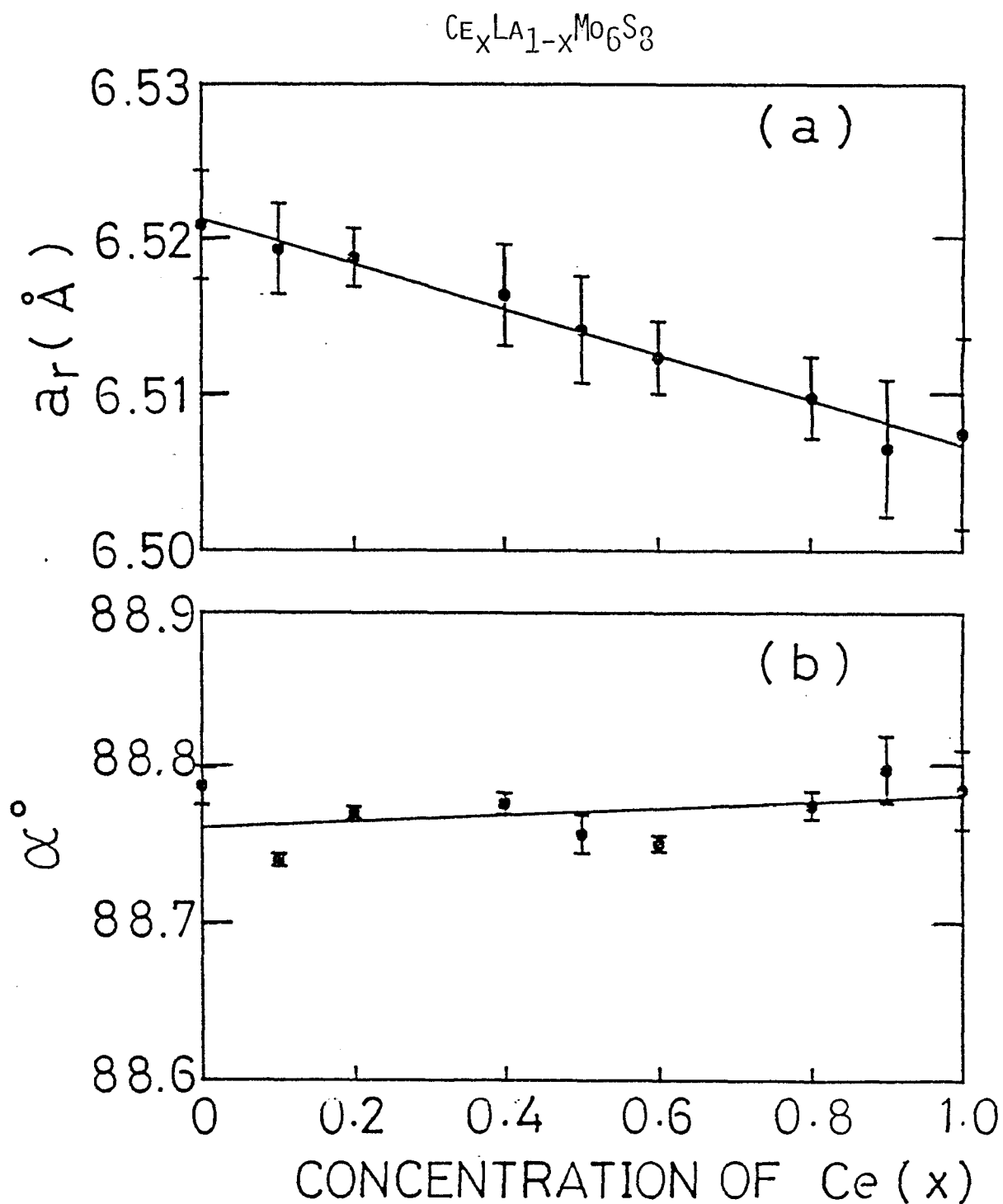


FIG.6 (a) Concentration dependence of lattice constant  $a_r(x)$  and (b) angle  $\alpha(x)$  of the rhombohedral unit cell in the system  $\text{Ce}_x\text{La}_{1-x}\text{Mo}_6\text{S}_8$ .

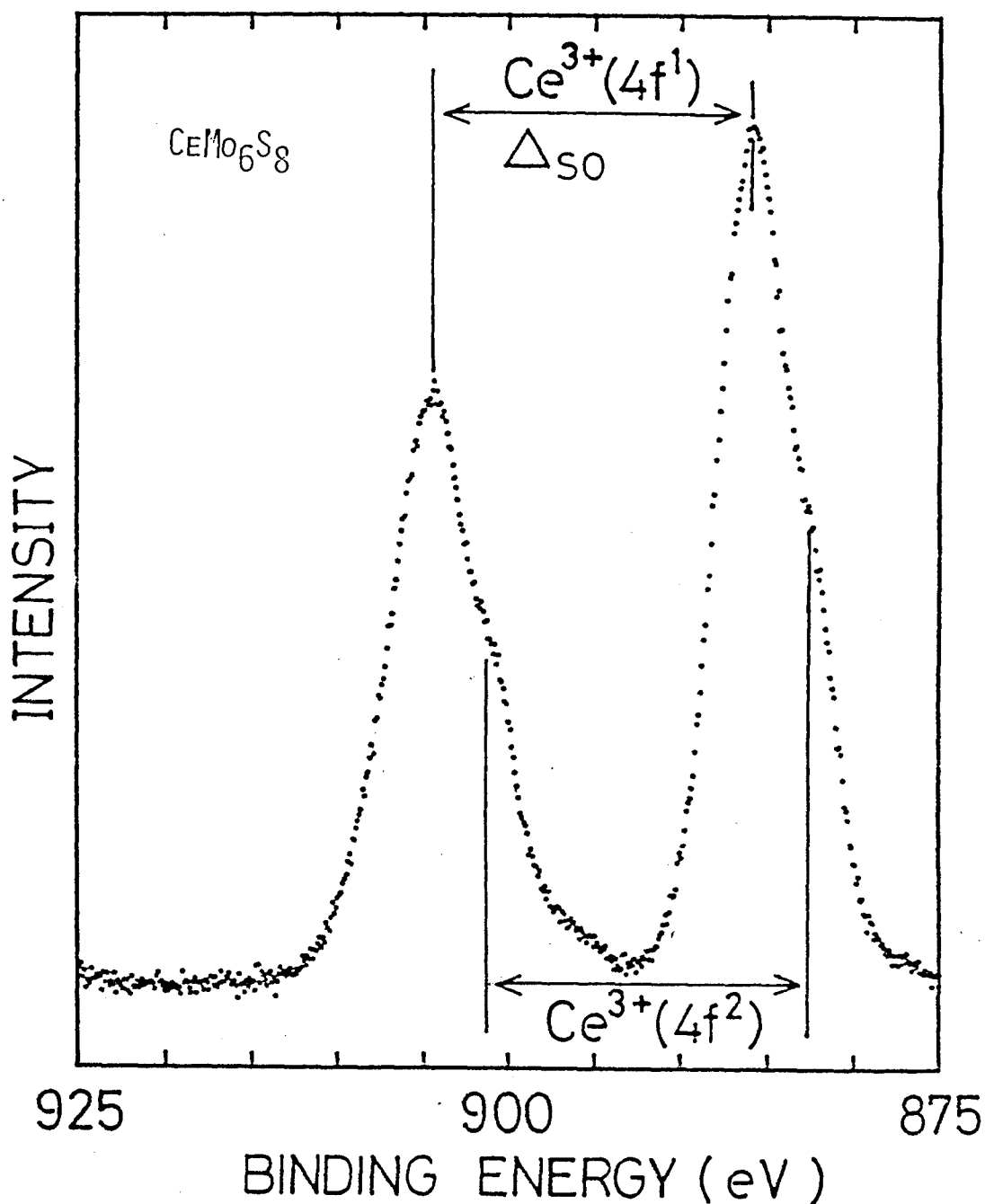


FIG.7 Ce 3d XPS spectrum of  $\text{CeMo}_6\text{S}_8$ . The peaks are labelled by the valence of Ce in the initial state and the number of 4f electrons in the final state.  $\Delta_{\text{SO}} = 18.6$  eV is the spin-orbit splitting. The peaks are normalized to the height of the  $3d_{5/2}$  peak.

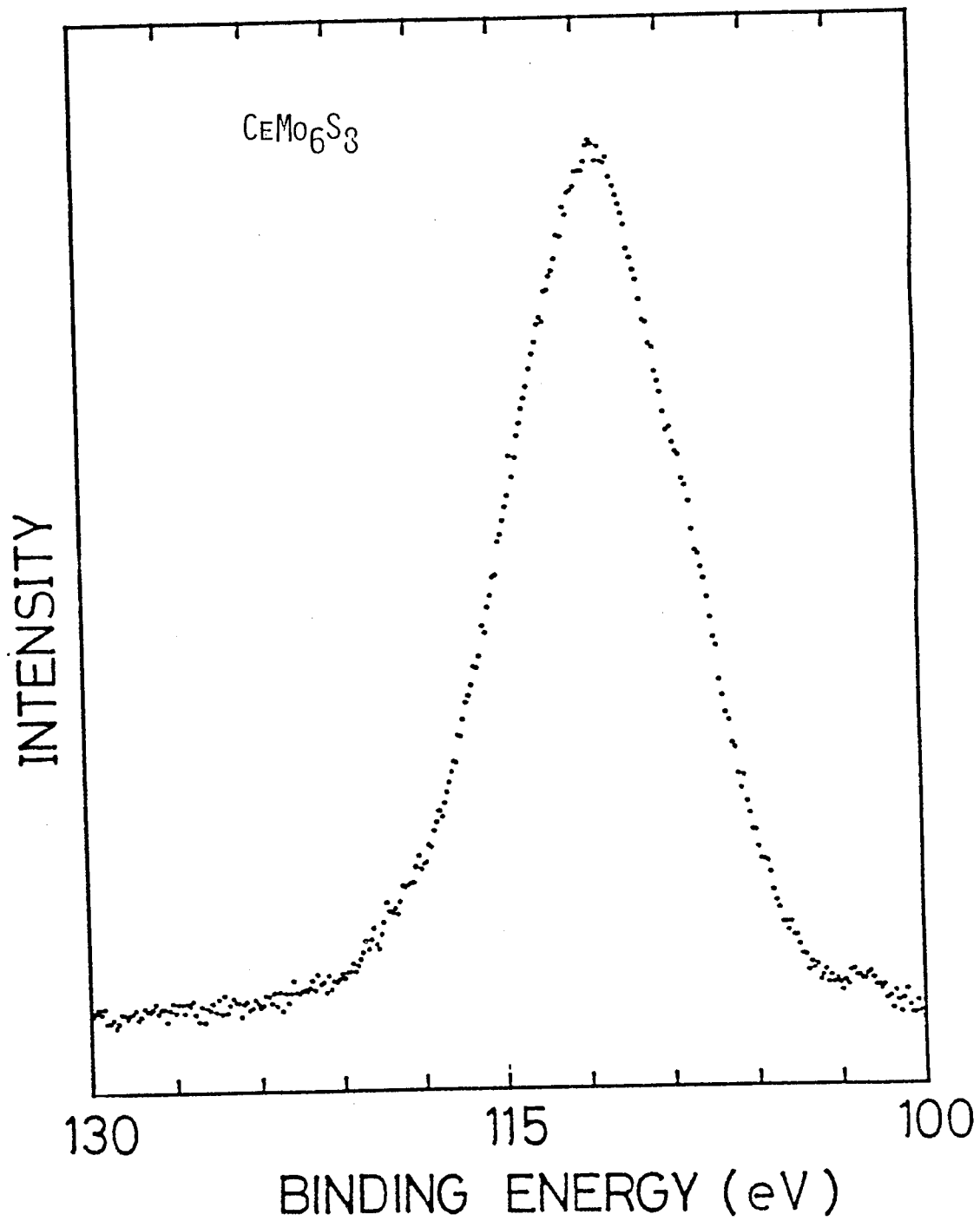


FIG.8 Ce 4d XPS spectrum of CeMo<sub>6</sub>S<sub>8</sub>. The spectrum is normalized to the height of the main peak.

eV. The peaks due to  $4d_{3/2}$  and  $4d_{5/2}$  are poorly resolved due to multiplet effects and the peak due to  $Ce^{4+}(4f^0)$ , which might be appeared around 120 eV<sup>12)</sup> if  $Ce^{4+}$  is mixed, is not found above the noise level. If we assume that the relative intensity of the peaks due to  $Ce^{4+}$  and  $Ce^{3+}$  ions is proportional to the mixing ratio of these states in the sample, the amplitude of  $Ce^{4+}$  state must be less than 2 %. The results are summarized in Table 1.

From the experimental results that the concentration dependence of lattice constant  $a_r(x)$  in  $Ce_xLa_{1-x}Mo_6S_8$  follows the Vegard's law and the relative intensity of the XPS peaks  $I(Ce^{4+})/I(Ce^{3+})$  is less than 2 %, it is concluded that  $CeMo_6S_8$  is not a mixed valence compound and the valence of Ce is trivalent.

TABLE 1 Binding Energies for  $\text{CeMo}_6\text{S}_8$

		B. E. ( eV )			B. E. ( eV )	
		$3d_{3/2}$	$3d_{5/2}$	$\Delta_{\text{s.o.}}(3d)$	$4d_{3/2}$	$4d_{5/2}$
$\text{Ce}^{3+}$	$(4f^1)$	904.5	885.9	18.6	111.9	
	$(4f^2)$	901.3	882.6	18.7		
$\text{Ce}^{4+}$	$(4f^0)$	—	—		—	—

$$\text{Ce}^{4+} / \text{Ce}^{3+} \approx \frac{I(4f^0)}{I(4f^1 + 4f^2)} \lesssim 1.7\%$$

#### § 4. SUPERCONDUCTING PROPERTIES

Superconducting transition temperature  $T_c$  defined by a midpoint of the resistive transition was obtained as a function of Ce concentration in the dilute system  $Ce_xLa_{1-x}Mo_6S_8$  as shown in Fig.9. In the figure the  $T_c$  is reduced by that of  $LaMo_6S_8$   $T_{c0} = 5.6$  K. The vertical bar of experimental points means the transition width from 10 % to 90 % of the transition curve. When the concentration of Ce is increased, the  $T_c$  is decreased with the initial decrease of  $-(dT_c/dx)_{x=0} = 0.2$  K/at.%Ce. It is rather small compared with the case of Ce impurities in  $La_{1-y}Th_y$ <sup>14)</sup> where the valence of Ce is strongly fluctuated; for instance, Ce ions on the La-rich side is magnetic and non-magnetic on Th-rich side, and the initial decrease is  $1 \sim 6$  K/at.%Ce depending on the Th concentration. The weak depression of  $T_c$  in the present compounds suggests the weak coupling between the Ce ions and the conduction electrons.

Transition width becomes broad near  $x = 0.14$  as shown in the figure. The transition curve of electrical resistance for the sample with  $x = 0.14$  is shown in Fig.10. It shows a gradual decrease, leaving a small trace of residual resistance at 0.4 K with decreasing temperature. So, the critical concentration for the break of superconductivity is likely to be  $x_c = 0.14$ .

The upper critical field  $H_{c2}$  was also measured as a function of temperature for the compositions with  $0 \leq x \leq 0.13$ . The  $H_{c2}$  is defined by the field of midpoint of the resistive transition. The results are shown in Fig.11. The  $H_{c2}(T)$  of non-magnetic superconductor  $LaMo_6S_8$  is well explained by the universal curve<sup>15)</sup> determined

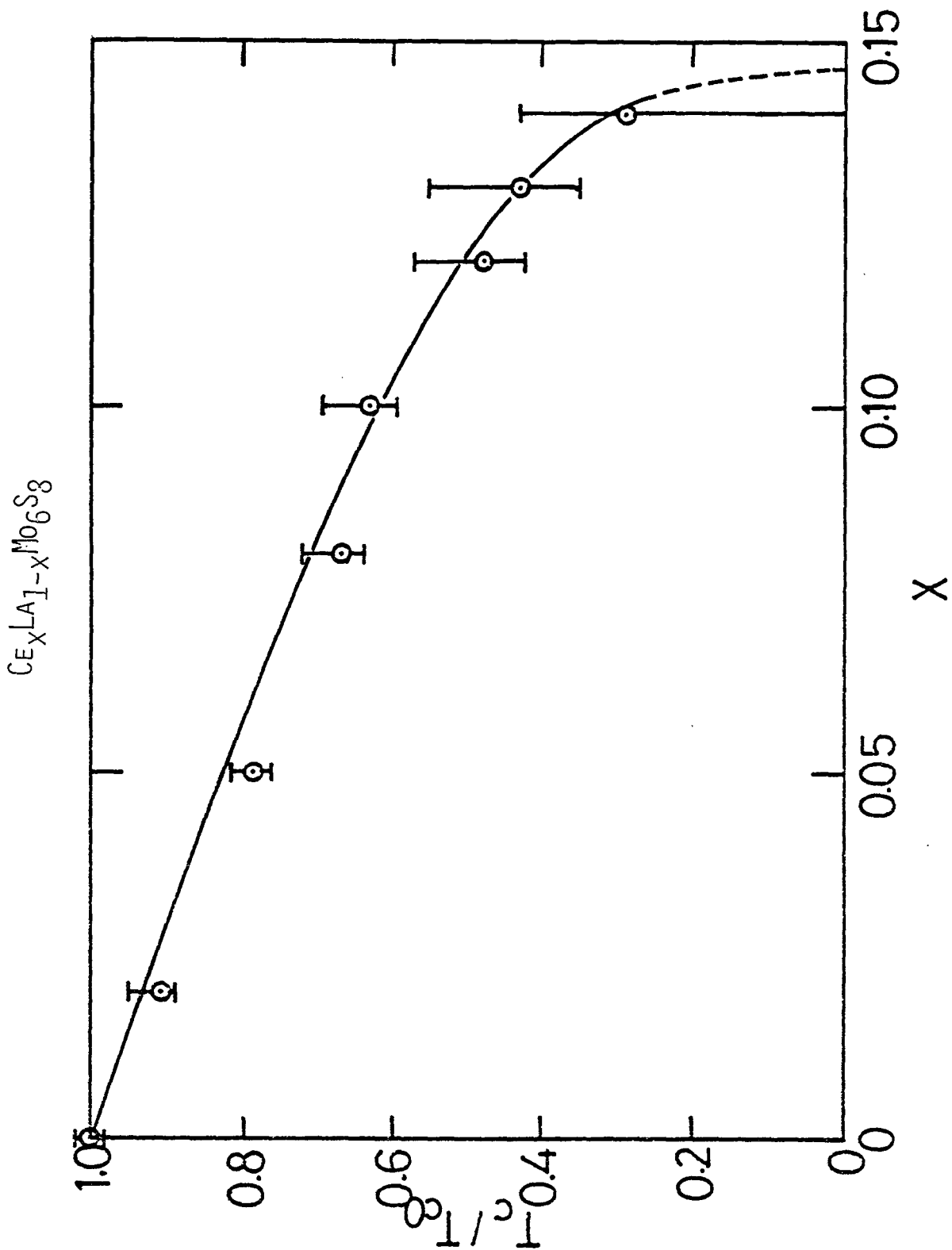


FIG.9 Superconducting transition temperature as a function of Ce concentration in the system  $Ce_xLa_{1-x}Mo_6S_8$ .  $T_c$  is reduced by that of  $LaMo_6S_8$   $T_{c0} = 5.6$  K. White circle and vertical bar of the data points mean the  $T_c$  defined by a midpoint and 10 % to 90 % of the resistive transition curve, respectively.

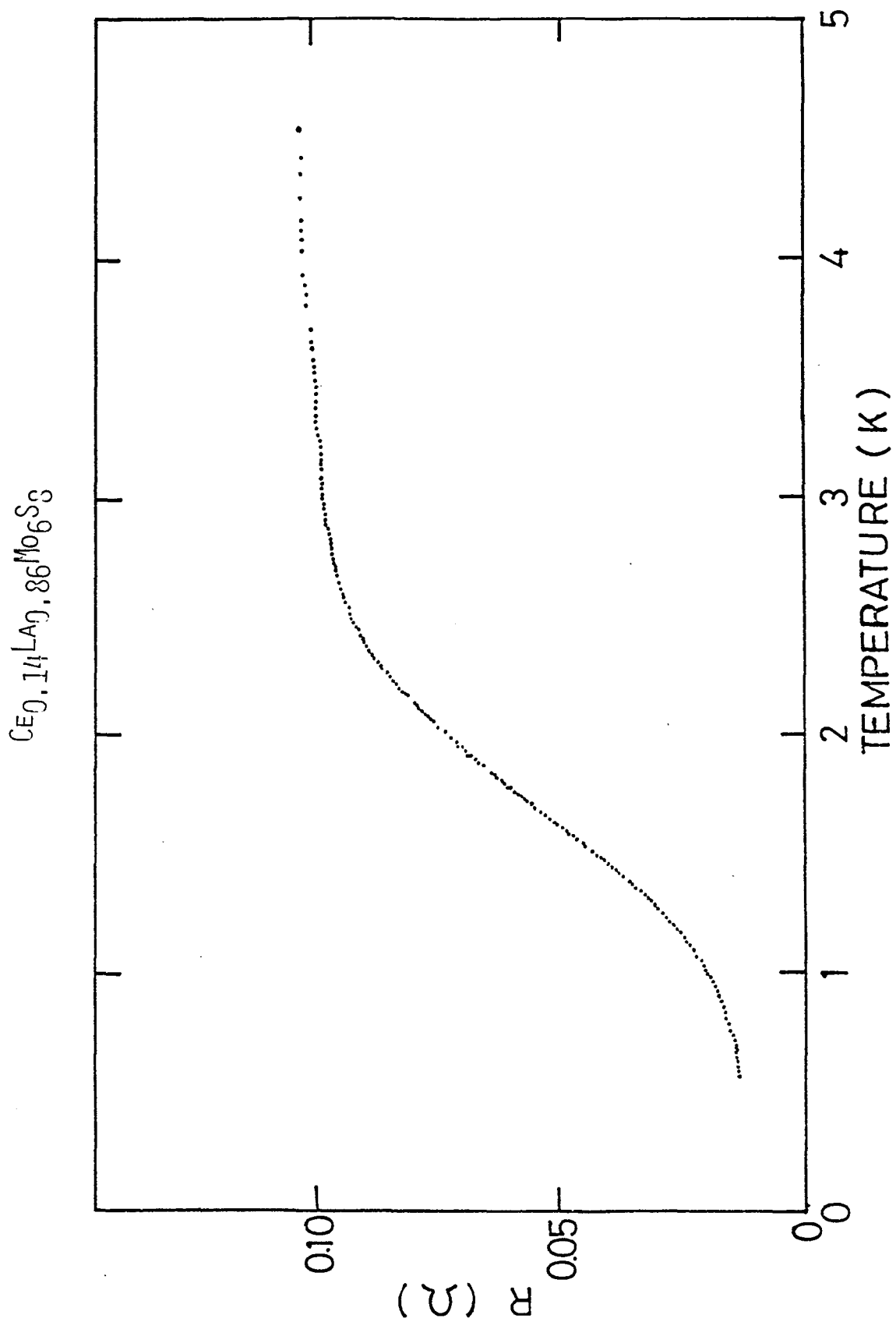


FIG.10 Transition curve of electrical resistance for  $\text{Ce}_{0.14}\text{La}_{0.86}\text{Mo}_6\text{S}_8$ . Transition is rather broad, leaving a small trace of residual resistance at 0.4 K.



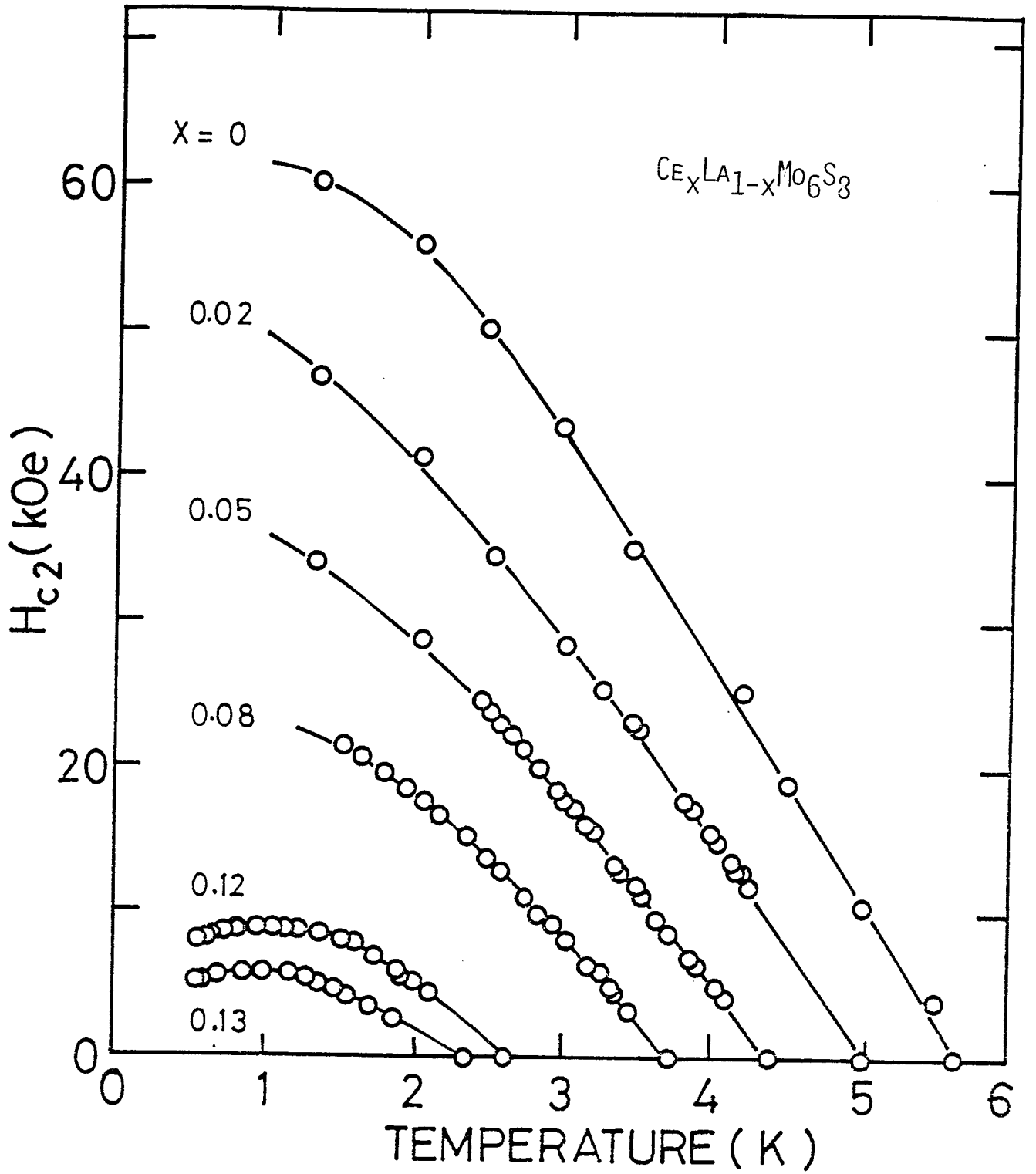


FIG.11 Temperature dependence of  $H_{c2}$  as a parameter of Ce concentration  $x$  in the system  $Ce_xLa_{1-x}Mo_6S_8$ .

by the following relation

$$\ln(1/t) = \psi(1/2 + h/2t) - \psi(1/2) , \quad ( 2-2 )$$

where  $t = T/T_c$ ,  $h = 0.281 \cdot H_{c2}(T)/H_{c2}(0)$  and  $\psi(z)$  is the digamma function. On the other hand, the  $H_{c2}(T)$  curves for the compositions with  $x = 0.12$  and  $0.13$  show a broad maximum near 1.2 K. It suggests a characteristic behavior of the Kondo effect for the case with small  $T_K/T_{c0}$  and relatively high concentration of Kondo impurities.<sup>16)</sup>

To check the magnetic state of Ce impurity in the compounds, as usually done, we plot the initial slope of  $H_{c2}(T)$  curve,  $(dH_{c2}/dT)_{T_c}$  as a function of  $T_c$  in Fig.12, where both the initial slope and  $T_c$  are reduced by those of  $\text{LaMo}_6\text{S}_8$ . Here we apply the theory of Kondo effect in superconductivity given by Matsuura-Ichinose-Nagaoka ( hereafter we call the theory as MIN )<sup>16)</sup>. In the figure the calculated curves by the MIN theory are given by solid lines as a parameter of  $T_K/T_{c0}$  ( see APPENDIX I ), together with the curve of broken line calculated by the AG theory<sup>6)</sup>. For  $T_K/T_{c0} > 1$  the initial slope increases abruptly with decreasing the  $T_c$  in low temperature. In the case of  $T_K/T_{c0} < 1$ , on the other hand, it decreases monotonically with decreasing the  $T_c$  and the curve becomes close to AG curve with approaching  $T_K/T_{c0} = 0$ . For  $T_K/T_{c0} \sim 1$ , the curves obtained by numerical calculations are unstable in the low temperature region, so they are not shown in the figure. Our experimental data deviate clearly from the AG curve and distribute over the MIN curves with the value of parameter  $T_K/T_{c0} =$

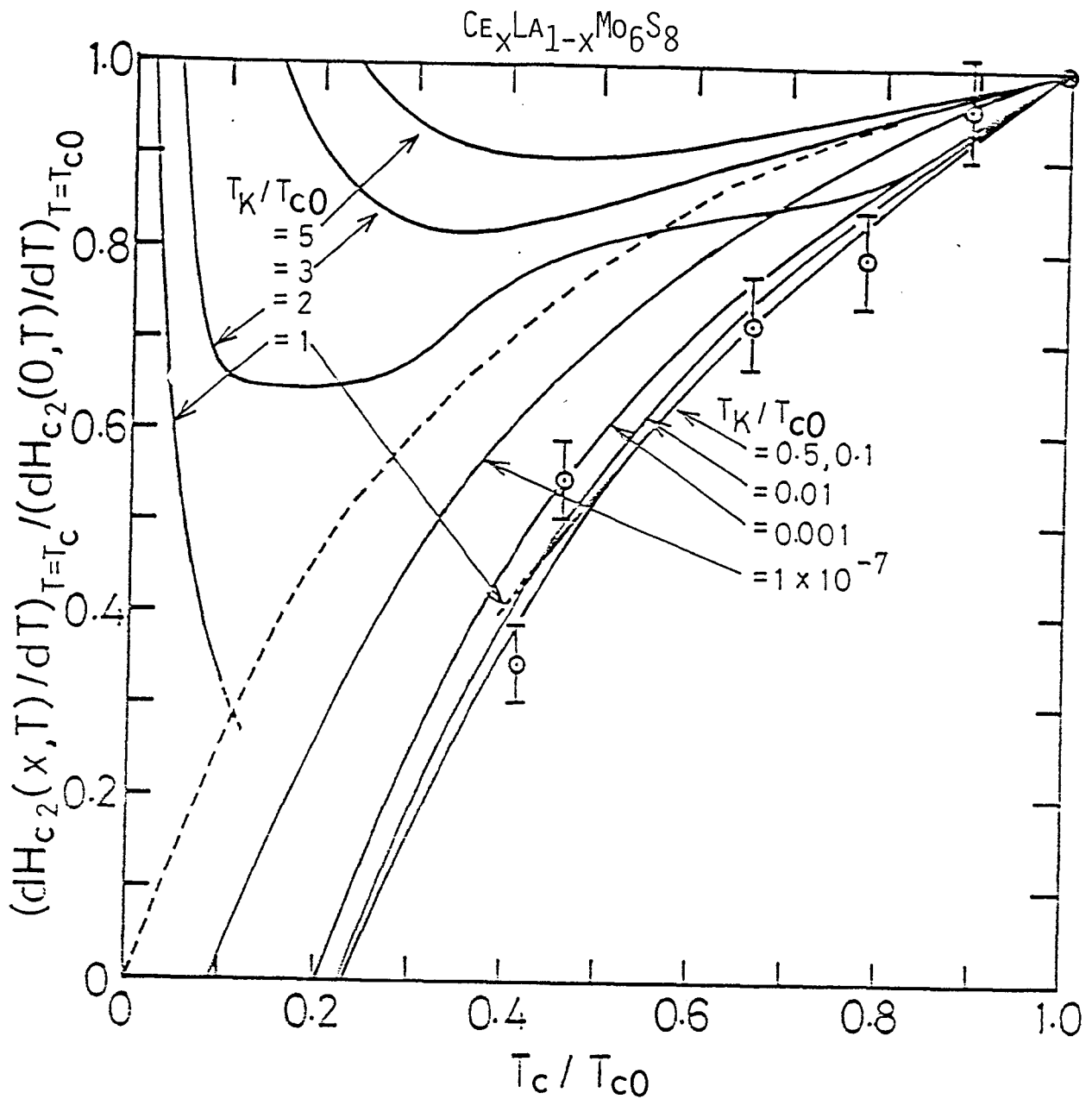


FIG.12 The initial slope of the  $H_{c_2}(T)$  curve,  $(dH_{c_2}/dT)_{T_c}$  as a function of reduced temperatures  $T_c/T_{c0}$ . The initial slope is also reduced by that of  $\text{LaMo}_6\text{S}_8$ . Solid lines are calculated by the theory of MIN.<sup>16)</sup> A broken line is for the AG theory<sup>6)</sup>. The MIN curves obtained by numerical calculations are unstable in the low-temperature region for  $T_K/T_{c0} \sim 1$ , so they are not shown in the figure.

0.001  $\sim$  1 within our experimental errors.

Next, we try to explain the results of Ce-concentration dependence of  $T_c$  by applying the MIN theory. The relations used in the calculation of  $T_c(x)$  are shown in APPENDIX I. In the case we have two adjustable parameters  $T_K/T_{c0}$  and  $N(0)$ ,  $N(0)$  being the density of state per atom. For the value of  $T_K/T_{c0}$  we use the range  $T_K/T_{c0} = 0.001 \sim 1$  obtained from the above discussion on the relation  $(dH_{c2}/dT)_{T_c}$  versus  $T_c$ . Best fitting curves of  $T_c(x)$  are calculated for the typical values of  $T_K/T_{c0} = 10^{-3}, 10^{-2}, 10^{-1}, 0.5$  and 1 in the range by adjusting the density of state  $N(0)$ . The results are shown in Fig.13 together with the experimental data. Five theoretical curves; A, B, C, D and E in the figure have the value of  $N(0) = 0.53, 1.00, 2.20, 3.95$  and  $4.90$  per (eV $\cdot$ atom) for  $T_K/T_{c0} = 10^{-3}, 10^{-2}, 10^{-1}, 0.5$  and 1, respectively. They show a good fitting with experimental data except for lower temperature region. Considering the most realistic range of the  $N(0)$  in the Chevrel compounds as  $0.2 \leq N(0) \leq 1$ ,<sup>17)</sup> the most reasonable value of the Kondo temperature is estimated to be  $T_K/T_{c0} = 0.001 \sim 0.01$  with  $T_{c0} \approx 6$  K from the superconducting data in  $Ce_xLa_{1-x}Mo_6S_8$ . A broad transition and a small trace of residual resistance at 0.4 K for the concentration  $x = 0.14$  as shown in Fig.10 may reflect the reenter to normal state from the superconducting state at low temperature, as expected from the theoretical curves B and C in Fig.13.

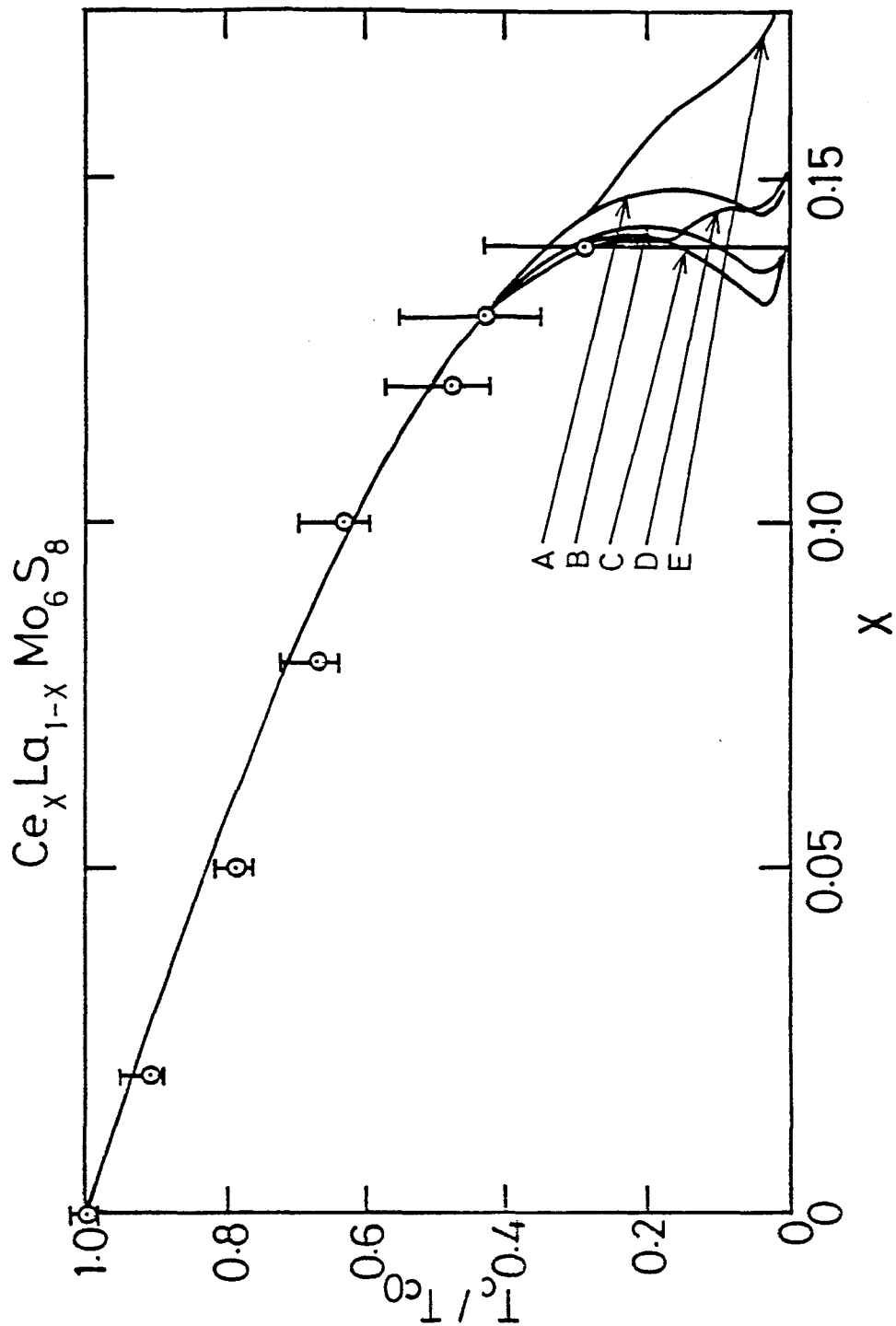


FIG.13 Theoretical curves of  $T_c(x)$  by applying the MIN theory. A, B, C, D and E correspond to  $T_K/T_{c0} = 10^{-3}$ ,  $10^{-2}$ ,  $10^{-1}$ , 0.5 and 1 K, and  $N(0) = 0.53$ , 1.00, 2.20, 3.95 and 4.90 /eV·atom, respectively. Experimental data are also shown.

#### § 4. MAGNETIC PROPERTIES

High field magnetization was measured for  $\text{CeMo}_6\text{S}_8$  up to 300 kOe. Fig.14 shows the magnetization  $M$  per Ce ion for the compound as a function of the applied field at 4.2, 2.0 and 1.3 K. In the high field region above 160 kOe, the magnetization shows a linear increase with increasing field. The high field susceptibility above 200 kOe at 1.3 K,  $\chi_{\text{hf}}$ , is  $1.07 \times 10^{-5}$  emu/g. Dashed line shows the magnetization due to the high field susceptibility at 1.3 K. By subtracting the dashed line from the magnetization curve in the figure, we get a magnetization curve which saturates in a high field region as shown in Fig.14(c). The saturated moment is increased with decreasing temperature.

Temperature dependence of the magnetic susceptibility was measured for five samples with different concentrations of Ce  $x = 1.0, 0.8, 0.5, 0.3$  and 0 in  $\text{Ce}_x\text{La}_{1-x}\text{Mo}_6\text{S}_8$ . To extract the contribution of Ce impurity, the magnetic susceptibility of  $\text{LaMo}_6\text{S}_8$ , which has an almost constant value of  $2.6 \times 10^{-4}$  emu/mole and a small increase at low temperatures due to magnetic impurities, was subtracted from the data. In Fig.15 we present the temperature dependence of the inverse magnetic susceptibility per mole Ce as a parameter of Ce-concentrations. It is remarkable that the magnetic susceptibility per mole Ce is independent of the Ce concentration and shows the same temperature dependence within our experimental errors. Above 120 K, it follows effectively the Curie-Weiss law  $\chi = C/(T-\theta)$  with  $C = 2.45 \pm 0.05 \mu_B/\text{Ce}$  and  $\theta = -38 \pm 3$  K. The Curie constant is a little bit small for the value of free  $\text{Ce}^{3+}$ ,

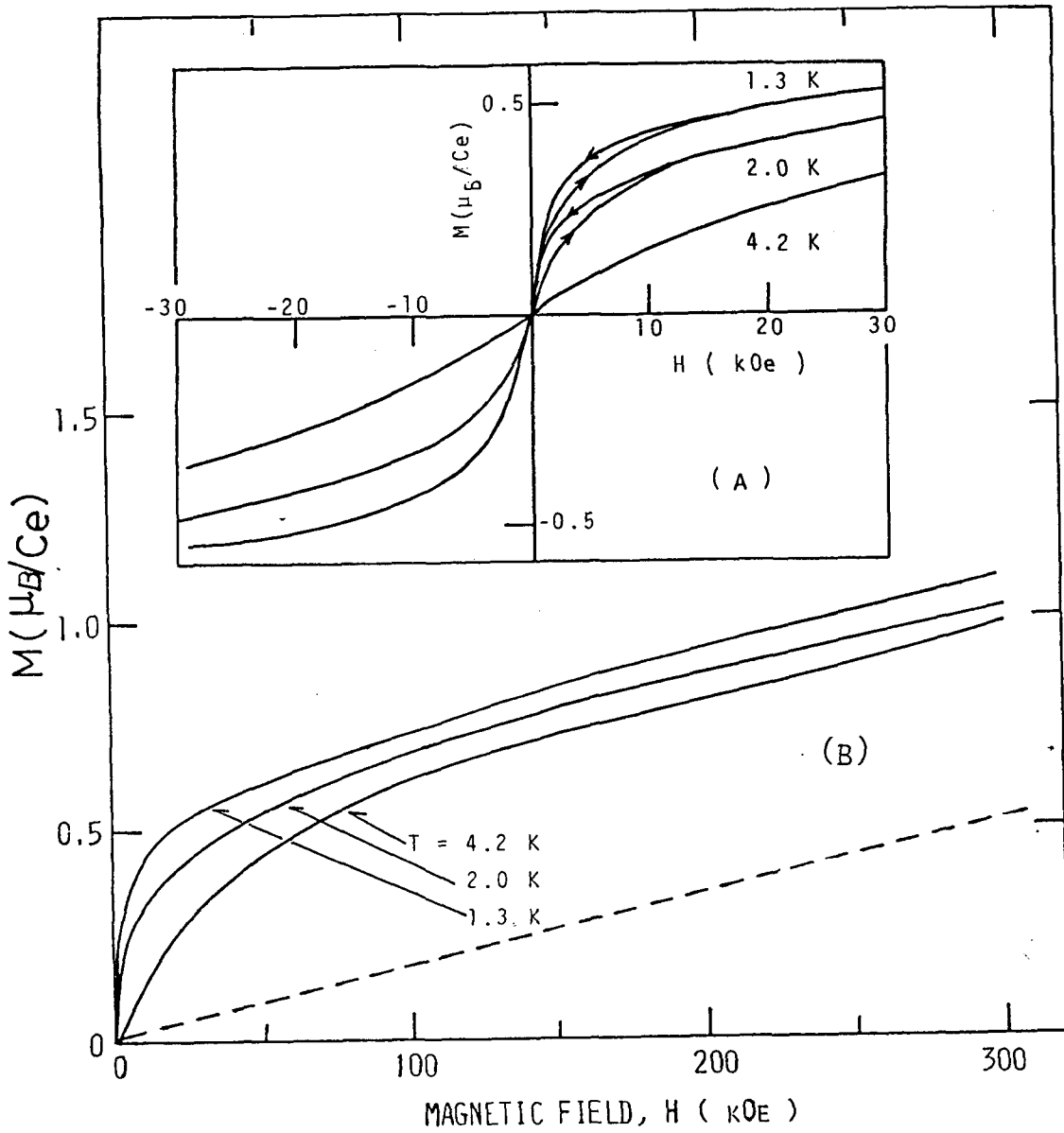
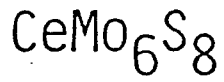


FIG.14 Magnetization process of  $\text{CeMo}_6\text{S}_8$  for (A) low field region and (B) high field region, respectively. Dashed line means the magnetization due to the high field susceptibility at  $1.3$  K.

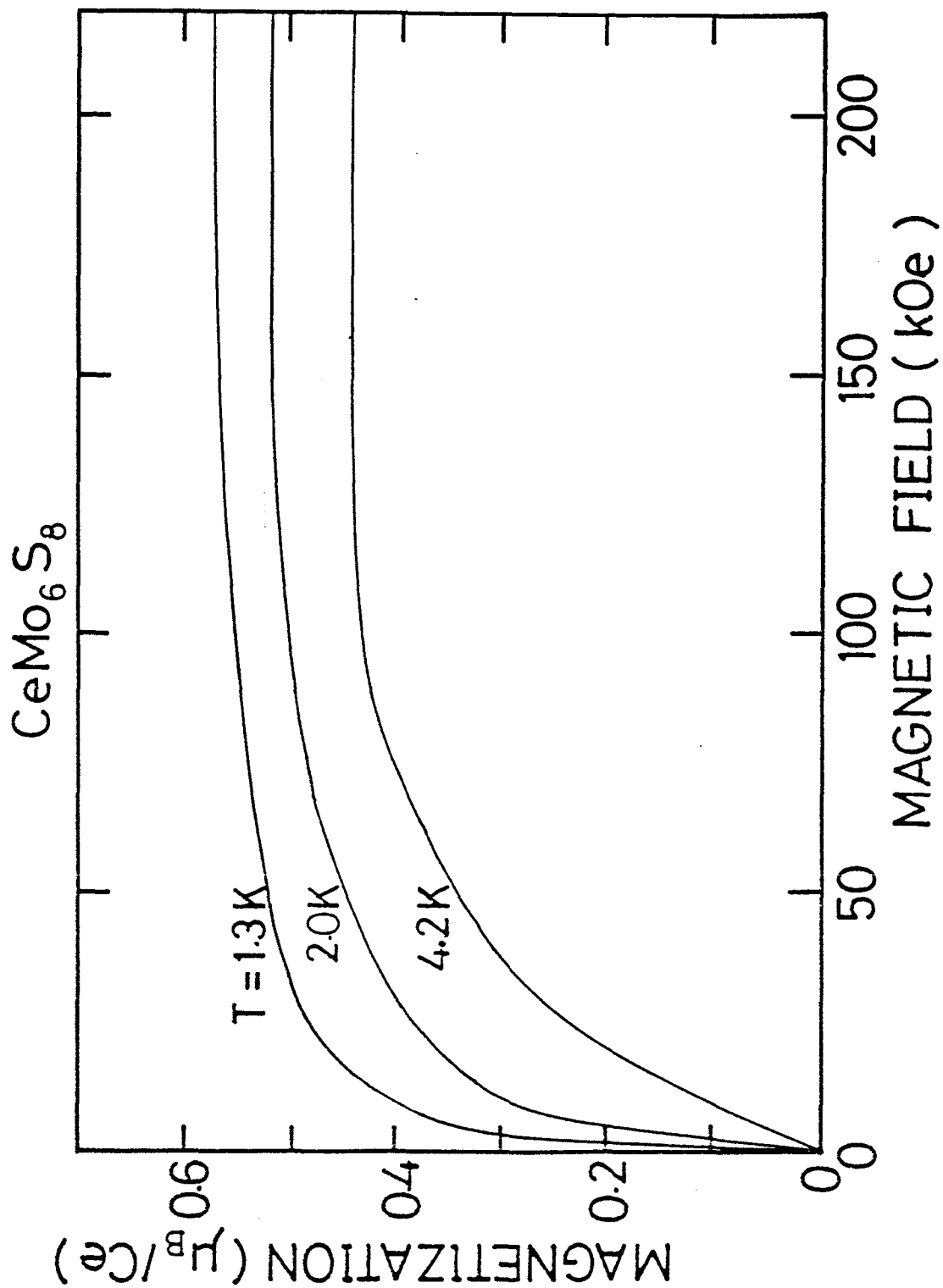


FIG.14(c) Magnetization curves of  $\text{CeMo}_6\text{S}_8$  which are subtracted the dashed line from the magnetization curves in Fig.14(B).



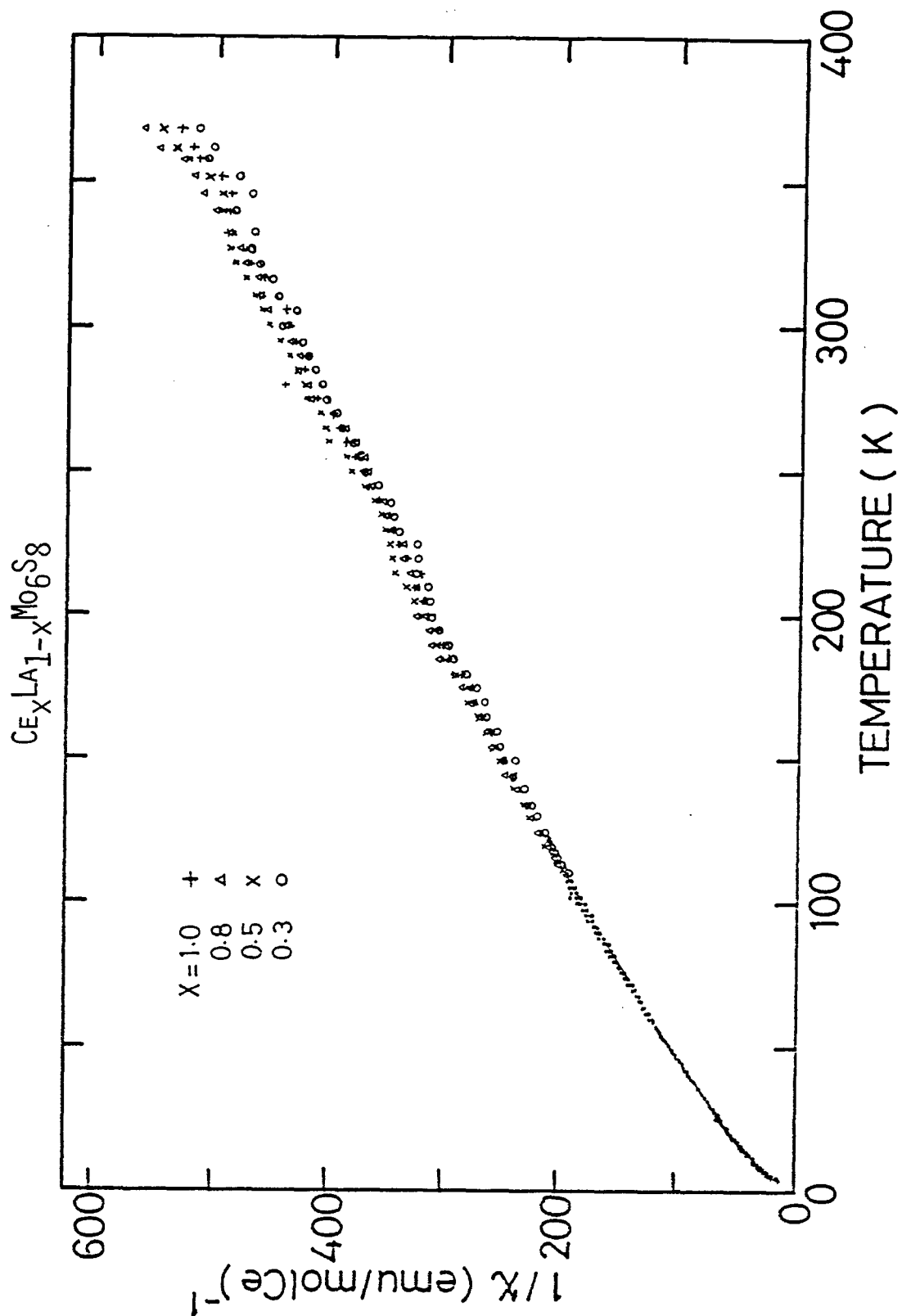


FIG.15 Temperature dependence of the magnetic susceptibility as a parameter of Ce concentration  $x$  in the system  $\text{Ce}_x\text{La}_{1-x}\text{Mo}_6\text{S}_8$ . The susceptibility is almost independent of the Ce concentration.

2.54  $\mu_B$ /Ce, and the Weiss constant is large compared to the  $T_N = 2.5$  K of  $\text{CeMo}_6\text{S}_8$ . These facts suggest that the magnetic susceptibility is mainly determined by a single site character of Ce, including the exchange interaction with conduction electrons.

In a first approximation, we tried to explain the results in Fig.15 in terms of the cubic crystal field splitting and Kondo effect by applying the DeGennaro and Borchhi's equation<sup>18)</sup> which is shown in APPENDIX II. As a first step, we calculated only the effect of crystal field splitting on the susceptibility. In Fig.16 the curves for the splitting  $\Delta = |\Gamma_7 - \Gamma_8| = 1000, 500$  and  $200$  K with  $\Gamma_7$  ground state and  $\Gamma_8$  ground state are given by A, B, C and a, b, c, respectively. As seen in the figure, two cases are clearly discriminated on the temperature dependence at low temperatures: the susceptibility for  $\Gamma_7$  ground state steeply increases at low temperature compared with that for  $\Gamma_8$  ground state. The case of  $\Delta = 0$  is given by a linear line O which follows the Curie law with Curie constant  $C = N(g\mu_B)^2 J(J+1)/3k_B = 0.0804$ . Experimental data of  $\text{CeMo}_6\text{S}_8$  are also plotted by dotted circles. It is found that their temperature dependence belong to the group with  $\Gamma_8$  ground state.

Thus, on taking account of the combined effect of Kondo and crystal field splitting, we choose a best value of  $\Delta$  with  $\Gamma_8$  ground state to fit with experimental data. Kondo temperature  $T_K$  is taken to be in the range  $T_K = 0.01 \sim 0.1$  K as is estimated in the preceding section of superconductivity in  $\text{Ce}_x\text{La}_{1-x}\text{Mo}_6\text{S}_8$ . Within those limitations for  $\Delta$  and  $T_K$ , the other parameter of band width  $D$  is adjusted to obtain a best fitting curve. Three typical examples of best fitting curves are shown in Fig.17(a), (b) and (c) for the set of

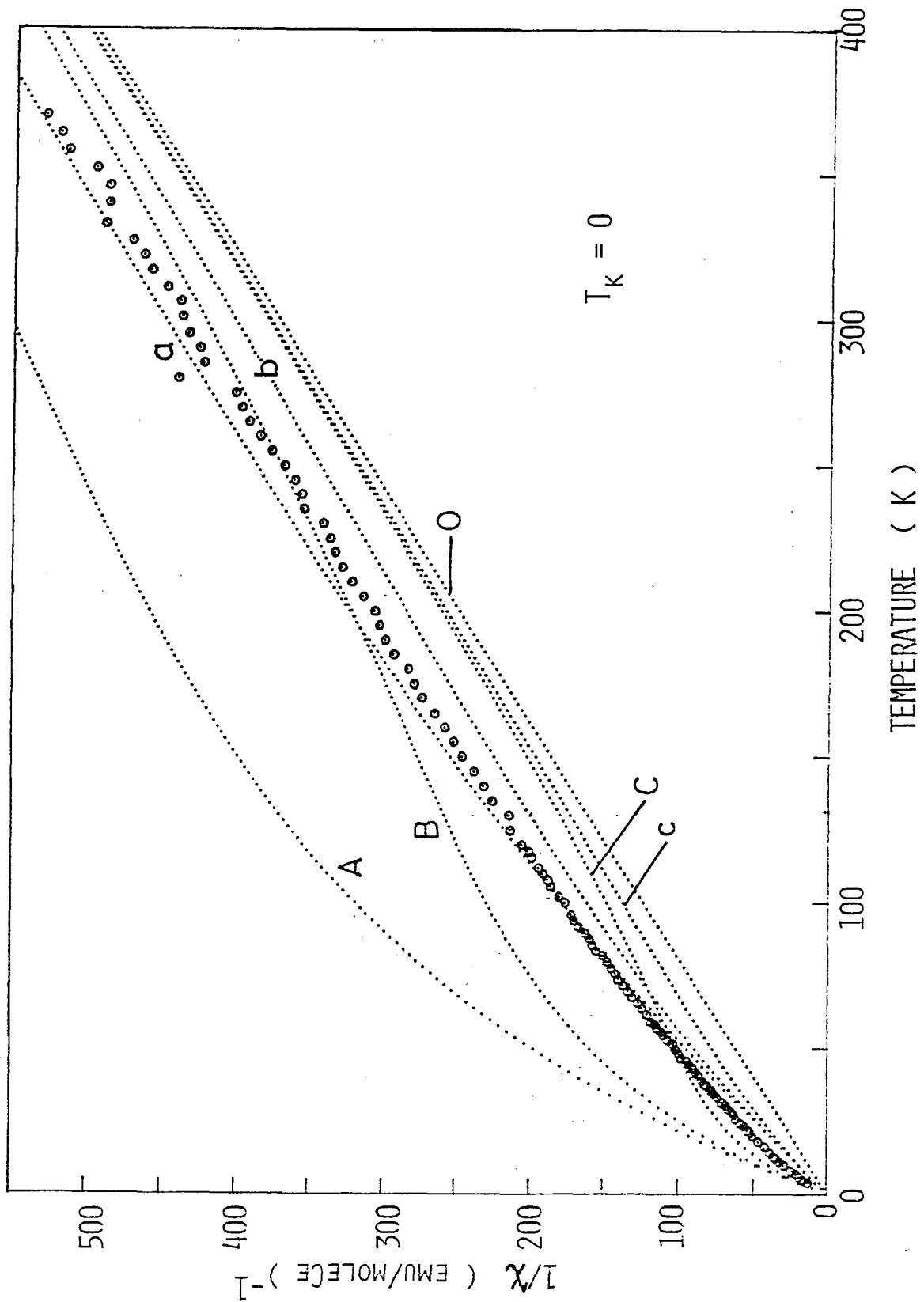


FIG.16 The calculated curves using DeGennaro and Borchì equation with no Kondo effect ( $T_K = 0$ ) but only crystal field splitting. A, B and C correspond  $\Delta = 1000, 500$  and  $200$  K, respectively with  $\Gamma_7$  ground state. a, b and c are in the same manner with  $\Gamma_8$  ground state. O gives the line with Curie law ( $\Delta = 0$ ). Experimental data for  $\text{CeMo}_6\text{S}_8$  is also given by dotted circles.

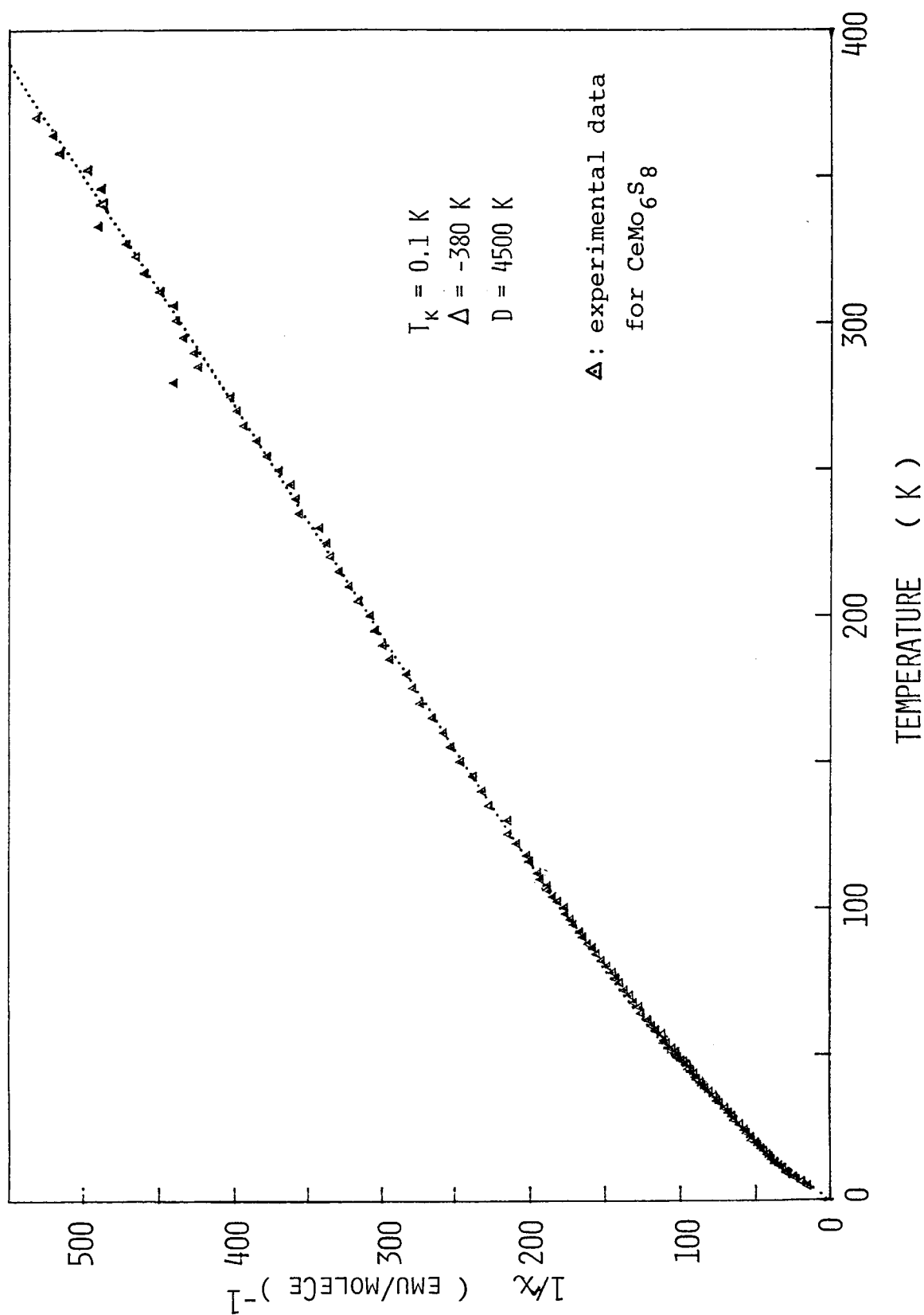


FIG.17(a) Example of best fitting curve by using DeGennaro Borchhi equation with the parameters;  $T_K = 0.1 \text{ K}$ ,  $\Delta = -380 \text{ K}$  and  $D = 4500 \text{ K}$ .

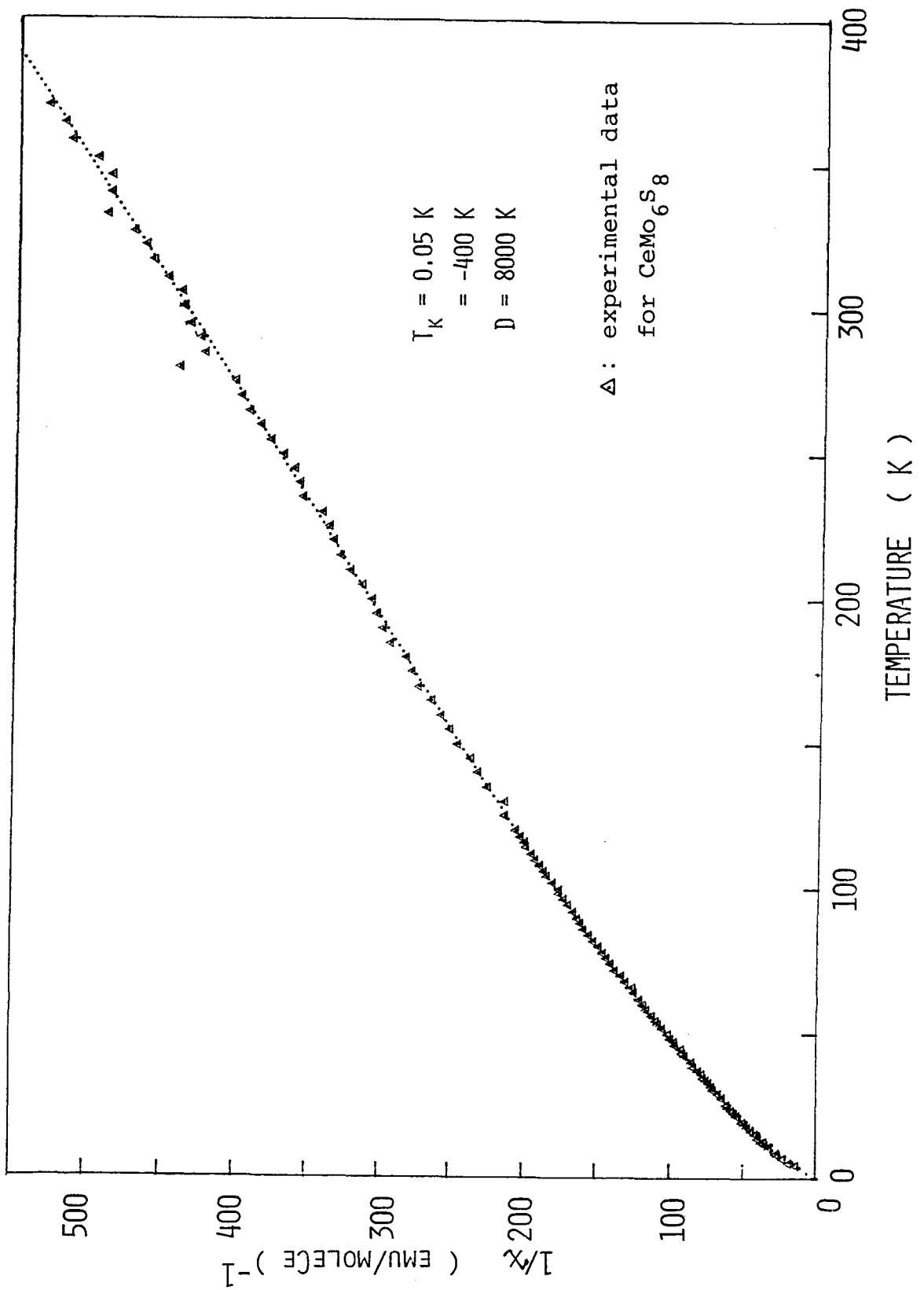


FIG.17(b) Example of best fitting curve by using DeGennaro Borchì equation with the parameters;  $T_K = 0.05 \text{ K}$ ,  $\Delta = -400 \text{ K}$  and  $D = 8000 \text{ K}$ .

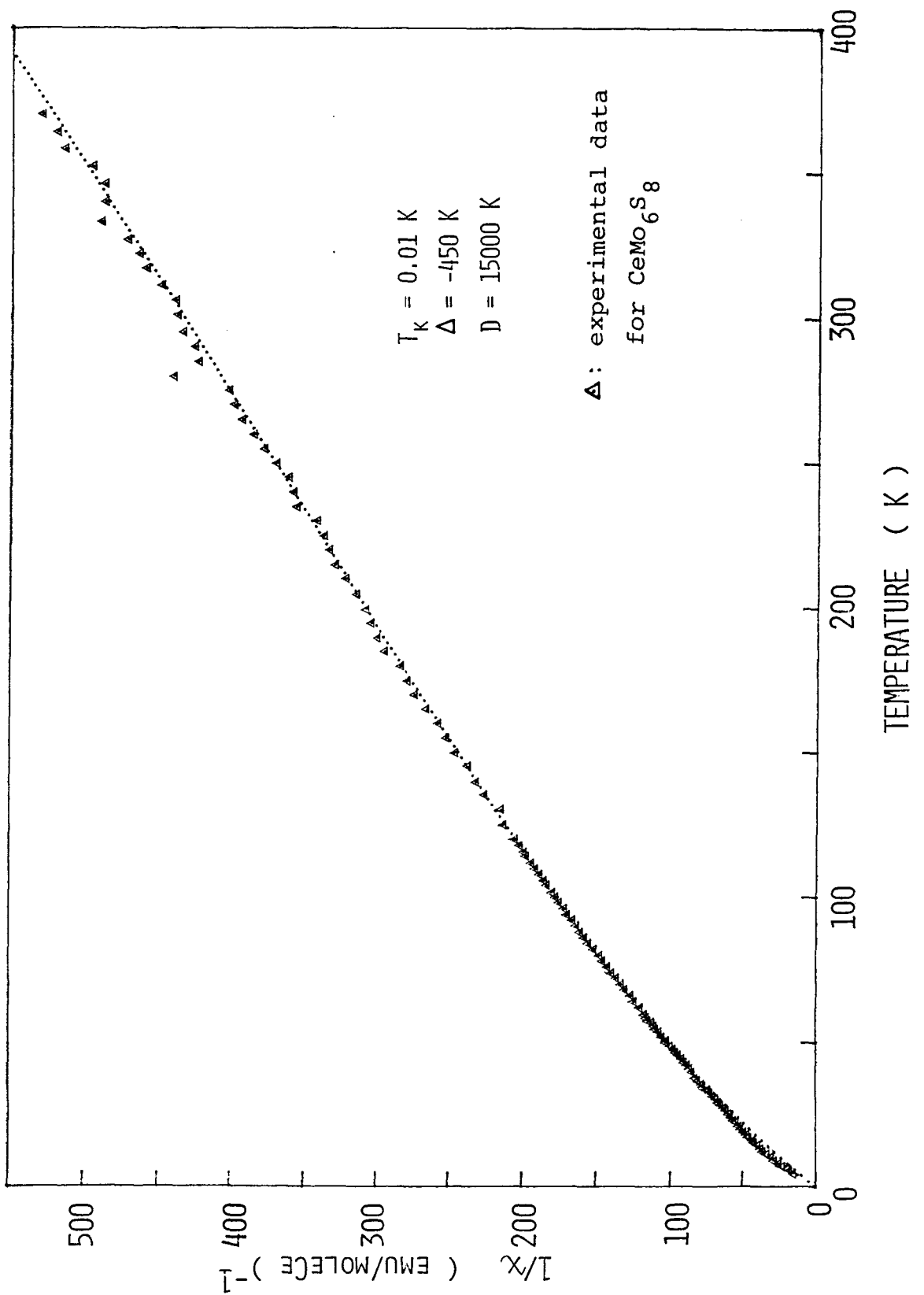


FIG.17(c) Example of best fitting curve by using DeGennaro Borchhi equation with the parameters;  $T_K = 0.01 \text{ K}$ ,  $\Delta = -450 \text{ K}$  and  $D = 15000 \text{ K}$ .

parameters ( $T_K$ ,  $\Delta$ ,  $D$ ) to be (0.01K, 450K, 15000K), (0.05K, 400K, 8000K) and (0.1K, 380K, 4500K), respectively, though it is difficult to obtain a unique set of parameters for the theory having three adjustable parameters. From this fitting procedure, it is suggested that the most probable value of crystal field splitting  $\Delta$  is about 400 K with  $\Gamma_8$  ground state and the value of band width is  $D = 4500 \sim 15000$  K.

On the other hand, temperature dependence of the magnetic entropy calculated from the data ( Fig.1 ) given by Maple et al.<sup>4)</sup> is shown in Fig.18. A plateau in a temperature region from  $T_N$  to 7 K suggests the doublet ground state of crystal field splitting though the entropy is somewhat small comparing the ideal value  $R \ln 2$  expected for the doublet. A sharp decrease below  $T_N$  is due to the magnetic ordering. A tendency to rise up near 7 K with increasing temperature suggests that the first excited doublet exists about 10 K above the ground doublet.\* Hence, considering the preceding discussion of magnetic susceptibility, we finally propose the scheme of crystal field splitting in the compound  $CeMo_6S_8$  as shown in Fig.19. Two lower lying doublets separated by about 10 K give the effective contribution to the magnetic susceptibility at lower temperatures. In a first approximation, however, the preceding analysis as the quartet ground state is effective at high temperatures above 10 K. This model is also consistent with  $C_3$  symmetry of the crystal structure in the compound  $CeMo_6S_8$ .

---

\* The value 10 K is only a speculation because the specific heat above 8 K is not measured.

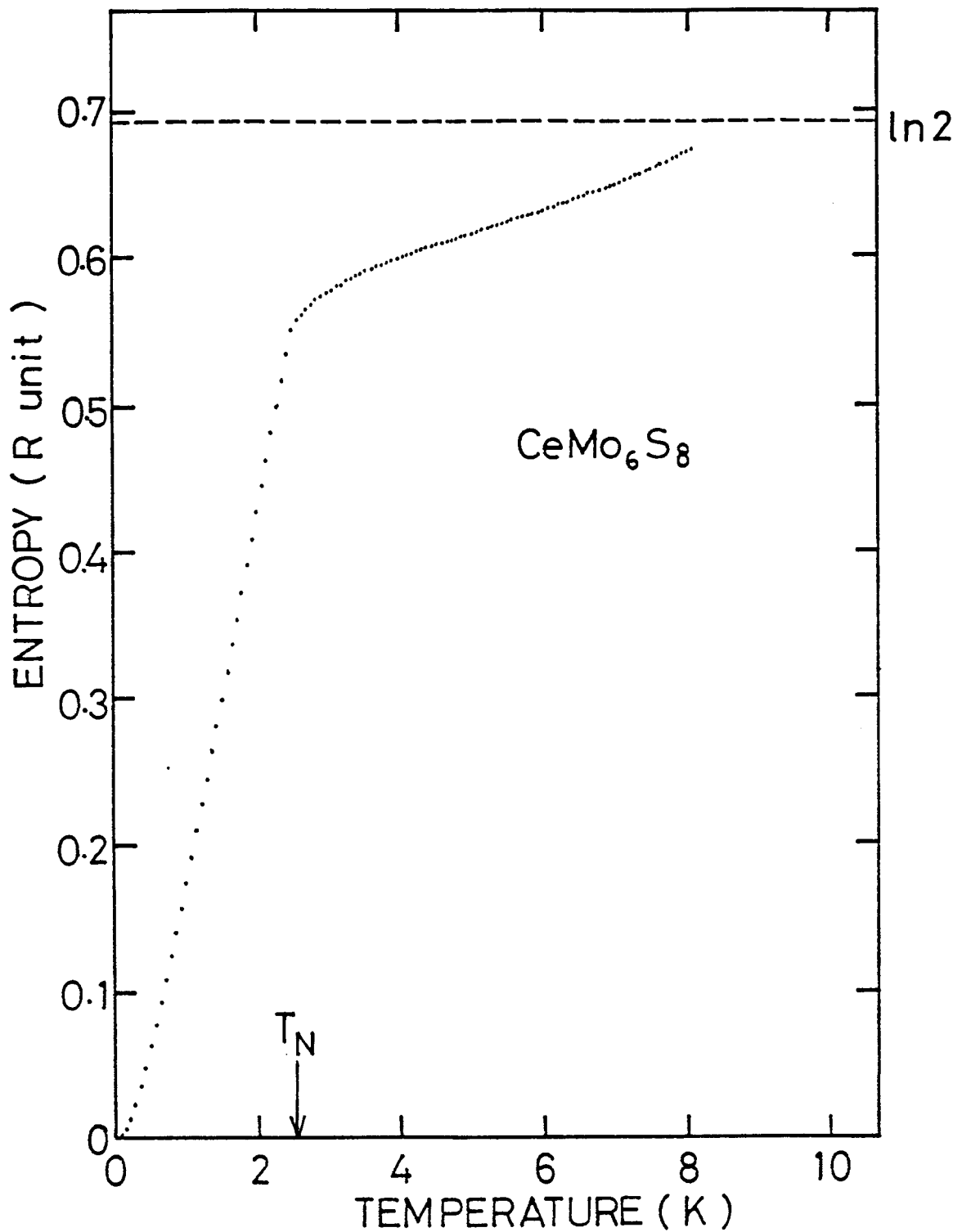


FIG.18 Temperature dependence of magnetic entropy of CeMo<sub>6</sub>S<sub>8</sub> from the data of magnetic specific heat measurement by Maple et al.<sup>3)</sup> ( see Fig.1 ).



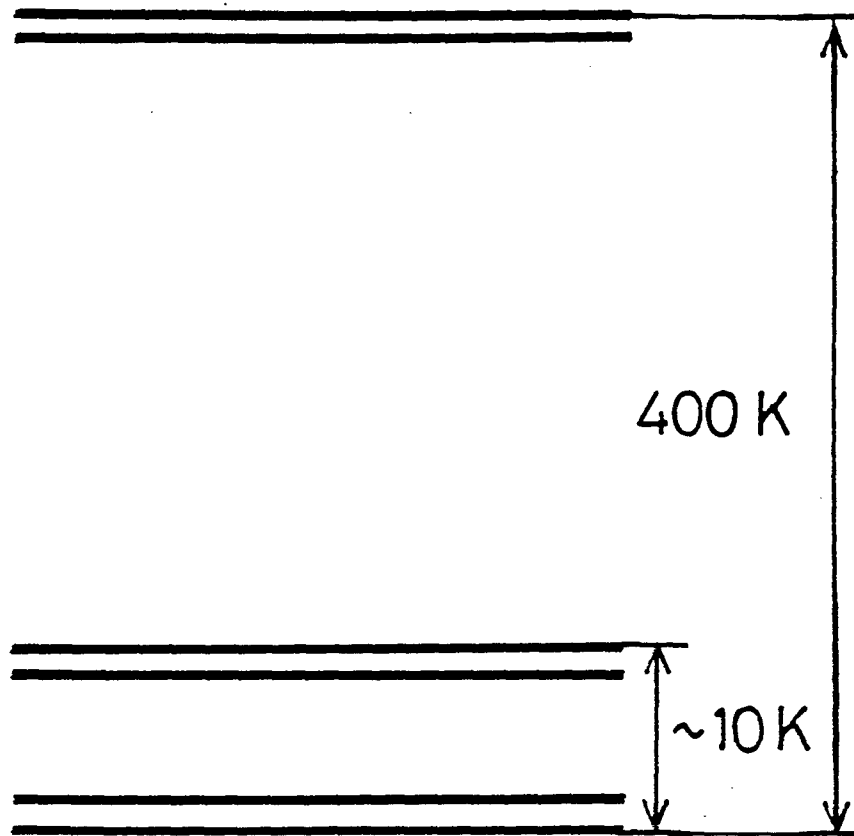
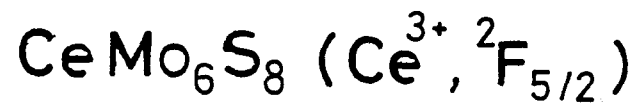


FIG.19 Crystal field splitting of  $\text{CeMo}_6\text{S}_8$  proposed in the present work.

A typical example of temperature dependence of the electrical resistance for the system  $\text{Ce}_x\text{La}_{1-x}\text{Mo}_6\text{S}_8$  is shown in Fig.20 as a parameter of Ce concentration. The resistance is normalized by the value at 300 K because of the difficulty to estimate the absolute value for the present sintered material. The resistance of Ce-doped samples in zero field has a minimum around 14 K, showing the peak at 2.5 K, 1.9 K and 1.4 K for  $x = 1.0, 0.7$  and  $0.5$ , respectively, and then followed by a decrease with decreasing temperature. The resistance minimum at 14 K is thought to be due to the Kondo effect. The peak temperature 2.5 K of  $\text{CeMo}_6\text{S}_8$  coincides with the antiferromagnetic ordering temperature<sup>4)</sup>. Thus, assuming the temperature of the resistance peak to be the antiferromagnetic ordering temperature  $T_N$ , the concentration dependence of  $T_N$  is obtained as shown in Fig.21.  $T_N$  decreases linearly with decreasing the concentration in the region of  $x > 0.5$ . For the concentration  $x = 0.2$ , a clear peak does not appear down to 0.5 K. The magnetic phase around  $x = 0.2 \sim 0.4$  may be complicated. Detailed measurements will be left. In the figure a phase boundary for the superconducting state is also shown by a broken line.

As shown in Fig.20, a large negative magnetoresistance is found below 10 K for the sample with high concentration of cerium. Details of the temperature dependent magnetoresistance for  $\text{CeMo}_6\text{S}_8$  are obtained as a parameter of applied field up to 20 kOe as is shown in Fig.21. The resistance shows the logarithmic temperature dependence at zero field in the temperature range from resistance minimum to the peak and decreases with decreasing temperature, showing a small kink around 0.8 K. The resistance below 0.8 K shows  $T^2$ -

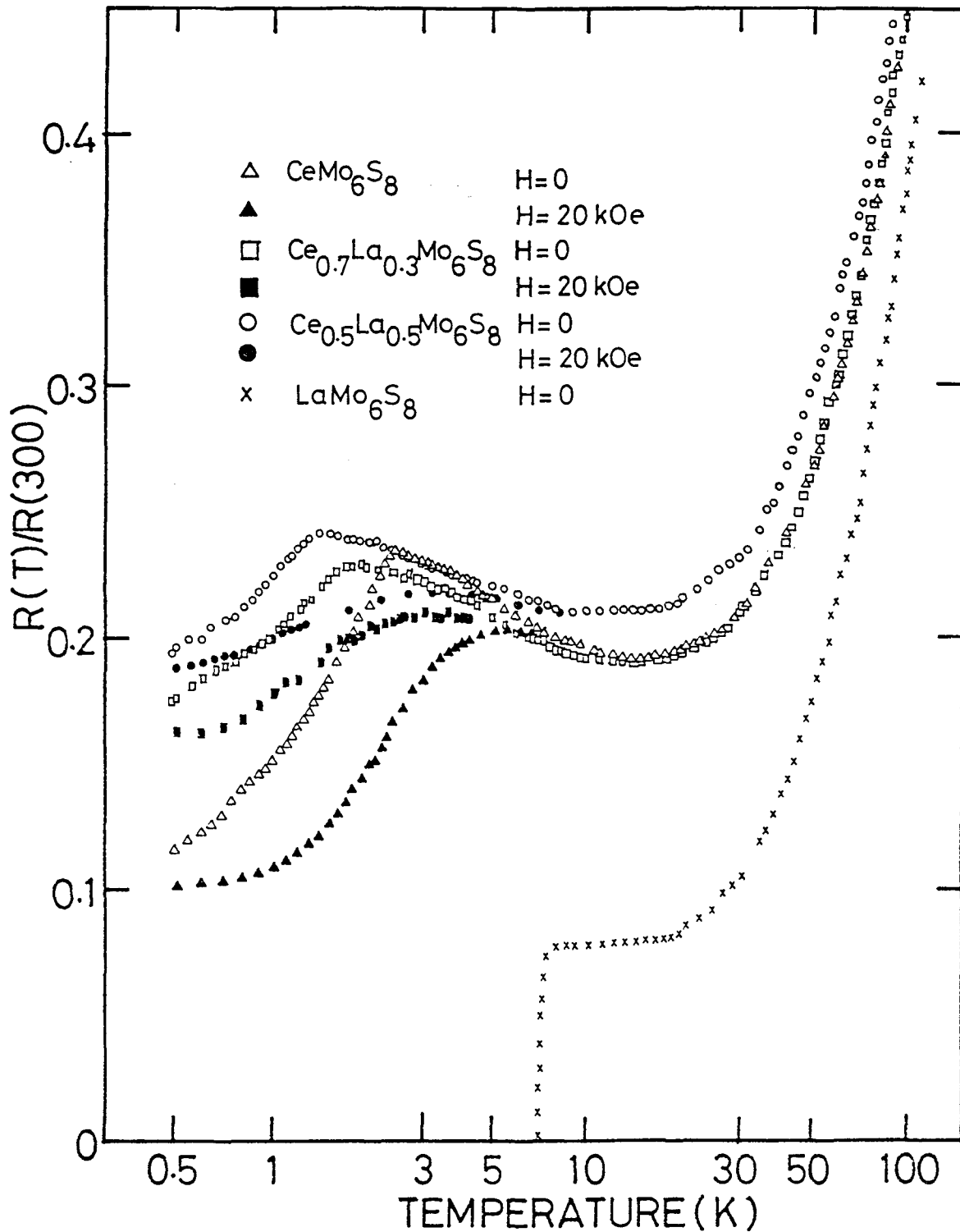


FIG.20 Temperature dependence of the electrical resistance for  $x = 1.0, 0.7, 0.5$  and  $0$  in  $\text{Ce}_x\text{La}_{1-x}\text{Mo}_6\text{S}_8$  under the magnetic field  $H = 0$  and  $20 \text{ kOe}$ . Negative magnetoresistance is found below about  $10 \text{ K}$ .

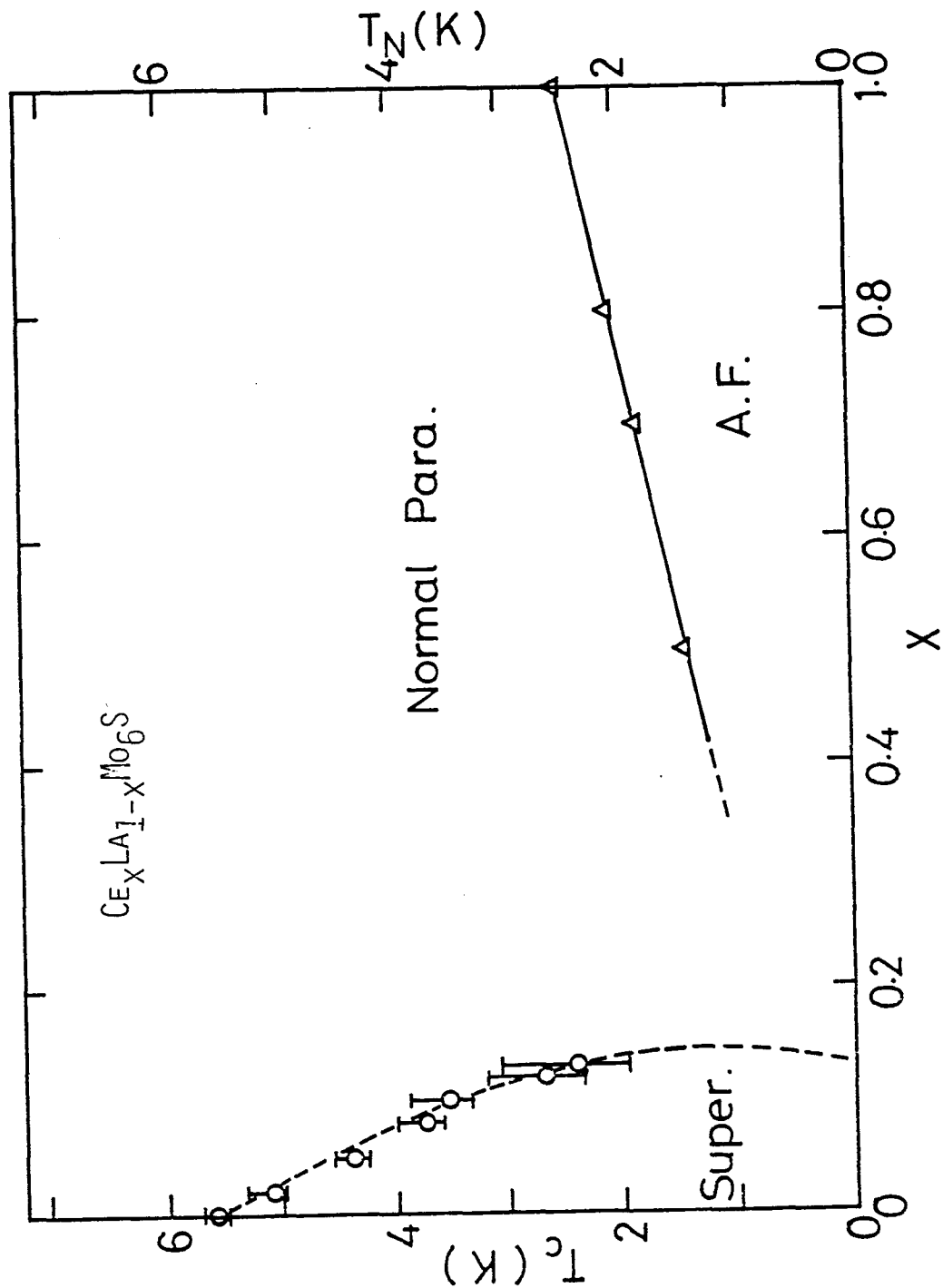


FIG.21 Phase diagram of the system  $Ce_xLa_{1-x}Mo_6S_8$ . Super. and A.F. mean the superconducting and antiferromagnetic ordering state, respectively.

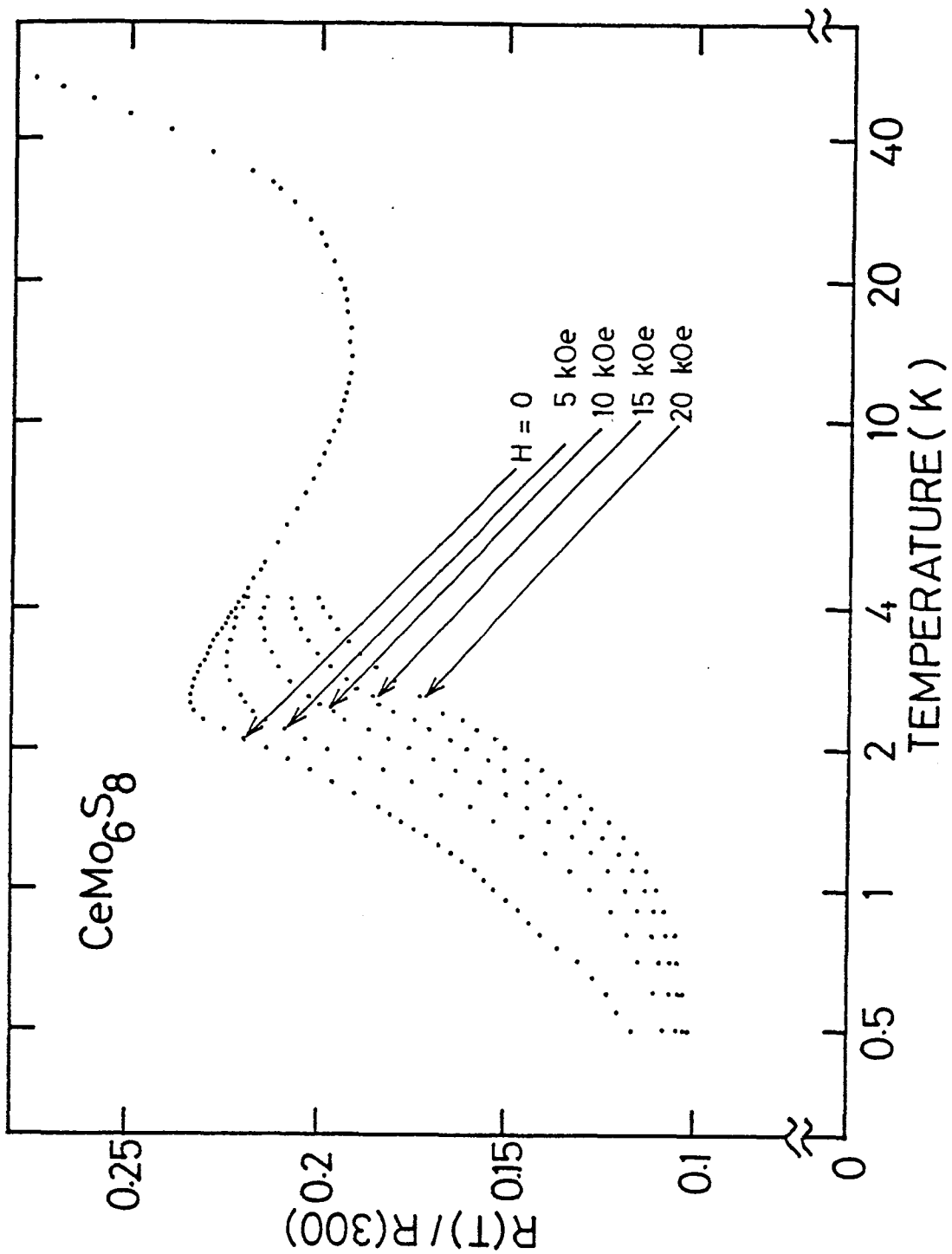


FIG.22 Temperature-dependent resistance of CeMo<sub>6</sub>S<sub>8</sub> as a parameter of applied magnetic field.

dependence as shown in Fig.23 and the slope decreases with increasing the applied magnetic field. Residual resistance reduced by the resistance at 300 K is estimated to be about 0.1 from the extrapolation to zero temperature in the figure. The difference in the resistance due to magnetic field,  $\Delta R = -[R(0,T) - R(H,T)]/R(0,300)$ , is plotted for several magnetic fields as a function of temperature in Fig.24. As the temperature is decreased from 4.2 K, the difference  $\Delta R$  is negatively increased with a shoulder at 2.4 K as indicated by an arrow and shows a broad minimum around 0.8 K. The minimum position is shifted to higher temperature with increasing the applied magnetic field. The shoulder at 2.4 K is attributed to the effect of spin fluctuation at the magnetic ordering as typically seen in the weak ferromagnets such as MnSi.<sup>19)</sup>

A clear logarithmic dependence of the magnetoresistance was observed in the compound below 1.2 K as is shown in Fig.25.

The behavior of the magnetoresistance is qualitatively consistent with the model based on the Kondo scattering at single site given by Zlatic<sup>20)</sup> and Beal-Monod et al.<sup>21)</sup>. However, the quantitative analysis is difficult at the present time. Concerning the theoretical problems for the dense Kondo materials such as Ce-compounds, they are currently under investigation. On this point, it may be needed to accumulate a more detailed experimental data for various type of dense Kondo materials.

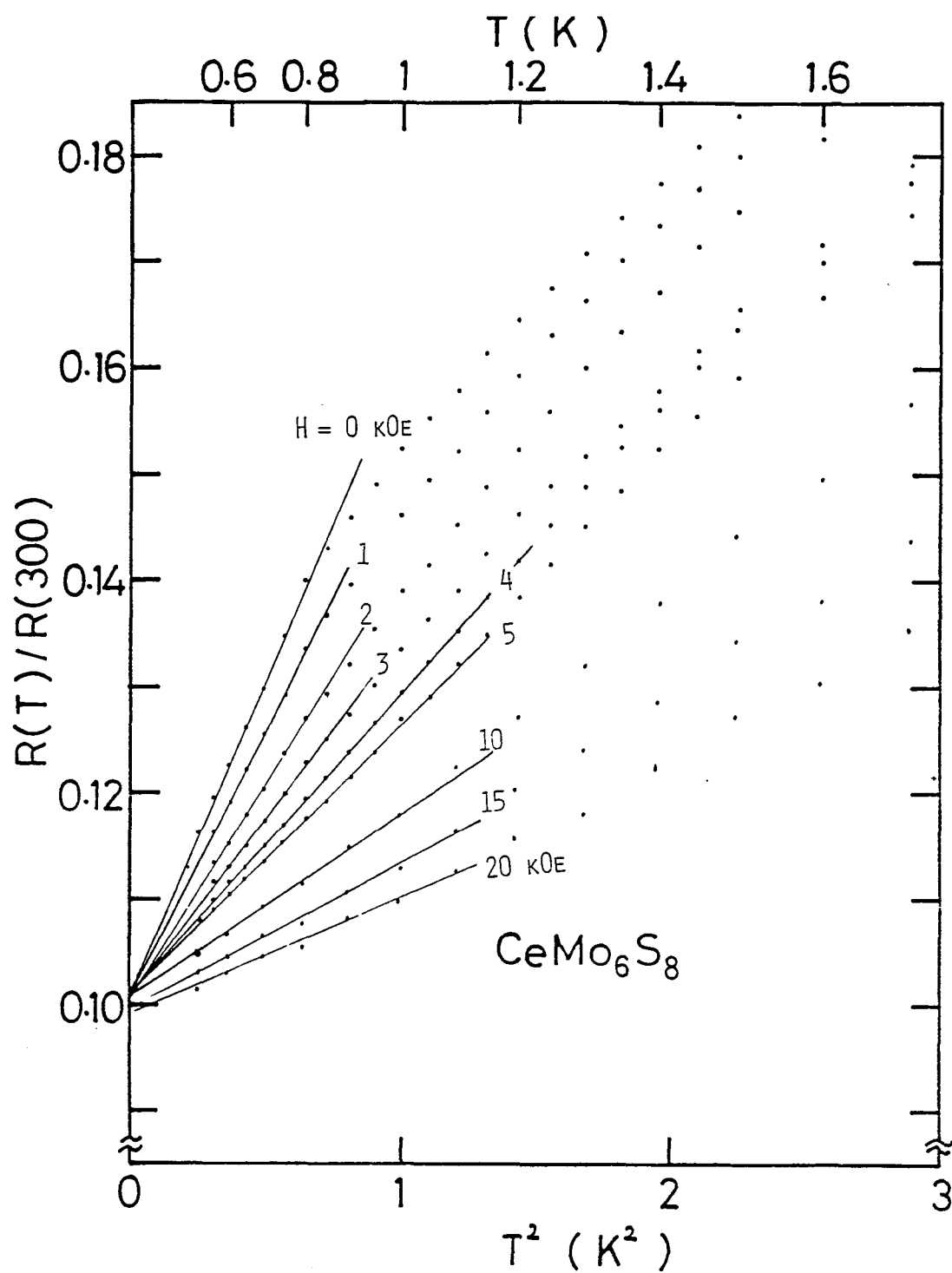


FIG.23 Magnetoconductance of  $CeMo_6S_8$  as a function of  $T^2$

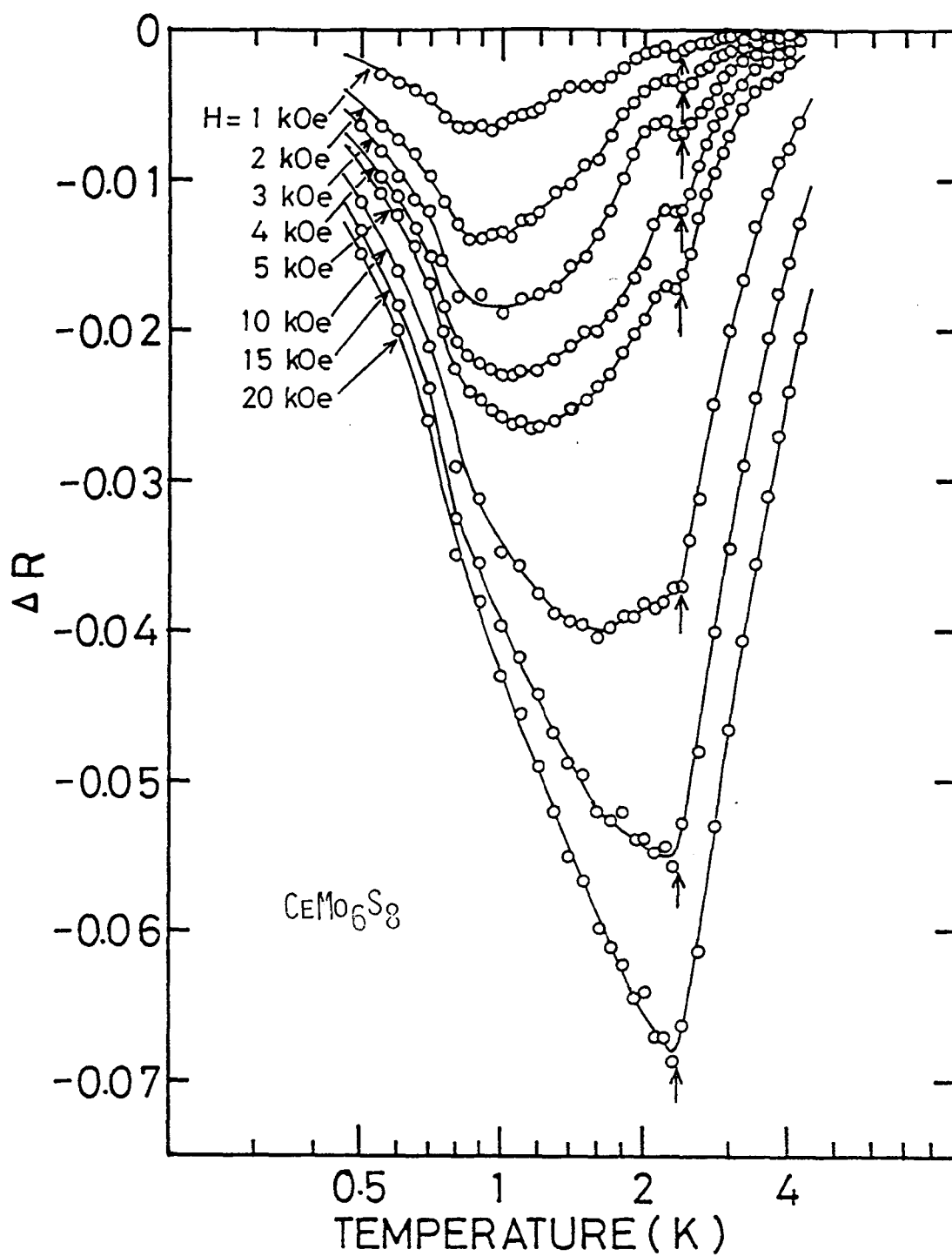


FIG.24 Temperature dependence of magnetoresistance of  $\text{CeMo}_6\text{S}_8$  for various magnetic fields. A weak shoulder indicated by an arrow is found near  $T_N$ .  $\Delta R$  is defined as  $\Delta R = -[R(0, T) - R(H, T)] / R(0, 300)$ .



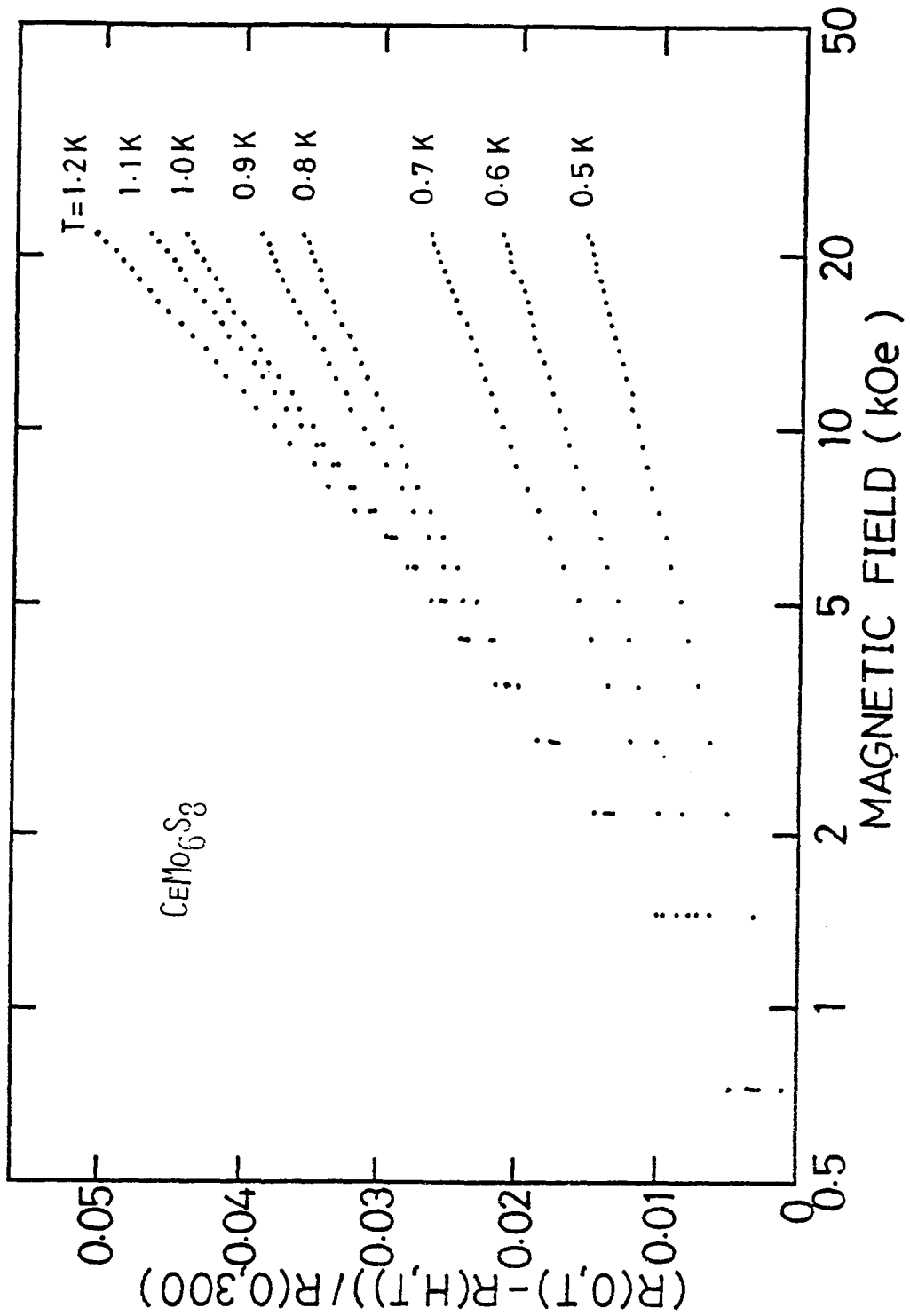


FIG.25 Magnetoconductance of  $\text{CeMo}_6\text{S}_8$  as a parameter of temperature below 1.2 K, which shows a clear  $\log H$  dependence.

## § 6. CONCLUDING REMARKS

We have presented the experimental results for  $\text{Ce}_x\text{La}_{1-x}\text{Mo}_6\text{S}_8$ ; lattice constant, XPS,  $T_c(x)$ ,  $H_{c2}(T)$ ,  $M(H)$ ,  $\chi(T)$  and  $R(H,T)$ .

Concentration dependence of lattice constant  $a_r(x)$  in  $\text{Ce}_x\text{La}_{1-x}\text{Mo}_6\text{S}_8$  follows the Vegard's law. Relative intensity of the XPS peaks  $I(\text{Ce}^{4+})/I(\text{Ce}^{3+})$  is less than 2 %. From these results it is concluded that  $\text{CeMo}_6\text{S}_8$  is not a mixed valence compound and the valence of Ce is trivalent.

Superconducting transition temperature and the upper critical field in the dilute system of  $\text{Ce}_x\text{La}_{1-x}\text{Mo}_6\text{S}_8$  ( $x \leq 0.14$ ) were obtained as a function of concentration and temperature, respectively. These superconducting properties with low  $x$  were well explained by the MIN theory based on the Kondo effect with a range of  $T_K/T_{c0} = 0.001 \sim 0.01$  with  $T_{c0} \approx 6$  K.

Magnetization measurement for  $\text{CeMo}_6\text{S}_8$  shows a rather small saturation moment about  $0.6 \mu_B$  and a large high field susceptibility  $\chi_{hf} \sim 1 \times 10^{-5}$  emu/g. Temperature dependence of the magnetic susceptibility per mole Ce is almost independent of the Ce concentration. This fact suggests that contribution of the exchange interaction between Ce spins and conduction electrons is dominant compared to the Ce spin-spin interaction. As a first approximation, the susceptibility is explained by the crystal field splitting and Kondo effect, which is consistent with the results from the superconducting properties. Considering the crystal structure and the experimental results in magnetic susceptibility and specific heat, we proposed a model of crystal field splitting which consists of three doublets with the

excited energy of 10 K and 400 K in  $\text{CeMo}_6\text{S}_8$ .

Concentration dependence of  $T_N$  is determined from the temperature dependent resistance of  $\text{Ce}_x\text{La}_{1-x}\text{Mo}_6\text{S}_8$ . A large negative magnetoresistance is found below 10 K for the sample with high concentration of cerium. Magnetoresistance of  $\text{CeMo}_6\text{S}_8$  is qualitatively explained by the model based on the Kondo scattering at single site. However, the quantitative analysis is difficult at the present time.

APPENDIX I -- CALCULATION OF  $T_c$  AND  $H_{c2}$  BY MIN THEORY --

According to their theory,  $T_c$  is given by

$$\ln(T_{c0}/T_c) = -\phi(T_c, n) + \frac{n}{4T_K\rho} \frac{[\phi_1(T_c, n)]^2}{1 + (n/4T_K\rho)\phi_2(T_c, n)} , \quad (A-11)$$

where

$$\phi(T, n) = 2\pi T \sum_{\omega>0} \left[ \frac{1}{\omega + n\alpha(\omega)} - \frac{1}{\omega} \right] , \quad (A-12)$$

$$\phi_k(T, n) = 2\pi T \sum_{\omega>0} \frac{f(\omega)^k}{\omega + n\alpha(\omega)} , \quad (A-13)$$

$$f(\omega) = \left[ 1 + \frac{\pi|\omega|}{4T_K} \right]^{-2} , \quad (A-14)$$

$$\alpha(\omega) = \begin{cases} \frac{1}{\pi\rho} \left[ \left( \frac{\pi|\omega|}{4T_K} \right) - \frac{1}{2} \left( \frac{\pi|\omega|}{4T_K} \right)^2 \right] , & \frac{\pi|\omega|}{4T_K} < 1 , \\ \frac{1}{2\pi\rho} \frac{(3/4)\pi^2}{(\ln(\pi|\omega|/4T_K))^2 + (3/4)\pi^2} , & \frac{\pi|\omega|}{4T_K} > 1 , \end{cases} \quad (A-15)$$

$$\omega = (2m+1) T , \quad (m = 0, \pm 1, \pm 2, \pm 3, \dots) , \quad (A-16)$$

where  $T_K$  and  $T_{c0}$  denote the Kondo temperature and the transition temperature of a superconductor with no magnetic impurities, respectively,  $n$  the impurity concentration and  $\rho$  the density of state of conduction electrons per atom per spin. These equations can be calculated with two parameters;  $T_K/T_{c0}$  and  $\tilde{n} = n/(2\pi)^2 T_{c0}\rho$ .

The equation to determine the upper critical field  $H_{c2}$  can be obtained by a slight modification of (A-11); i.e. it is given by

$$\ln(T_{C0}/T_C) = -\tilde{\phi}(T_C, H_{C2}, n) + \frac{n}{4T_K \rho} \frac{[\tilde{\phi}_1(T_C, H_{C2}, n)]^2}{1 + (n/4T_K \rho) \tilde{\phi}_2(T_C, H_{C2}, n)},$$

where

( A-17 )

$$\tilde{\phi}(T, H, n) = 2\pi T \sum_{\omega > 0} \left[ \frac{1}{\omega + n\alpha(\omega) + DeH} - \frac{1}{\omega} \right],$$

( A-18 )

$$\tilde{\phi}_k(T, H, n) = 2\pi T \sum_{\omega > 0} \frac{f(\omega)^k}{\omega + n\alpha(\omega) + DeH},$$

( A-19 )

where D is the diffusion constant which we assume is determined by nonmagnetic impurities.  $(dH_{C2}/dT)_{T_C}$  is calculated by using the equation near  $T_C(H=0)$ .  $(dH_{C2}/dT)_{T_C}$  and  $T_C$  are combined through the parameter  $\tilde{n}$ . Therefore, in  $(dH_{C2}/dT)_{T_C}$  versus  $T_C$  plot,  $\tilde{n}$  does not appear explicitly as a parameter, but only  $T_K/T_{C0}$  appears.

APPENDIX II -- CALCULATION OF  $\chi$  BY DeGennaro-Borchi EQUATION --

According to their theory, magnetic susceptibility is given by the sum of two contribution;  $\chi_0$  and  $\chi_2$ .  $\chi_0$  gives the crystal field contribution as obtained by Murao and Matsubara<sup>22)</sup>.  $\chi_2$  is the term of the Kondo effect with the crystal field splitting.

$$\chi_0 = (C/T)F(T) , \quad (A-21)$$

$$F(T) = (4/7)(e^{\beta\Delta}+2)^{-1} [(1/12)(26+5e^{\beta\Delta})+(8/3)(\beta\Delta)^{-1}(e^{\beta\Delta}-1)] , \quad (A-22)$$

where  $C = N(g\mu_B)^2 J(J+1)/3k_B$  is the Curie constant,  $\beta = 1/k_B T$  and  $\Delta$  is an energy separation between a doublet and a quartet ( of which the doublet is lower ).

$$\chi_2 = (C/T)(2\Gamma\rho)^2 \ln(k_B T/D)\psi(T) , \quad (A-23)$$

$$\begin{aligned} \psi(T) = \frac{1}{189} \frac{1}{e^{\beta\Delta}+2} [ 986 + 125e^{\beta\Delta} + 960 \frac{e^{\beta\Delta}}{e^{\beta\Delta}+2} + \frac{1}{\beta\Delta}(e^{\beta\Delta}-1) \\ \times ( 1216 + 960 \frac{e^{\beta\Delta}-2}{e^{\beta\Delta}+2} - 480 \frac{e^{\beta\Delta}+1}{e^{\beta\Delta}-1} + \frac{960}{\beta\Delta} ) ] , \end{aligned} \quad (A-24)$$

where  $\Gamma$  is the parameter of s-f exchange interaction;  $H_{sf} = -\Gamma \vec{J} \cdot \vec{s}$ .  $\rho$  is the density of state. In order to determine  $T_K$  from  $2\Gamma\rho$ , the usual formula  $T_K = D e^{-1/2} |\Gamma| \rho$  is modified by considering the influence of the crystal field on the Kondo effect as follows,

$$\psi(T_K) = (2\Gamma\rho)^{-1} , \quad (A-25)$$

where

$$\begin{aligned} \Psi(T) = & [ 15 + 192(1+e^{\beta\Delta})^{-1} + 78e^{-\beta\Delta} ]^{-1} \\ & \times \{ [-25+96(1+e^{\beta\Delta})^{-1}+70e^{-\beta\Delta}] \ln k_B T/D + [20+48(1+e^{\beta\Delta})^{-1} \\ & +4e^{-\beta\Delta}] \ln(|k_B^2 T^2 - \Delta^2|/D^2) \} . \quad ( A-26 ) \end{aligned}$$

Thus, we can calculate the magnetic susceptibility  $\chi = \chi_0 + \chi_2$ , with three parameters  $T_K$ ,  $D$  and  $\Delta$ .

## REFERENCES

- 1) For instance, "Valence Fluctuations in Solids" eds. L.M.Falicov, W.Hanke and M.B.Maple (North-Holland, 1981).
- 2) M.Ishikawa,  $\phi$ .Fischer and J.Muller: "Superconductivity in Ternary Compounds II" -eds. M.B.Maple and  $\phi$ .Fischer (Springer-Verlag, Berlin Heidelberg New York, 1982) p.143.
- 3) T.Jarlborg and A.J.Freeman: Phys. Rev. Lett. 44 (1980) 178.
- 4) M.B.Maple, L.E.DeLong, W.A.Fertig, D.C.Johnston, R.W.McCallum and R.N.Shelton: "Proc. Int. Conf. on Valence Instabilities and Related Narrow-Band Phenomena" ed. R.D.Parks (Plenum, New York, 1977) p.17.
- 5) M.Pelizzone, A.Treyvaud, P.Spitzli and  $\phi$ .Fischer: J. Low Temp. Phys. 29 (1977) 453.
- 6) A.A.Abrikosov and L.P.Gor'kov: Soviet Phys.- JETP 12 (1961) 1243.
- 7) Y.Takigawa and K.Okuda: J. Phys. Soc. Jpn. 55 (1986) 465.
- 8) K.Okuda, K.Kadowaki, K.Sugiyama, S.Noguchi and M.Date: Physica 108B (1981) 1273.
- 9) K.Okuda, Y.Takigawa, S.Noguchi, M.Honda and M.Date: J. Magn. Magn. Mat. 54-57 (1986) 441.
- 10) S.Noguchi, K.Okuda, Y.Takigawa, M.Yamada, M.Honda and M.Date: to be published in J. Phys. Soc. Jpn.
- 11) L.Vegard: Z. Phys. 5 (1925) 17.
- 12) R.Lasser, J.C.Fuggle, M.Beyss, M.Campagna, F.Steglich and F.Hulliger: Physica 102B (1980) 360.
- 13) G.Praline, B.E.Koel, R.L.Hance, H.I.Lee and J.M.White: J. Electron Spectroscopy and Related Phenomena 21 (1980) 17.



- 14) C.A.Luego, J.G.Huber, M.B.Maple and M.Roth: Phys. Rev. Lett. 32 (1974) 54
- 15) K.Maki: Physics 1 (1964) 127
- 16) T.Matsuura, S.Ichinose and Y.Nagaoka: Prog. Theor. Phys. 57 (1977) 713.
- 17)  $\phi$ .Fischer: Appl. Phys. 16 (1978) 1
- 18) S.DeGennaro and E.Borchi: Phys.Rev. Lett. 30 (1973) 377.
- 19) K.Kadowaki, K.Okuda and M.Date: J. Phys. Soc. Jpn. 51 (1982) 2433.
- 20) V.Zlatic: J. Phys. F11 (1981) 2147.
- 21) M.T.Beal-Monod and R.A.Weiner: Phys. Rev. 170 (1968) 552.
- 22) T.Murao and T.Matsubara: Prog. Theor. Phys. 18 (1957) 215.

## ACKNOWLEDGEMENTS

The author wishes to express his sincere gratitude to Professor Muneyuki Date for his valuable suggestions and enlightening discussions, and for his continuous encouragement throughout the present work.

He is indebted to Professor Kiichi Okuda of Department of Electronics, University of Osaka Prefecture for his valuable suggestions and many stimulating discussions throughout the present work.

He is also indebted to Dr. Yasuo Takigawa of Osaka Electro-Communication University for supplying  $Ce_xLa_{1-x}Mo_6S_8$  and XPS and lattice constant measurements of the compounds.

He would like to thank Dr. Kazuo Kadowaki for resistance measurements below 1 K and his helpful suggestions in experimental techniques. He also would like to thank Dr. Tatsuru Yosida for high field magnetization measurements below 1 K. He also would like to thank Dr. Kiyohiro Sugiyama for the cooperation and experimental suggestion in the high field measurements. He is indebted to Mr. Makoto Honda and Mr. Minoru Yamada as colabolators especially in the static measurements. He is also indebted to Mr. Takato Masuda for computer calculation.

Finally, the author wishes to thank all the members of Date Laboratory.